INVESTIGATION OF THE USE OF NANOFLUIDS TO ENHANCE THE IN-VESSEL RETENTION CAPABILITIES OF ADVANCED LIGHT WATER REACTORS

by

Ryan Christopher Hannink

B.S. Mechanical Engineering/Nuclear Engineering
University of California, Berkeley, 2003

Submitted to the Department of Nuclear Science and Engineering and the Engineering Systems Division in partial fulfillment of the requirements for the degree of

MASTER OF SCIENCE IN NUCLEAR SCIENCE AND ENGINEERING
and
MASTER OF SCIENCE IN TECHNOLOGY AND POLICY
at the
MASSACHUSETTS INSTITUTE OF TECHNOLOGY

June 2007

Author.....
Department of Nuclear Science and Engineering and Engineering Systems Division
May 11, 2007

Certified by.....
Jacopo Buongiorno
Assistant Professor of Nuclear Science and Engineering
Thesis Supervisor

Certified by.....
Lin-Wen Hu
Associate Director for Research Development at the MIT Nuclear Reactor Laboratory
Thesis Supervisor

Certified by.....
George E. Apostolakis
Professor of Nuclear Science and Engineering and Engineering Systems
Thesis Reader

Accepted by.....
Dava Newman
Professor of Aeronautics and Astronautics and Engineering Systems
Director of the Technology and Policy Program

Accepted by.....
Jeffrey Coderre
Associate Professor of Nuclear Science and Engineering
Chairman, Committee for Graduate Studies

INVESTIGATION OF THE USE OF NANOFLUIDS TO ENHANCE THE IN-VESSEL RETENTION CAPABILITIES OF ADVANCED LIGHT WATER REACTORS

by

Ryan Christopher Hannink

Submitted to the Department of Nuclear Science and Engineering and the Engineering Systems Division on May 11th, 2007 in partial fulfillment of the requirements for the degrees of
MASTER OF SCIENCE IN NUCLEAR SCIENCE AND ENGINEERING
and
MASTER OF SCIENCE IN TECHNOLOGY AND POLICY

Abstract

Nanofluids at very low concentrations experimentally exhibit a substantial increase in Critical Heat Flux (CHF) compared to water. The use of a nanofluid in the In-Vessel Retention (IVR) severe accident management strategy, employed in Advanced Light Water Reactors, was investigated. A model simulating the two-phase flow and heat transfer on the reactor vessel outer surface quantified the increase in decay power that can be removed using a nanofluid, predicting that the use of a nanofluid will allow a stable operating power ~40% greater than the power allowable using water to be achieved, while holding the Minimum Departure from Nucleate Boiling Ratio (MDNBR) constant.

A nanofluid injection system that would take advantage of the enhanced CHF properties of the nanofluid in order to provide a higher safety margin than the current IVR strategy or, for given margin, enable IVR at higher core power, is proposed. A risk-informed analysis has revealed that this injection system has a reasonably high success probability of 0.99, comparable to the success probability without the injection system.

Potential regulatory, environmental, and health risk issues were analyzed, and it was concluded that the current regulatory regimes are adequate for ensuring that the implementation of nanofluids in IVR will not endanger public health and safety. However, experimental verification of nanofluid CHF enhancement at prototypical IVR conditions and periodic nanofluid property testing as a surveillance requirement are needed to reduce the key uncertainties related to nanofluid performance. Finally, a periodic review of the health and environmental risks of nanofluids and, if necessary, follow-up research are recommended to ensure the health of the public and environment.

Thesis Supervisors:

Jacopo Buongiorno, Assistant Professor of Nuclear Science and Engineering

Lin-Wen Hu, Associate Director for Research Development at the MIT Nuclear Reactor Laboratory

ACKNOWLEDGEMENTS

First and foremost, I want to express my gratitude to my supervisors Professor Jacopo Buongiorno and Dr. Lin-Wen Hu for their abundant and valuable input over the past two years. I greatly appreciate their enthusiasm and generosity. Additionally, I want to thank Professor George Apostolakis for his input and insights throughout the process of my research.

I am also grateful to Richard Wright of Westinghouse Electric Company for his informational support, to Eric Forrest and Tim Lucas for their help with the experimental aspects of my thesis, and to Dr. In-Cheol Bang, C.J. Fong, Jiyong Oh, and the numerous others who have provided feedback on different aspects of my research and thesis.

Finally, thanks to my parents, Don and Leslie, and my sister, Erin, for their continual love and support.

This work was supported by the U.S. Nuclear Regulatory Commission under contract NRC-04-02-079.

CONTENTS

LIST OF FIGURES

LIST OF TABLES

1. INTRODUCTION

1.1 Motivation and Background

The threat of global warming resulting from man-made emissions of greenhouse gases has spurred interest in carbon-free energy sources. The electric power sector is a substantial greenhouse gas contributor, emitting roughly a third of the total greenhouse gases worldwide. Because electricity demand worldwide is expected to continue its rapid expansion in the future, carbon-free electricity sources are needed if the atmospheric carbon dioxide concentration is to be held to a sufficiently low level. Of the carbon-free electricity sources, only nuclear power can provide baseload electricity and be expanded to meet increasing electricity demand. Increasing the amount of electricity generated by nuclear power plants will displace other baseload electricity sources, primarily coal power plants, reducing the world's greenhouse gas emissions. This is of particular importance in developing countries, such as China, where the electricity demand growth will be the greatest and where the coal plants emit greenhouse gases and other pollutants at the highest rate.

One way to increase the amount of electricity generated by nuclear power plants is to increase the power that each plant produces. In Advanced Light Water Reactor (ALWR) systems, such as the Westinghouse AP1000 and the Korean APR1400, the power that a plant can produce is limited by its ability to mitigate the consequences of hypothetical severe accidents in which the core melts and relocates to the bottom of the reactor vessel. The AP1000 and APR1400 employ an In-Vessel Retention (IVR) strategy to mitigate these consequences. The IVR strategy consists of flooding the reactor cavity with water and removing the residual heat from the core through the reactor vessel lower head. This heat removal is limited by the occurrence of Critical Heat Flux (CHF) on the reactor vessel outer surface. Recent experiments have found that nanofluids, colloidal dispersions of nanoparticles (solid particles ranging in size from 1 to 100 nanometers) in a base fluid (typically water), have a higher CHF than water alone. Therefore, in theory, using a nanofluid as a coolant in IVR instead of water would allow an increase in the power of these ALWRs.

1.2 Objectives and Overview

The effect of using a nanofluid in IVR will be quantified by modeling the two-dimensional flow and heat transfer on the reactor vessel outer surface. The model will then be used to predict the increase in residual heat that can be removed by using a nanofluid to cool the reactor vessel outer surface and maintaining a constant safety margin. The details of the model are discussed in Chapter 2 and the results of the model are discussed in Chapter 3.

Using the results of the thermal hydraulic model, a risk-informed design of a conceptual nanofluid injection system is developed and proposed. The integration of the nanofluid injection system with the other systems in the nuclear power plant is considered and Probabilistic Risk Assessment (PRA) is used to quantify the impact of adding the nanofluid injection system on the IVR performance of the plant. The design and analysis of the nanofluid injection system is discussed in Chapter 4.

Lastly, the adequacy of the current regulatory regimes for ensuring that the implementation of the proposed nanofluid injection system will not endanger public health or safety is investigated. The regulatory regimes include the regime for regulating severe accidents in nuclear power plants and the regimes for regulating adverse health and environmental effects from toxic substances. The regulatory impact of using nanofluids in IVR is discussed in Chapter 5.

2. DESCRIPTION OF THE THERMAL-HYDRAULIC MODEL

This model is based upon the assumption that in the case of a core relocation severe accident, the vessel will be cooled solely through natural circulation provided by the fluid in the flooded reactor cavity.

2.1 Geometry, Heat Flux, and Inlet Condition Assumptions

In the Advanced Light Water Reactors (ALWRs) that this model represents, the reactor vessel is surrounded by thermal insulation, which is necessary for normal operation. This model defines the gap between reactor vessel outer surface and the thermal insulation to be the rising portion of the coolant flow path. The falling portion of the flow path (downcomer) is outside of this gap in the reactor cavity.

This model takes the Westinghouse AP1000 as a representative of ALWRs that employ an IVR strategy. The vessel and insulation geometry is based on the geometry of the AP1000 as defined in the University of California at Santa Barbara report, "Limits of Coolability in the AP1000-Related ULPU-2400 Configuration V Facility" (UCSB Report) [1]. The model's geometry is based on the 3" baffle position shown in the report. The inlet was modified from the geometry in the UCSB Report to account for the total inlet area for a full hemispherical reactor vessel. The UCSB Configuration V facility models the full reactor vessel by taking a section of the full hemisphere. Figure 1 shows this configuration.

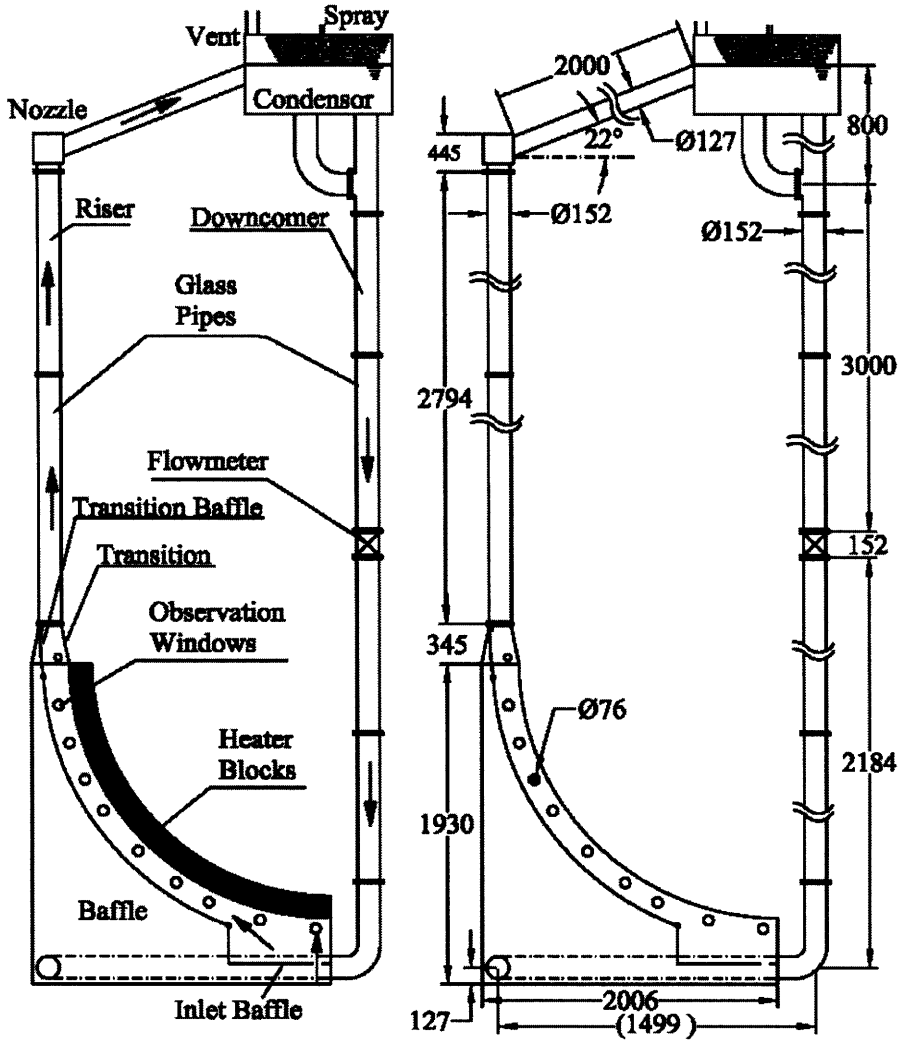

Figure 1: Geometry taken from UCSB Report (dimensions in mm)[1]

The heat flux profile is based on the heat flux profile detailed in the UCSB Report [1]. Three test configurations were used in the model (labeled T48A, T40B, and T40D in the report) and are illustrated in Figure 2. An angle of 0° corresponds to the bottom of the reactor vessel where the surface is downward-facing and horizontal, while an angle of 90° corresponds to the side of the reactor vessel where the surface is outward-facing and vertical.

[1] Taken from [1].

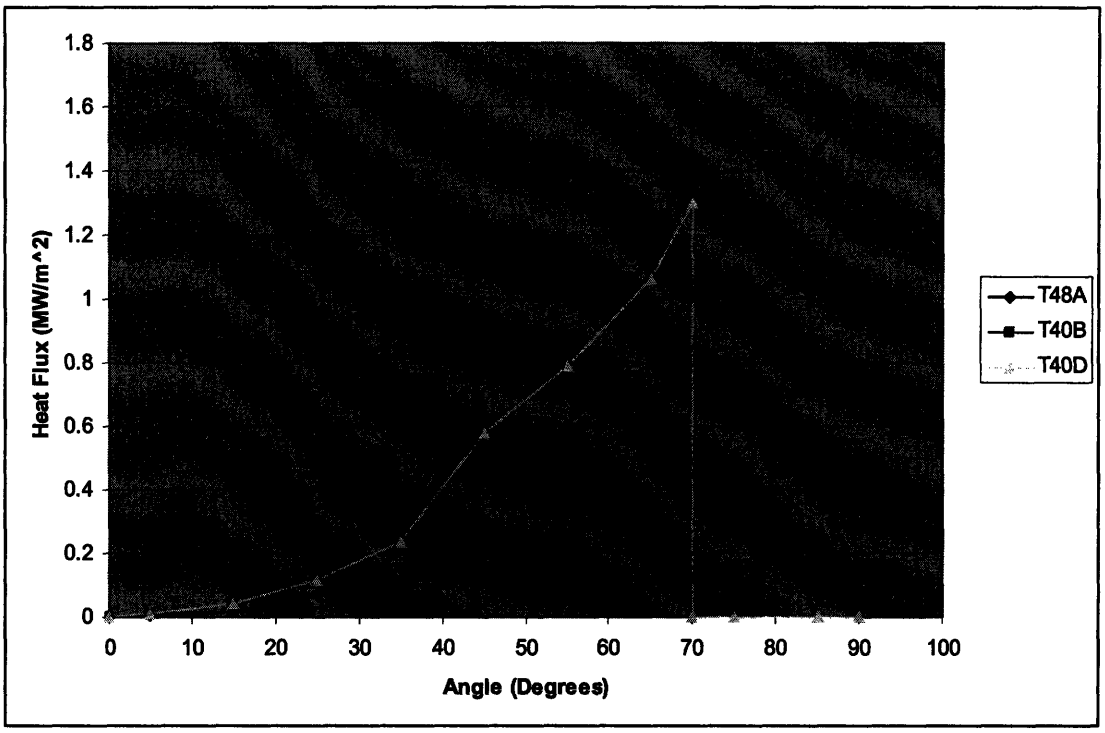

Figure 2: Heat Flux Profiles used in Model

The inlet conditions in this model are also based on the information given in the UCSB Report [1], namely that the fluid is saturated and at atmospheric pressure in the condenser at the top of the loop. Therefore, the fluid is assumed to enter the gap between the reactor vessel outer surface and the insulation at a temperature of 373 K at a pressure of 1.57 atm.[2]

A summary of the key model parameters is given in Table I.

Table I: Key Model Parameters

Vessel Inner Diameter	4.02 m
Vessel Height	6.14 m
Lower Head Height	2.31 m
Typical Gap Size	0.076 m
Inlet Temperature	373 K
Inlet Pressure	1.57 atm

2.2 Summary of Code Operation and Outputs

The code uses a given heat flux, flow geometry, and mass flow rate to calculate the flow quality, void fraction, and temperature throughout the flow path. Combining this

[2] The inlet conditions are calculated assuming no heat loss in the downcomer and a downcomer height of 6.14 m.

information with the properties of the fluid, the density and flow velocity throughout the flow path are determined. The properties and parameters above are calculated at nodes along the flow path. The results of the calculations at each node are used to calculate the properties and parameters of the next node. The first node is at the bottom of the lower head (an angle of 0°). The lower head is divided into 142 nodes spaced roughly at intervals of 0.57°. The riser section of the flow path is divided in 190 equally spaced nodes. From the flow data, the gravity, acceleration, friction and form terms are calculated. The mass flow rate is then adjusted until the momentum balance is satisfied. Finally, the flow data are used with a critical heat flux correlation, modified to account for the effect of a nanofluid, to determine the Critical Heat Flux (CHF) and the Departure from Nucleate Boiling Ratio (DNBR).

The code can be used to determine the mass flow rate for different power levels and thus the MDNBR for these different power levels. By comparing the MDNBR with water as the coolant to the MDNBR with a nanofluid as the coolant, one can quantify the power increase that can be achieved with a nanofluid while keeping the safety margin (*i.e.*, MDNBR) the same. It must be emphasized that the thermodynamic and thermophysical properties of nanofluids at the low concentrations of interest here are practically identical to those of water [2], so the thermal-hydraulic model can be used for water and nanofluids indifferently. The only difference is in the treatment of CHF, as explained in Section 2.7.

2.3 Onset of Subcooled Boiling

The fluid undergoes subcooled boiling as it flows through the gap. The onset of subcooled boiling occurs when the wall temperature exceeds the saturation temperature of the fluid at the local pressure. The wall temperature is determined using the Dittus-Boelter Heat Transfer Correlation, solved for wall temperature and shown in Equation (2.1).

$$T_{wall} = T_{bulk} + \frac{q''}{\frac{k}{D_H}\left(0.023 \cdot (\mathrm{Re})^{0.8} \cdot (\mathrm{Pr})^{0.4}\right)} \tag{2.1}$$

where: T_{wall} = wall temperature, T_{bulk} = bulk fluid temperature, q'' = heat flux, k = liquid thermal conductivity, D_H = hydraulic diameter of channel, Re = Reynolds number of liquid coolant, Pr = Prandtl number of liquid coolant

The bulk temperature and the associated properties of the bulk fluid are determined based on the energy balance, shown in Equation (2.2).

$$T_{bulk} = T_{sat} + \frac{x_e \cdot (h_g - h_f)}{c_p}$$
$$x_e = \frac{h - h_f}{h_g - h_f}, h = h_{inlet} + \frac{1}{\dot{m}} \int_{vessel} q'' dA_{surface} \quad (2.2)$$

where: T_{sat} = saturation temperature of the liquid, x_e = equilibrium quality, h = enthalpy, h_f = saturation enthalpy of liquid, h_g = saturation enthalpy of gas, h_{inlet} = enthalpy at the inlet, $A_{surface}$ = incremental surface area of the reactor vessel, $\dot{m}$ = mass flow rate

2.4 Calculation of Flow Quality in Heated and Unheated Sections

2.4.1 Heated Section

In the heated section of the flow path the Levy model [3] is used:

$$x = x_e - x_{e,onb} \cdot e^{\left(\frac{x_e}{x_{e,onb}} - 1\right)} \quad (2.3)$$

where: x = flow quality, $x_{e,onb}$ = equilibrium quality at the onset of nucleate boiling

2.4.2 Unheated Section

The UCSB Report observes that the voids quickly collapse upon entering the unheated section of the flow path. In order to match the model with the UCSB Report's experimental results, the flow quality, x, is forced to go quickly to zero upon the fluid entering the unheated section of the flow path.

As the liquid flows up the riser, the pressure is reduced and the liquid reaches saturation. The pressure is further reduced after saturation has been reached and flashing occurs. The quality is then given by equating the quality and the equilibrium quality, as shown in Equation (2.4).

$$x = x_e = \frac{h - h_f}{h_g - h_f} \quad (2.4)$$

2.5 Calculation of Void Fraction

The void fraction, α, is determined using the EPRI correlation [4], shown in Equation (2.5).

$$\alpha = \frac{j_g}{C_0 \cdot (j_f + j_g) + V_{gj}} \tag{2.5}$$

where: j_g = vapor superficial velocity, j_f = liquid superficial velocity, C_0 = distribution parameter, V_{gj} = drift flux parameter

The distribution parameter, C_0, is determined by Equation (2.6) and the drift flux parameter is determined by Equation (2.7).

$$\begin{aligned}
&C_0 = F_r \cdot C_{0v} + (1 - F_r) \cdot C_{0h} \\
&F_r = \left(\frac{90^\circ - \theta}{90^\circ}\right), C_{0v} = \frac{L}{(1 - K_0) \cdot \alpha^r + K_0} \\
&L = \frac{1 - e^{-C_1 \cdot \alpha}}{1 - e^{-C_1}}, C_1 = \frac{4 \cdot P_{crit}^2}{P \cdot (P_{crit} - P)}, K_0 = B_1 + (1 - B_1) \cdot \left(\frac{\rho_g}{\rho_f}\right)^{0.25} \\
&r = \frac{1.0 + 1.57 \cdot \left(\frac{\rho_g}{\rho_f}\right)}{(1 - B_1)}, B_1 = \min(0.8, A_1), C_{0h} = \left[1 + \alpha^{0.05} \cdot (1 - \alpha)^2\right] \cdot C_{0v}
\end{aligned} \tag{2.6}$$

where: θ = angle from vertical, P = pressure, P_{crit} = critical pressure

$$\begin{aligned}
&V_{gj} = F_r \cdot V_{gjv} + (1 - F_r) \cdot V_{gjh} \\
&V_{gjh} = V_{gjv}, V_{gjv} = 1.41 \cdot \left[\frac{(\rho_f - \rho_g) \cdot \sigma \cdot g}{\rho_f^2}\right]^{0.25} \cdot C_2 \cdot C_3 \cdot C_4 \cdot C_9 \\
&C_2 = \frac{1}{1 - e^{\frac{-C_5}{1 - C_5}}}, C_5 = \sqrt{\frac{150}{\left(\frac{\rho_f}{\rho_g}\right)}}, C_3 = \max\left(0.50, 2 \cdot e^{-\mathrm{Re}/60000}\right) \\
&C_4 = 1, if \rightarrow C_7 \geq 1, C_4 = \frac{1}{1 - e^{-C_8}}, if \rightarrow C_7 < 1 \\
&C_7 = \left(\frac{0.09144}{D_H}\right), C_8 = \frac{C_7}{1 - C_7}, C_9 = (1 - \alpha)^{B_1}
\end{aligned} \tag{2.7}$$

where: σ = surface tension

2.6 Momentum Balance

Knowing the properties of the fluid allows the mass flow rate to be determined through the momentum equation:

$$\Delta P_{gravity} = \Delta P_{acceleration} + \Delta P_{friction} + \Delta P_{form} \tag{2.8}$$

2.6.1 Gravity Term

The gravity term in the momentum equation is the driving force in natural circulation flow, shown in Equation (2.9). The difference between the average densities within the gap and outside of the gap provides this driving force.

$$\Delta P_{gravity} = \left(\rho_{cavity} - \rho_{channel}\right) \cdot g \cdot h \tag{2.9}$$

where: ρ_{cavity} = density of liquid inside of the cavity but outside of the channel, $\rho_{channel}$ = average height-weighted density of the two-phase mixture inside of the channel, g = acceleration due to gravity, h = height of channel

2.6.2 Acceleration Term

The acceleration term is determined by summing the incremental pressure losses due to acceleration within the gap:

$$\Delta P_{acceleration} = \sum_{gap} \frac{1}{\overline{A}} \left[\dot{m}^2 \left(\frac{1}{\rho^+_{m,o} \cdot A_o} - \frac{1}{\rho^+_{m,i} \cdot A_i} \right) \right]$$
$$\overline{A} = 0.5 \cdot \left(A_o + A_i\right), \frac{1}{\rho^+_m} = \frac{x^2}{\alpha \cdot \rho_g} + \frac{(1-x)^2}{(1-\alpha) \cdot \rho_f} \tag{2.10}$$

where: $\overline{A}$ = average area of incremental inlet and incremental outlet, A_i = area at the incremental inlet, A_o = area at the incremental outlet, $\rho^+_{m,o}$ = mixture density at the incremental outlet, $\rho^+_{m,i}$ = mixture density at the incremental inlet, x = coolant flow quality, ρ_g = density of vapor coolant, ρ_f = density of liquid coolant, α = void fraction of coolant

2.6.3 Friction Term

Similarly, the pressure loss due to the friction term is determined by summing the incremental friction losses within the gap, shown in Equation (2.11). The flow is assumed to be turbulent throughout the gap. This assumption is verified upon the determination of the mass flow rate and the subsequent calculation of the Reynolds Number.

$$\Delta P_{friction} = \sum_{gap} \frac{0.184 \cdot l \cdot G^2}{2 \cdot \mathrm{Re}^{0.2} \cdot D_H \cdot \rho_f} \cdot \Phi^2 \tag{2.11}$$

where: ρ_f = density of liquid coolant, G = mass flux, Re = Reynolds's Number of coolant, l = characteristic length = average length of incremental volume, D_H = hydraulic diameter of gap = $D_{exterior} - D_{interior}$, Φ^2 = two-phase friction multiplier

Because the flow is two-phase in some regions of the gap, the two-phase friction multiplier is included, shown in Equation (2.12) [3].

$$\Phi^2 = A_1 + \frac{3.24 \cdot A_2 \cdot A_3}{Fr^{0.045} \cdot We^{0.035}}$$

$$A_1 = (1-x)^2 + x^2 \cdot \left(\frac{\rho_f}{\rho_g}\right) \cdot \left(\frac{\mu_g}{\mu_f}\right)^{0.2}, A_2 = x^{0.78} \cdot (1-x)^{0.224}$$

$$A_3 = \left(\frac{\rho_f}{\rho_g}\right)^{0.91} \left(\frac{\mu_g}{\mu_f}\right)^{0.19} \left(1 - \frac{\mu_g}{\mu_f}\right) \tag{2.12}$$

$$We = \frac{G^2 \cdot D_H}{0.0589 \cdot \overline{\rho}}, Fr = \frac{G^2}{g \cdot D_H \cdot \overline{\rho}^2}, \overline{\rho} = \left(\frac{x}{\rho_g} + \left(1 - \frac{x}{\rho_f}\right)\right)^{-1}$$

where: Fr = Froude Number, We = Weber Number, μ_f = dynamic viscosity of liquid coolant, μ_g = dynamic viscosity of vapor coolant, $\overline{\rho}$ = average density of coolant

2.6.4 Form Term

The form term is given by Equation (2.13). It is based on the form pressure losses of the gap inlet structure and the gap outlet, which occurs as the two-phase mixture turns and exits the rising portion of the gap through four rectangular vents. Here the value of k_{inlet} is set equal to 0.5.

$$\Delta P_{form} = \frac{k_{inlet} \cdot \dot{m}^2}{2 \cdot \rho_{l,inlet} \cdot A_{inlet}^2} + \frac{k_{exit} \cdot \dot{m}^2}{2 \cdot \rho_{l,exit} \cdot A_{exit}^2} \cdot \Phi^2 \tag{2.13}$$

where: A_{inlet} = inlet area, A_{exit} = vent (exit) area, k_{exit} = form factor of vent (exit), $\rho_{l,inlet}$ = liquid density at the inlet, $\rho_{l,exit}$ = liquid density at the exit

Because the value of the form factor at the exit is difficult to determine theoretically, it is determined indirectly by using the experimental value of the mass flow rate and solving the momentum equation for the form factor at the exit.

2.7 CHF Correlation

An appropriate CHF correlation for this application, which accounts for surface orientation effects, is the SULTAN correlation [5], shown in Equation (2.14). This correlation is based on experimental results obtained from a hemispherical geometry similar to this model's geometry.

$$q''_{CHF} = A_0(s,P,G) + A_1(s,G)\cdot x_e + A_2(s)\cdot x_e^2 + A_3(s,P,G,x_e)\cdot\Theta + A_4(s,P,G,x_e)\cdot\Theta^2$$

$$A_0 = b_0 + b_1\cdot s\cdot\ln(G) + b_2/P^2 + b_3\cdot G + b_4\cdot s/P + b_5\cdot s/P^2 + b_6\cdot P\cdot(\ln(G))^2$$

$$A_1 = b_7(\ln(G))^2 + b_8 s\ln(G), A_2 = b_9 s,$$

$$A_3 = b_{10}\cdot(\ln(G))^2 + b_{11}\cdot s\cdot P + b_{12}\cdot x_e\cdot\ln(G), A_4 = b_{13}\cdot P + b_{14}\cdot\ln(G) + b_{15}\cdot x_e + b_{16}\cdot s$$

$$b_0 = 0.65444, b_1 = -1.2018, b_2 = -0.008388, b_3 = 0.000179, b_4 = 1.36899, \quad (2.14)$$

$$b_5 = -0.077415, b_6 = 0.024967, b_7 = -0.086511, b_8 = -4.49425, b_9 = 9.28489,$$

$$b_{10} = -0.0066169, b_{11} = 11.62546, b_{12} = 0.855759, b_{13} = -1.74177,$$

$$b_{14} = 0.182895, b_{15} = -1.8898, b_{16} = 2.2636$$

where: P = coolant pressure in [MPa], s = channel gap size in [m], G = mass flux in [kg/m^2·s], Θ = angle from horizontal [rad], q''_{CHF} = critical heat flux in [MW/m^2]

Figure 3 shows the relationship between CHF, x_e, and θ for G = 500 kg/m^2·s and Figure 4 shows the same relationship for G = 3000 kg/m^2·s. The figures show that CHF increases with increasing angle and with increasing mass flux, but decreases with increasing equilibrium quality. It should also be noted that although the correlation does give non-physical negative values for CHF is some instances, the flow parameter range in this model always results in positive values for CHF. For example, the equilibrium quality is smallest at small angles and the mass flux is smallest at large angles.

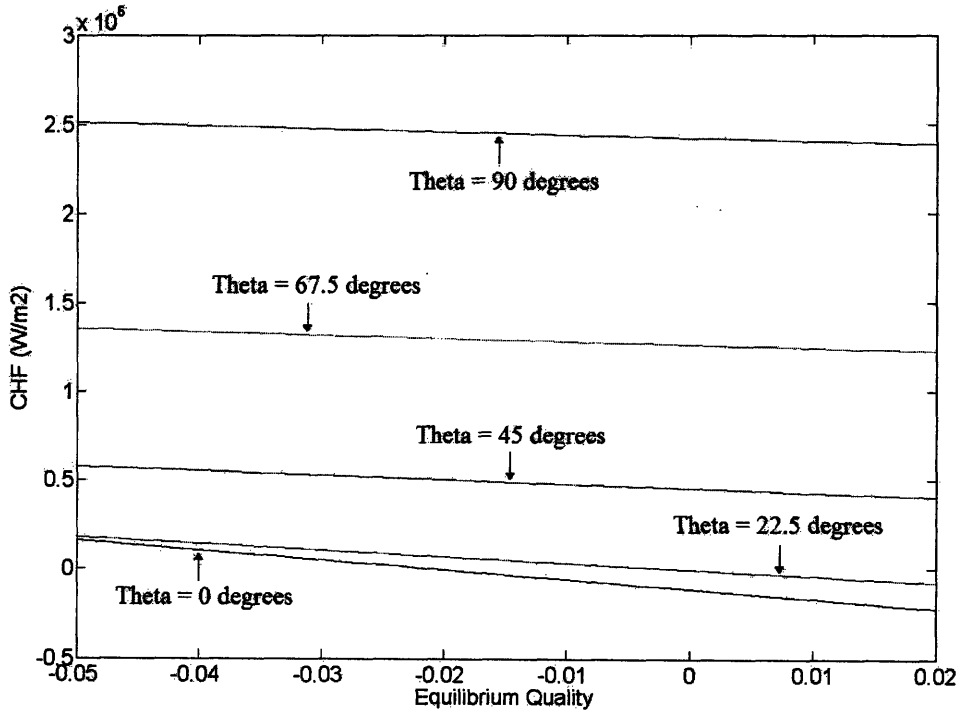

Figure 3: CHF versus Equilibrium Quality (G = 500 kg/m^2·s, P = 0.1 MPa)

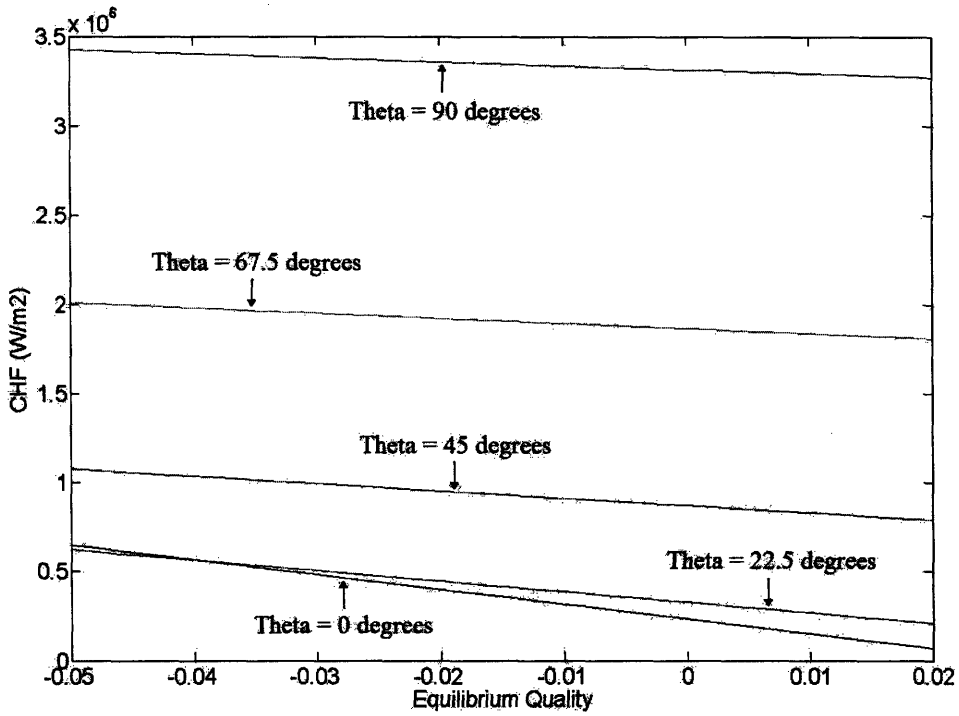

Figure 4: CHF versus Equilibrium Quality (G = 3000 kg/m^2·s, P = 0.1 MPa)

2.7.1 Effect of Nanofluids on CHF

Because CHF data for nanofluids at prototypical IVR conditions are lacking, in order to account for the effect that a nanofluid has on CHF, a multiplier that accounts for the increased CHF compared to water is used. This multiplier is dependant on orientation.

This model assumes that the CHF of a nanofluid is related to the CHF of water as described in [6]. The CHF for a nanofluid is expressed as a multiplier to the CHF of water and accounts for the orientation effects of nanofluid boiling. This relationship is illustrated in Figure 5.

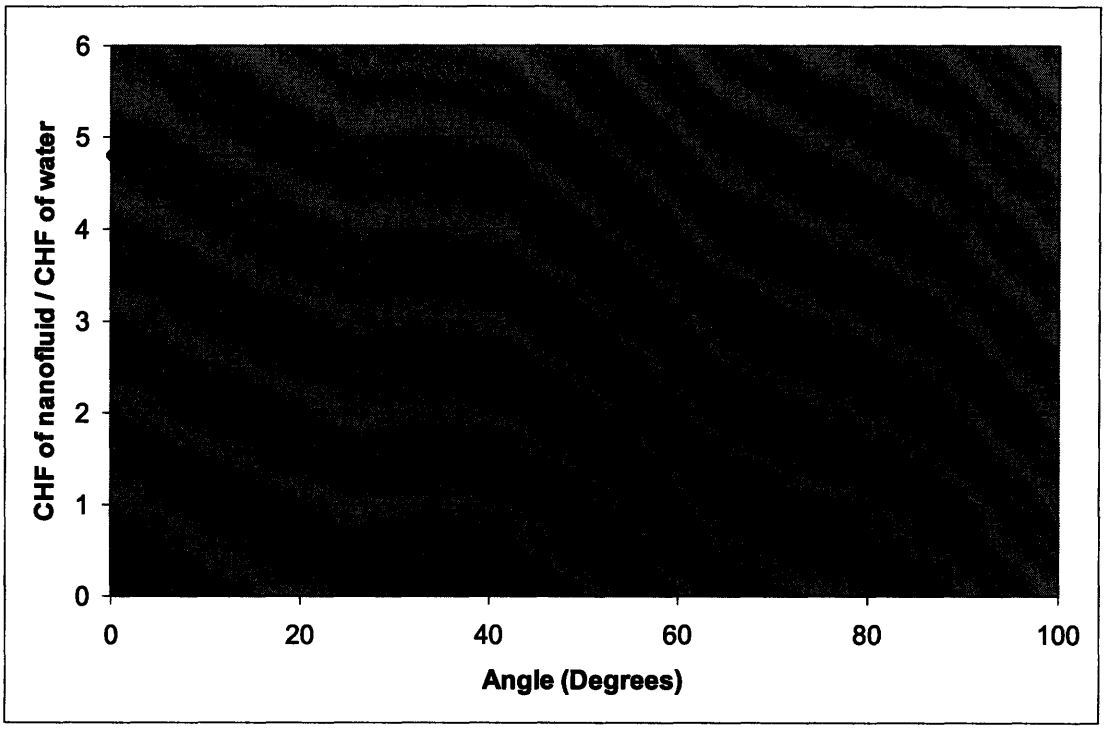

Figure 5: Nanofluid CHF Multiplier Angular Dependence

As in Figure 2, an angle of 0° corresponds to the bottom of the reactor vessel where the surface is downward-facing and horizontal, while an angle of 90° corresponds to the side of the reactor vessel where the surface is outward-facing and vertical.

Experimental results at the Massachusetts Institute of Technology (MIT) [2] found that a 0.001% by volume alumina nanofluid enhances CHF by a factor of approximately 1.4 compared to the pure water case. Combining the angular dependence in Figure 5 with the MIT experimental results by shifting the curve downwards, the nanofluid CHF multiplier used in the model is found (shown in Figure 6). The model assumes that when using a nanofluid as the coolant, the nanofluid will be uniformly mixed and behave according to the relationship shown in Figure 6.

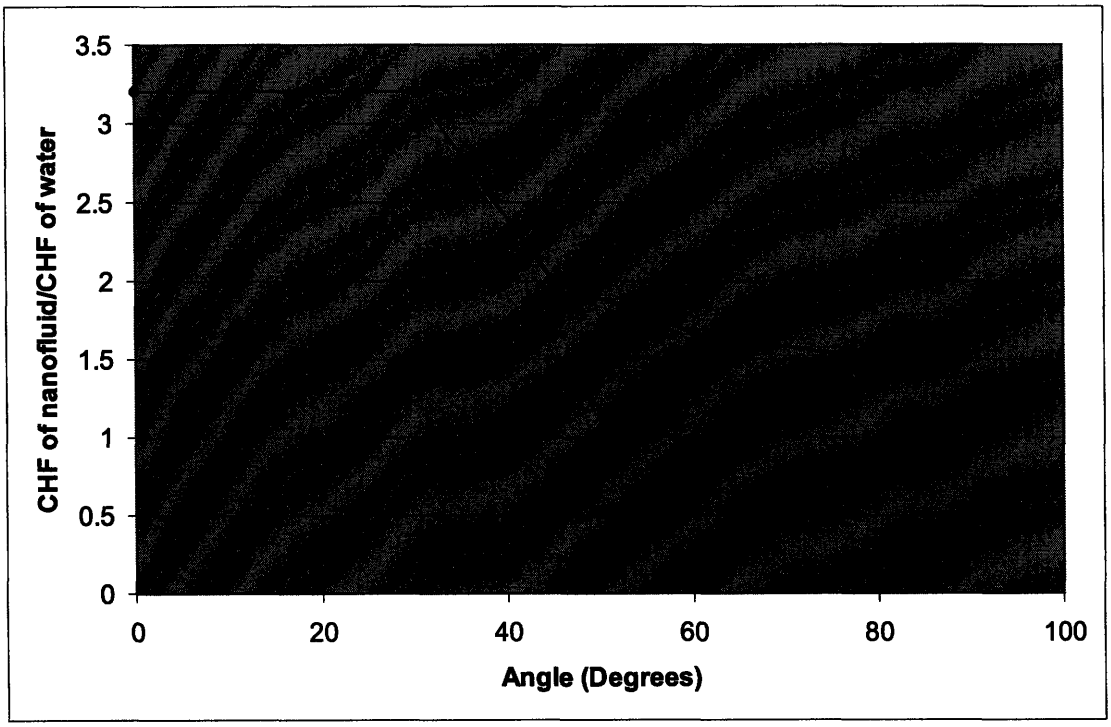

Figure 6: Nanofluid CHF Multiplier Used in Model

3. MODEL RESULTS AND DISCUSSION

Various relationships between the flow parameters produced by the model were compared to expected trends and experimental results in order to ensure that the model was reasonably accurate. All of the following graphs used the T48A heat flux profile shown in Figure 1 as the heat flux input into the model.

3.1 Graphs of Void Fraction and Quality

Figure 7 and Figure 8 illustrate void fraction versus height and quality versus height, respectively. Height refers to the vertical distance above the bottom of the reactor vessel lower head.

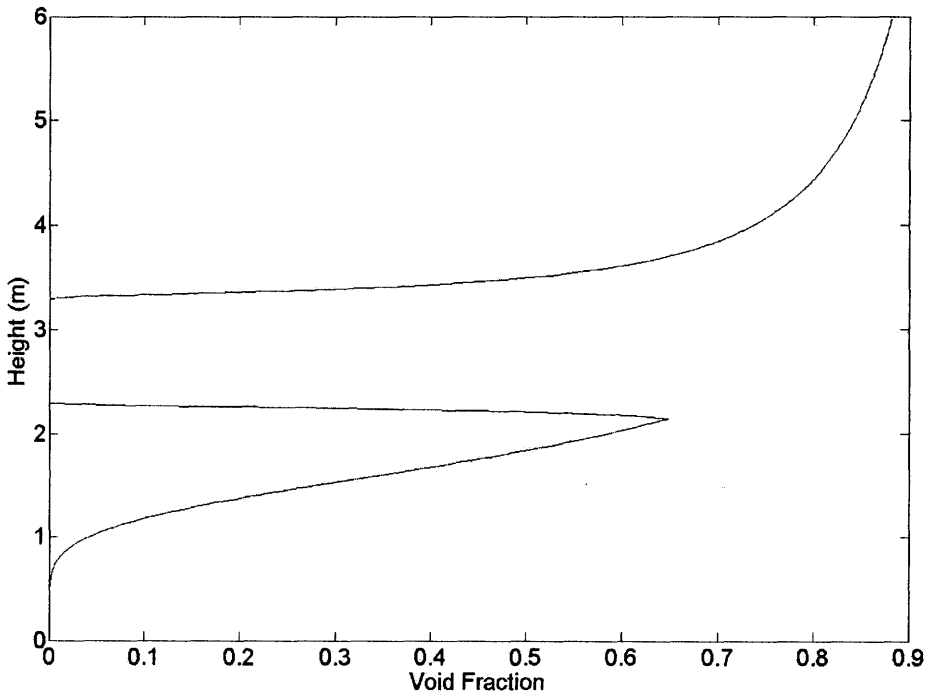

Figure 7: Void Fraction versus Height

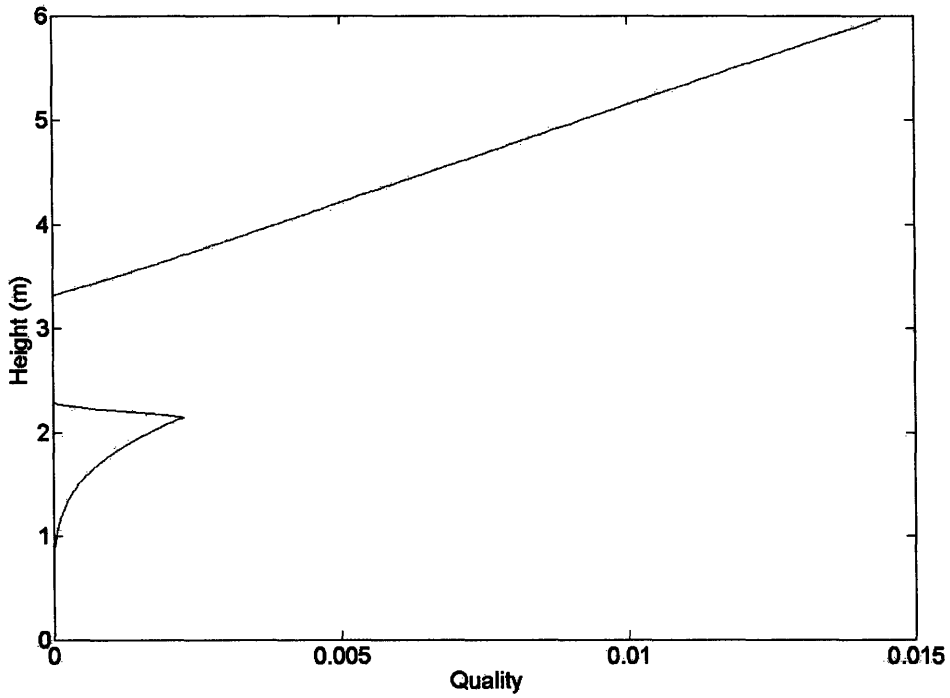

Figure 8: Quality versus Height

At a height of 2.1 m the heat flux goes to zero in the T48A heat flux profile. At this point the two-phase mixture is subcooled. The UCSB Report observed that the voids quickly collapsed [1]. In order to calibrate this model to these observations, the voids were forced to collapse under subcooled conditions as discussed in Section 2.4.2. Eventually as the pressure decreases with the increasing height, the fluid becomes saturated and the void fraction and quality increase due to flashing. These trends shown in Figures 7 and 8 are consistent with the experimental results documented in the UCSB Report.

3.2 Calculation of Exit Form Loss Factor

By inputting the three heat flux profiles in Figure 1 with their experimentally determined mass flow rates, one can determine a value for k_{exit}. A least-squared fit analysis of the values of k_{exit} associated with the different heat flux profiles gives a $k_{exit} = 1.35$. Table II shows that using this value of k_{exit}, the mass flow rates given by the model are within 2% of the experimental mass flow rates in all three cases.

Table II: Comparison of Mass Flow Rates at $k_{exit} = 1.35$

Heat Flux Profile	Power (MW)	UCSB Mass Flow Rate (kg/s)	Model Mass Flow Rate (kg/s)	Percentage Difference (%)
T48A	18.9	860	860	0.0
T40B	18.6	858.7	868	+1.1
T40D	10.3	785.3	769.5	-2.0

3.3 Graphs of CHF and DNBR

Figure 9 and Figure 10 illustrate the height dependence of CHF and DNBR for water and nanofluid, respectively. Note that the blip in the CHF graph at a height of 0.3 m is an effect of the geometry. The flow area is rapidly increasing from the inlet to the baffle, which strongly reduces the mass flux and CHF. However, the CHF starts to rise again because of the effect of the surface orientation. The notable feature of Figure 10 is that the worst-case (lowest) value of DNBR occurs very near the top of the heated section, which is consistent with experimental observations in the UCSB Report.

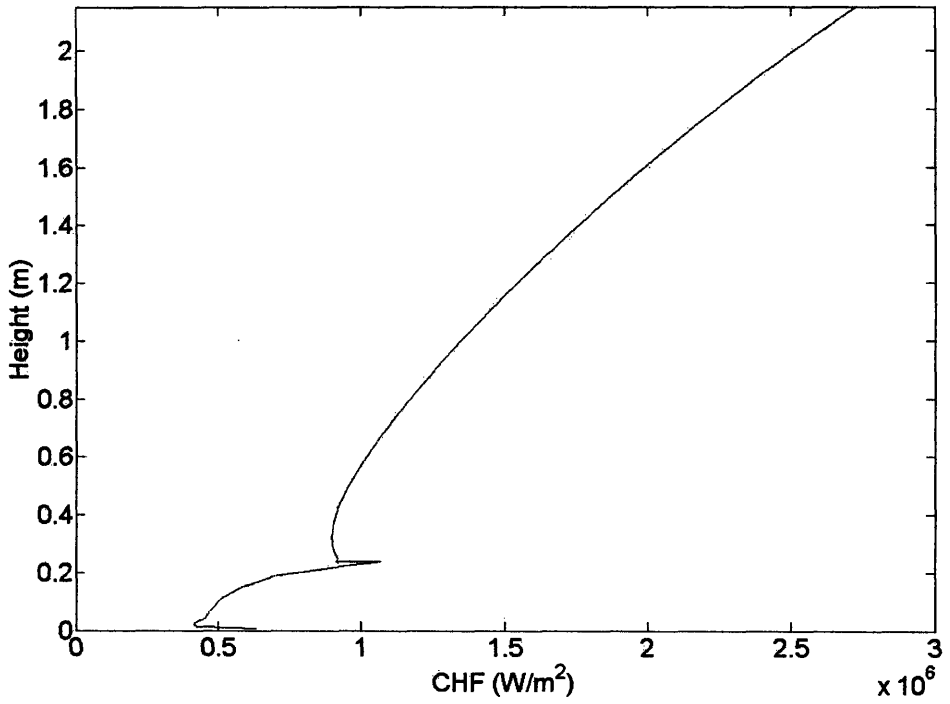

Figure 9: CHF versus Height

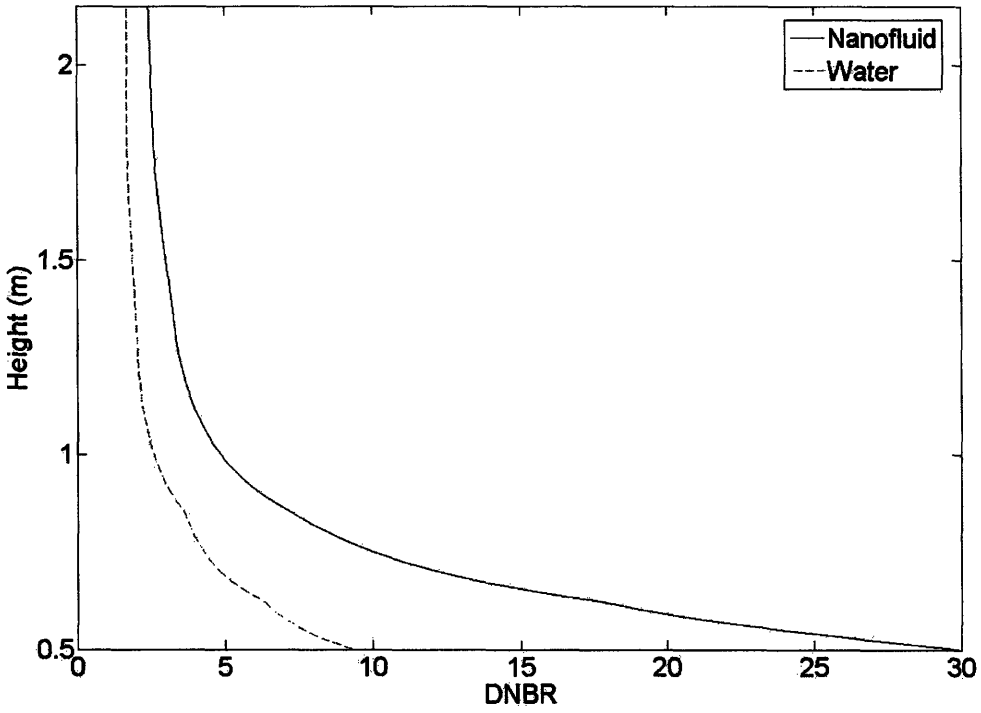

Figure 10: DNBR versus Height

3.4 DNBR at Increased Residual Power

The model can be used to determine the increase in residual power that a nanofluid can accommodate over water at the same safety margin (MDNBR). This is done by equating the MDNBR of pure water at the original residual power to the MDNBR of a nanofluid at an increased residual power. Figure 11 shows the model's predictions of the maximum power that can be achieved with a nanofluid as well as the corresponding mass flow rates.

Note that the mass flow rate versus power curve has a peak at around 30 MW. This trend is expected in a natural circulation system and is due to the competing effects of increasing gravity head (via the change in two-phase density) and hydraulic resistance (via the increase in two-phase multiplier), as the thermal power increases. A mathematical explanation of the peak is presented in Appendix A.1.

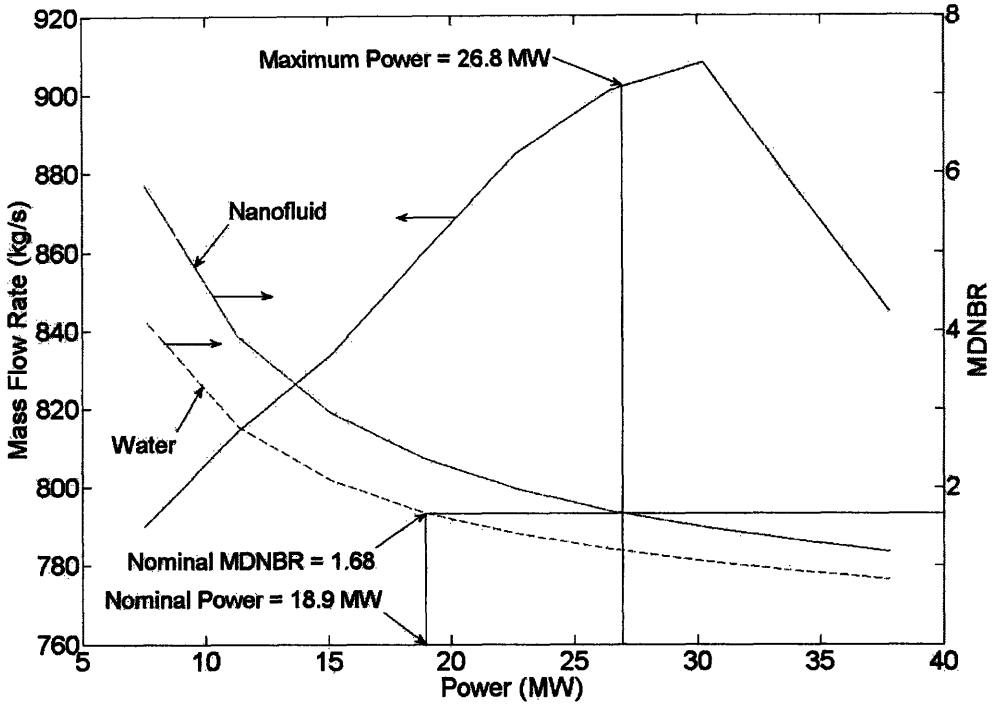

Figure 11: Operating Conditions versus Power

The maximum power achievable with nanofluids would appear to be 26.8 MW, or 142% of the power achieved using water at the same MDNBR value.

3.5 Effect of Flow Stability

At the higher power levels and corresponding mass flow rates, the stability of the system must be checked as large flow oscillations could cause premature CHF. There are three types of flow instabilities: (1) flow excursion oscillation (static), (2) density-wave oscillation (dynamic), and (3) pressure-drop (dynamic).

3.5.1 Flow Excursion Oscillation Instabilities

In non-dimensional terms, flow excursion instability in natural circulation flows occurs in the region in which $0.7<N_p/N_s<3.0$, where N_p is the phase change (Zuber) number and N_s is the subcooling number [7], defined in Equation (3.1). This system enters the region of instability at 32 MW as shown in Figure 12.

$$N_p = \frac{Q_0 \rho_f}{AGh_{fg}\rho_g}, N_s = \frac{\Delta h \rho_f}{h_{fg}\rho_g} \tag{3.1}$$

where: Q_0 = maximum power, Δh = subcooled enthalpy

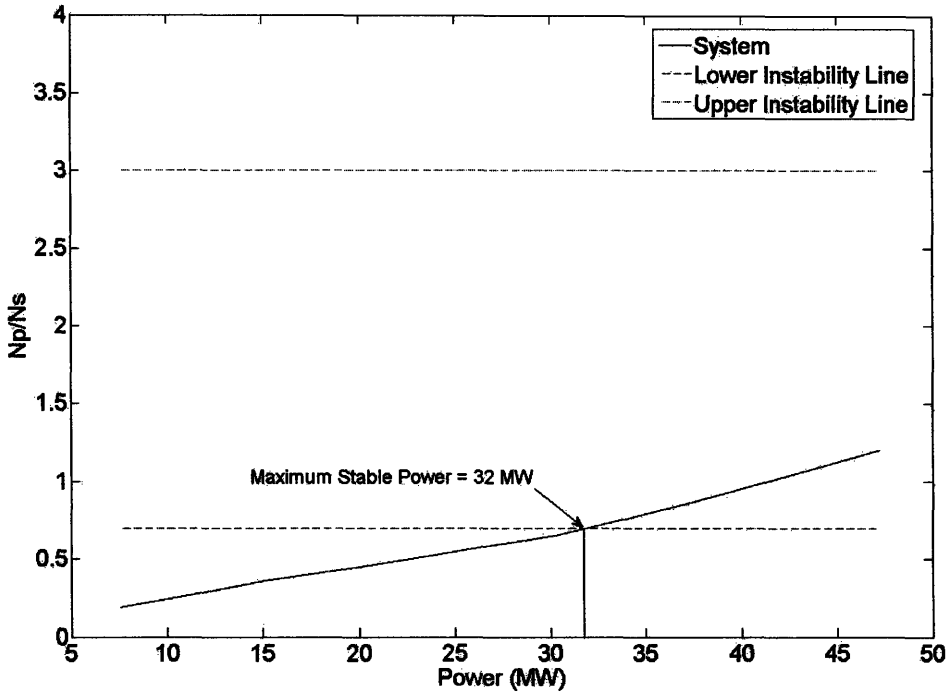

Figure 12: System Stability

3.5.2 Density-wave Oscillation Instabilities

Density-wave oscillation instabilities are investigated using the Saha, Ishii, and Zuber stability criterion [8]. For high subcooling numbers (N_s>3), a system is stable against density-wave oscillation instabilities when the inequality given in Equation (3.2) is satisfied.

$$N_s > N_p - \frac{2 \cdot \left(k_{inlet} + \frac{f_{tp} \cdot L}{2 \cdot D_H} + k_{exit} \right)}{1 + 0.5 \cdot \left(\frac{f_{tp} \cdot L}{2 \cdot D_H} + 2 \cdot k_{exit} \right)} \tag{3.2}$$

where: f_{tp} = two-phase friction factor, L = length of channel

Table III shows the system values for Equation (3.2) at various power levels.

Table III: Density-wave Oscillation Stability

Power	N_p	N_s	Right Hand Side of Inequality	Stability
7.6	6.8	36.1	5.2	Stable
11.3	9.8	36.1	8.1	Stable
15.1	12.7	36.1	11.0	Stable
18.9	15.4	36.1	13.6	Stable
22.7	18.0	36.1	16.2	Stable
26.5	20.6	36.1	18.7	Stable
30.3	23.6	36.1	21.7	Stable
34.0	27.3	36.1	25.4	Stable
37.8	31.4	36.1	29.4	Stable
39.7	33.5	36.1	31.5	Stable
47.3	42.7	36.1	40.7	Unstable

The system is stable against density-wave oscillation instabilities up to at least a power of 39.7 MW.

3.5.3 Dynamic Pressure-drop Instabilities

The necessary condition for this type of instability is that the pressure loss versus mass flow rate curve have a slope reversal around the equilibrium mass flow rate point [9]. Figure 13 illustrates that the slope does not reverse around any of the equilibrium mass flow rate points associated with power levels up to 34 MW.

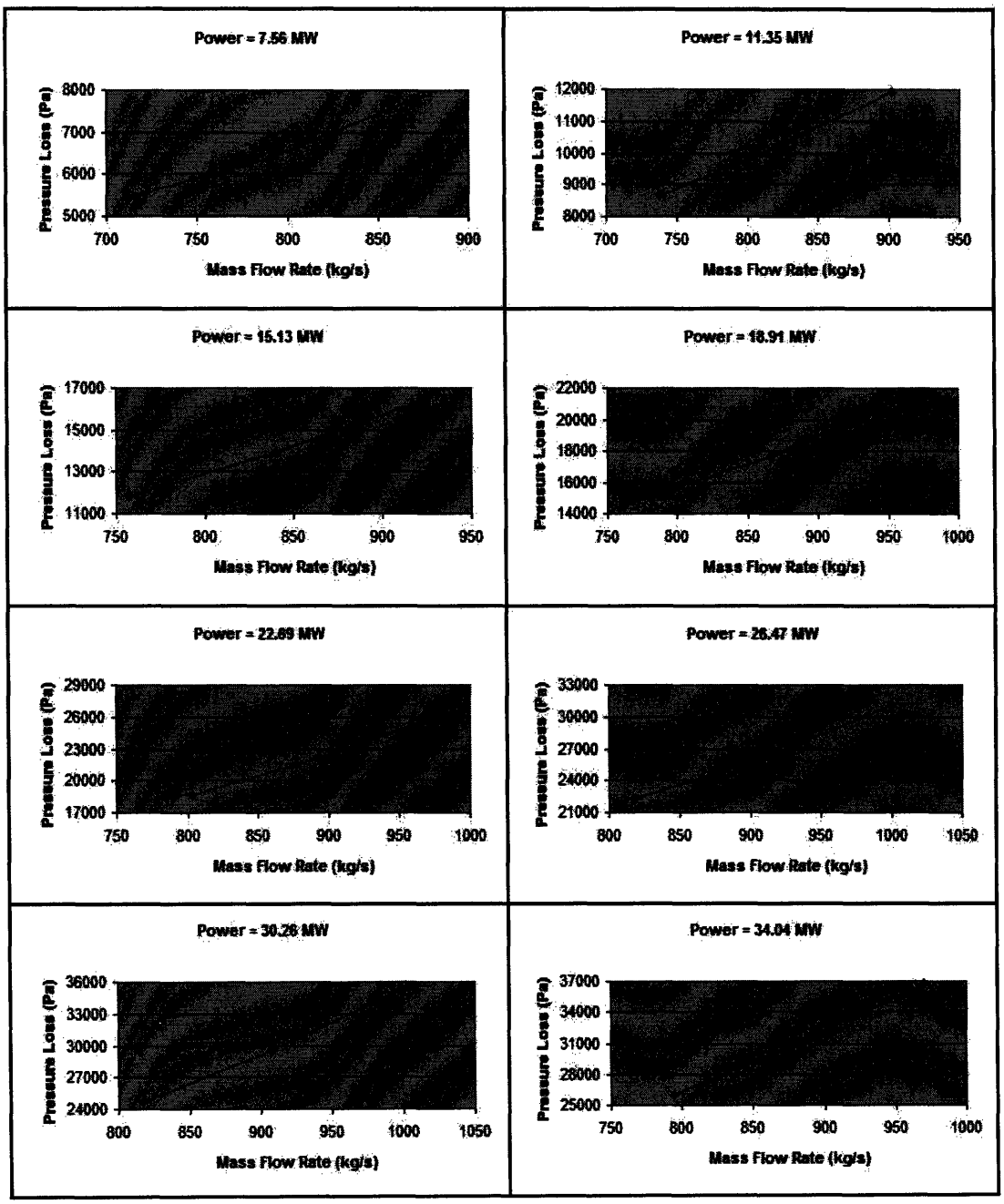

Figure 13: Pressure Loss versus Mass Flow Rate Curves at Varying Power Levels

3.5.4 Operating Range of the System

Flow excursion oscillation instabilities are the most limiting type of instability in this system. Figure 14 integrates Figure 11 and Figure 12 and shows the operating range of the system, including the maximum stable power and the associated mass flow rate. In this case, the operating power is limited by MDNBR not by stability.

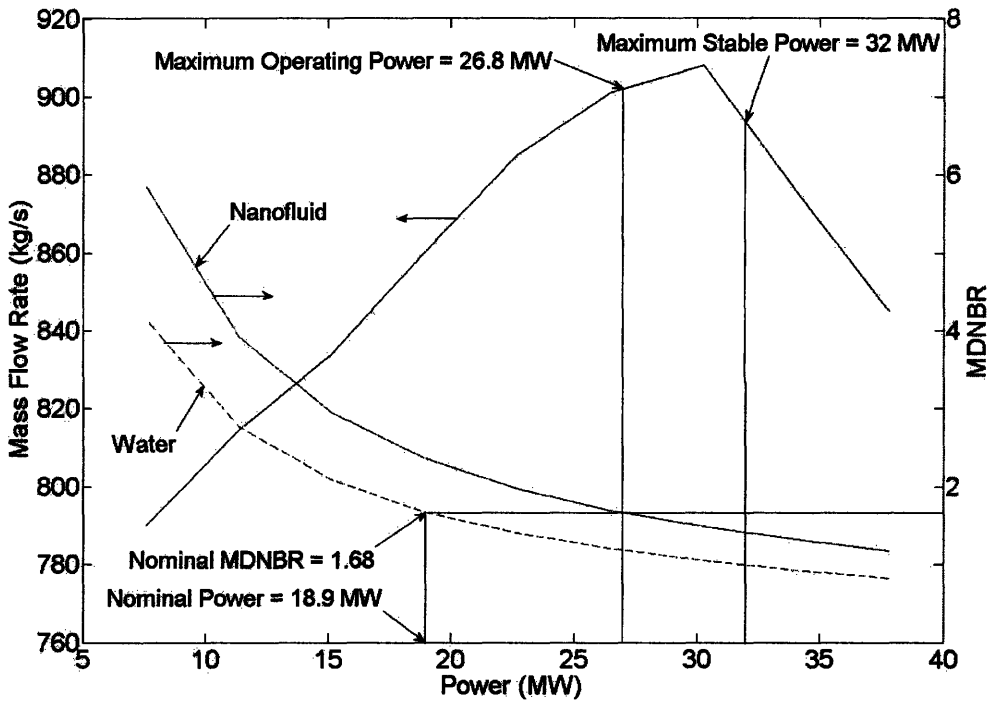

Figure 14: Operating Range of the System

3.6 Sensitivity Analysis on the Nanofluid CHF Multiplier

In order to see the sensitivity of the model results to the CHF nanofluid multiplier, a set of three multipliers were used as shown in Figure 15.

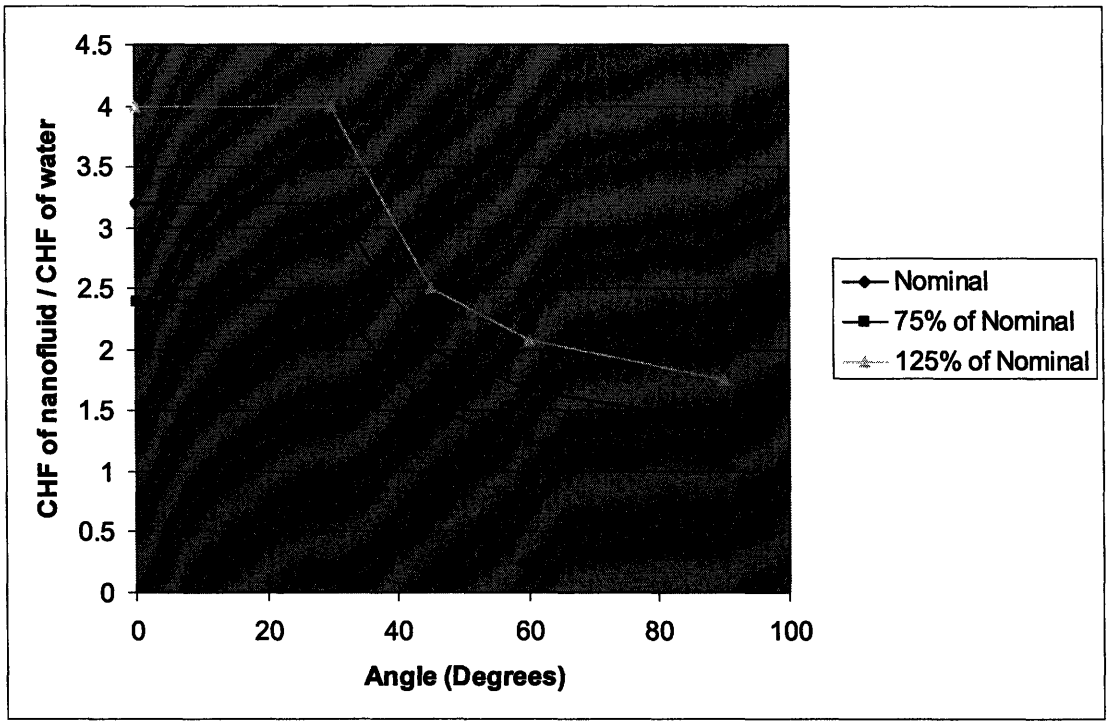

Figure 15: Set of Nanofluid CHF Multipliers used in Model

Figure 16 shows the impact of the nanofluid CHF multiplier on the maximum residual power that can be removed while keeping the MDNBR equal to that of water at nominal power (18.9 MW). Note that even assuming a nanofluid CHF multiplier that is 75% of the nominal multiplier shown experimentally, the power is still slightly higher than the 18.9 MW in the case of water (20 MW versus 18.9 MW). One can see that the effect of the CHF Nanofluid Multiplier varies roughly linearly with power: varying the CHF Nanofluid Multiplier by 25% in either direction roughly corresponds to a 25% change in power. Using Figure 15 one can also see that a power of 32 MW corresponds to 120% of the nominal nanofluid CHF multiplier. One will not be limited by stability unless the CHF nanofluid multiplier that is achieved is greater than 120% of nominal.

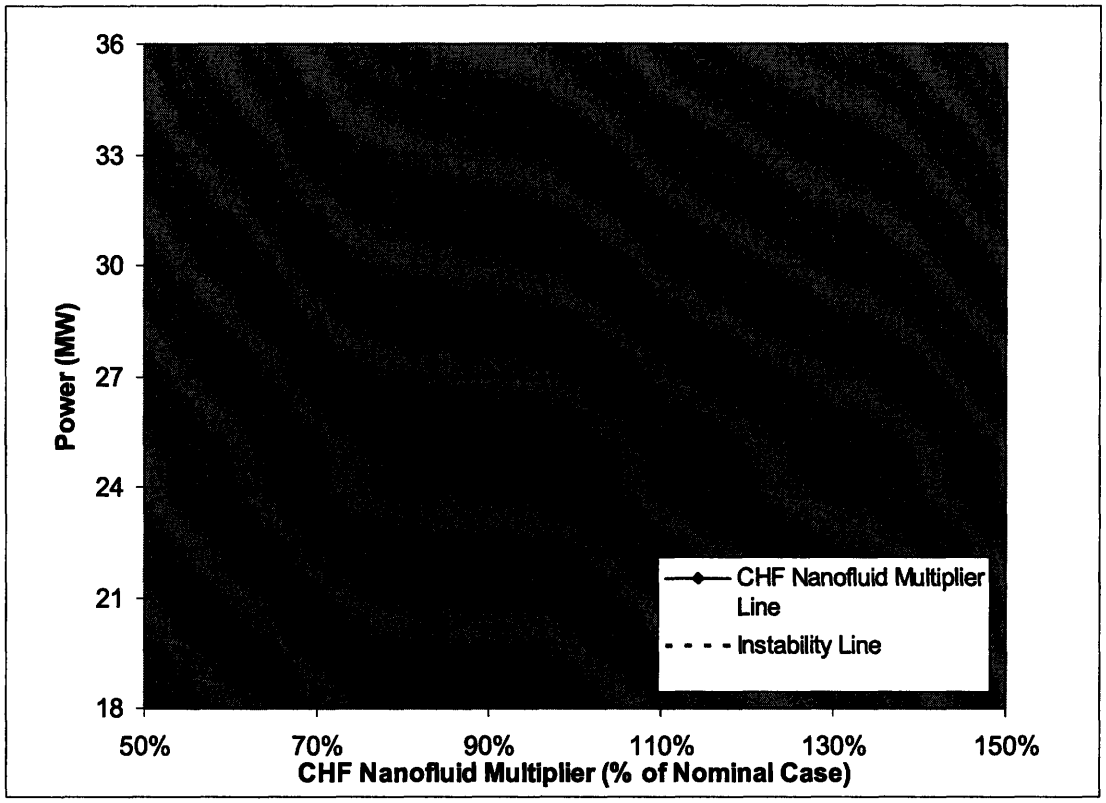

Figure 16: Sensitivity of Power to CHF Nanofluid Multiplier

The effect of varying the nanofluid CHF multiplier on the operating range of the system is shown in Figure 17. One can see that in the 125% case, the maximum stable operating power is limited by stability, while in the 100% and 75% cases the maximum stable operating power is limited by MDNBR.

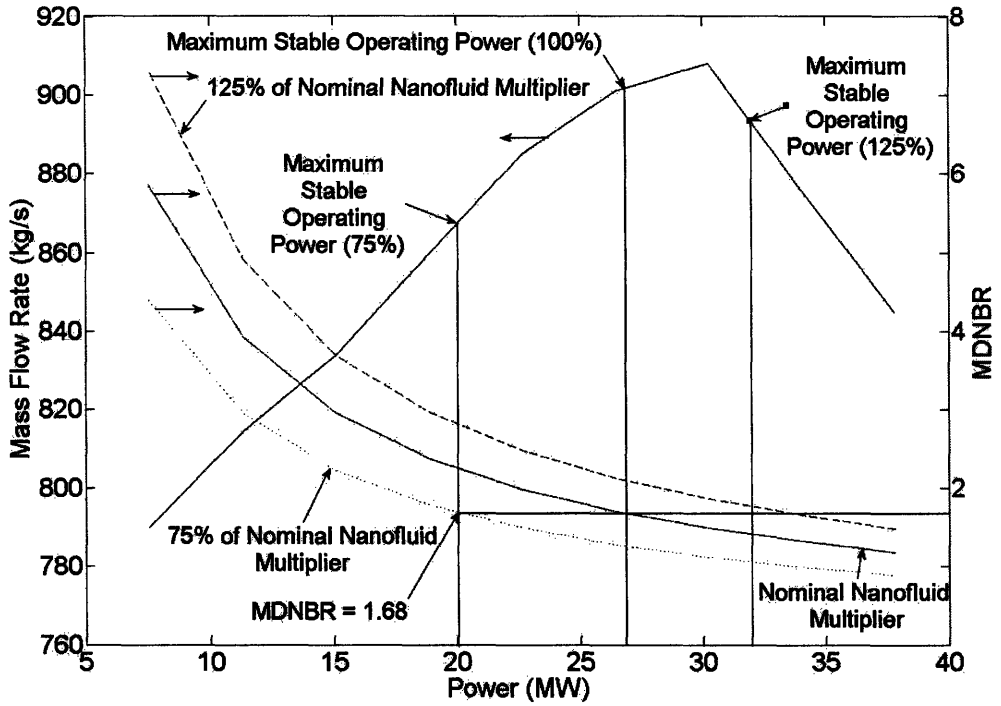

Figure 17: Effect of a Varying Nanofluid CHF Multiplier on Operating Range

3.7 Summary of the Model

Using energy and momentum balances, this model of the two-dimensional flow and heat transfer along the reactor vessel outer surface was created. It simulates the conditions of a severe accident in which the core melts and relocates to the bottom of the reactor vessel and shows that under those conditions the use of a nanofluid is more effective than water in an IVR strategy. This model fits the experimental results conducted with water reasonably well.

This model shows that the increase in residual power that a nanofluid provides and the nanofluid CHF multiplier are related roughly linearly, keeping the worst-case DNBR constant. This model predicts that using a nanofluid, a stable operating power that is 142% of water can be achieved.

Finding #1: Using a nanofluid as the coolant in IVR could allow a ~40% increase in the power compared to using water as a coolant, while maintaining the same safety margin.

4. CONCEPTUAL NANOFLUID INJECTION SYSTEM DESIGN

The results of the thermal hydraulic model presented in Chapters 2 and 3 show that nanofluids would be able to increase the DNBR margin in the IVR severe accident mitigation strategy. In order for this enhancement to be achieved at an actual nuclear power plant, a system must be designed that is able to deliver the nanofluid to the reactor cavity if the core melts and relocates during a severe accident. This system must also be integrated into the overall design of the power plant. This chapter of the report investigates these design requirements and proposes a conceptual nanofluid injection design for the Westinghouse AP1000 nuclear reactor, which is taken as a representative of ALWRs that employ an IVR strategy.

4.1 General Design Considerations

The most general considerations in the design of a nanofluid injection system are: (1) integration with the current reactor design and (2) quality control of the nanofluid before injection. The nanofluid injection system should interface with the current reactor design in a manner that does not interfere with the other functions of the reactor safety, control, and auxiliary systems. Because the nanofluid is only effective at enhancing CHF when it is a stable colloidal suspension, the system must be designed such that the quality of the nanofluid can be controlled effectively. In order to address these general considerations the current reactor design and procedures must be investigated.

4.1.1 Current IVR Strategy and Coolant Quality Control Procedures

The IVR severe accident mitigation strategy has the ultimate goal of preventing the molten core from breaching the reactor vessel. More specifically, upon the melting of the core and its relocation to the bottom of the reactor vessel, the core melt is contained by cooling the outer surface of the reactor vessel thus preventing the vessel from melting or even softening. The outer surface of the vessel is cooled passively by the natural circulation of the water in the reactor cavity after it has been flooded. Figure 18 and Figure 19 are views of the reactor vessel and cavity after flooding has occurred.

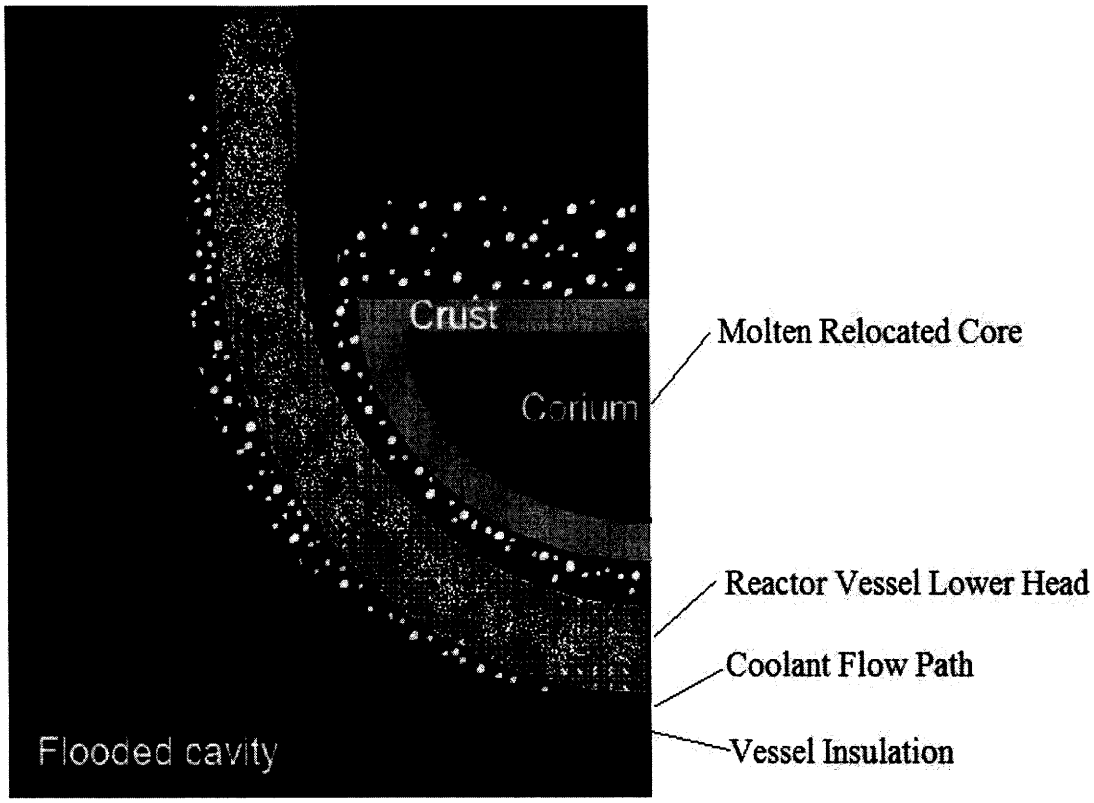

Figure 18: Detailed View of Reactor Cavity after Core Melt and Relocation[3]

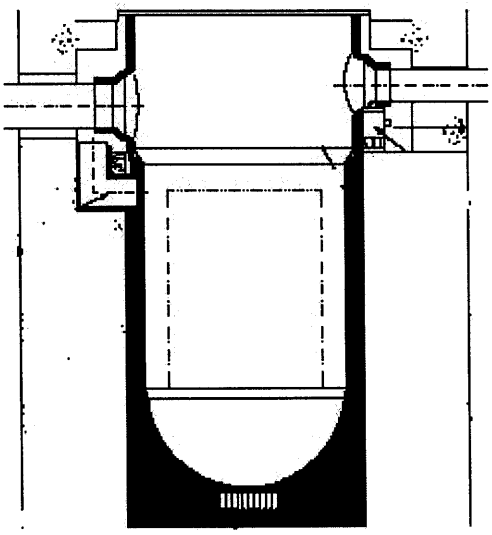

Figure 19: Overview of Flooded Reactor Cavity[4]

[3] Adapted from [10].
[4] Adapted from [11].

The critical factor in the current IVR strategy is ensuring that the cavity is flooded in sufficient time to prevent vessel breach. For an IVR strategy that uses a nanofluid, the cavity must be flooded with the nanofluid in sufficient time. The water that floods the reactor cavity comes from the Reactor Coolant System (RCS) and the In-Containment Refueling Water Storage Tank (IRWST). Under normal operation, the RCS removes heat from the reactor core which is eventually used for power generation. The RCS consists of two steam generators, four reactor coolant pumps, and one pressurizer [12]. The IRWST is a large tank inside the containment that provides water for refueling and for core emergency cooling after the RCS is depressurized [13]. Successful depressurization of the RCS is assumed for successful IVR implementation; therefore, the AP1000 PRA assumes that the reactor cavity is full of water from the RCS up to at least the 83' (25.3 m) elevation [12]. The remainder of the cavity is flooded either through the progression of the accident or through the operator action to manually drain the IRWST water into the containment through the IRWST recirculation lines [13]. Sufficient cavity flooding for IVR is defined as flooding up to the 98' (29.9 m) elevation. The floodable region of the containment extends up to the 107' 2" (32.7 m) elevation [13], which is the level that this analysis assumes the cavity eventually floods up to.

The quality of the coolant in the RCS and the IRWST is important because although the coolant is mainly water, the water notably contains boric acid (for long-term reactivity control) and lithium hydroxide (for pH control) [12]. The concentration of boric acid ranges from 2500 to 3000 ppm in the containment water [14]. The IRWST and RCS are sampled periodically to ensure proper chemistry [12]. In addition, the containment contains trisodium phosphate (in concentrations ranging from 3500 to 6000 ppm [14]) in order to maintain a pH between 7.0 and 9.5 after the cavity is flooded [12]. This pH range helps to retain the fission product particulates in the water, which in turn reduces the source term for radioactivity release into the environment if a core meltdown and containment breach were to occur.

4.1.2 Initial Design Options

Based on the current reactor design in the AP1000, the nanofluid must either replace water as the coolant in the IRWST and the RCS or nanoparticles must be mixed with the water to create a nanofluid in the event of a severe accident. Because the IRWST and RCS have a myriad of other functions not associated with IVR, having nanofluid in these systems at all times could potentially lead to problems with these functions. One of the potentially problematic issues with integration is maintaining the quality of the nanofluid in the presence of the other chemicals in these systems. Long-term interactions with the chemical environments in the RCS and IRWST as well as the agitation the nanofluid would undergo as part of these systems could lead to agglomeration of the nanoparticles in the nanofluid, resulting in a reduction in the desired CHF enhancement. In addition if agglomeration occurs, an additional system that mixes in nanofluids to maintain the proper nanoparticle concentration would be required. Because of these complications, the option to mix nanoparticles with the water from the RCS and IRWST in the event of a severe accident is more attractive.

Because only a very small amount of nanoparticles needs to be mixed into a base fluid to see the desired CHF enhancement, it is possible to store concentrated nanofluid in relatively small tanks.[5] This concentrated nanofluid can be mixed with the water from the IRWST and RCS to produce a large amount of nanofluid with an overall (low) concentration that corresponds to the desired CHF enhancement. By storing the nanofluid in separate storage tanks, it is easier to maintain the quality of the nanofluid and simpler to integrate the injection system with the rest of the safety systems.

4.1.2.1 Nanofluid Selection

A nanofluid must be properly selected in order to ensure that it remains stable during storage and after injection. Many nanofluids with oxide-based nanoparticles are stable for concentrations up to 20% by weight when their pH is adjusted to create like electric charges on the nanoparticle surface. For example, nanofluids made using alumina nanoparticles are stable when an acid is added to reduce the pH to around 4. If this concentrated nanofluid is injected into the flooded reactor cavity as envisioned in this system, it will be diluted and the pH will increase, potentially resulting in agglomeration of the nanoparticles and thus an unstable nanofluid. Under the severe accident scenarios that employ IVR, good nanofluid stability is needed for less than a day,[6] as the additional heat removal capabilities of a stable nanofluid over water are needed only towards the beginning of the severe accident while the decay heat is high. In order to evaluate the effects of dilution on nanofluid stability, dilution experiments were conducted. This experiment consisted of diluting concentrated alumina nanofluid (similar to the concentration in the storage tanks) to lower concentrations (sufficient to see the desired CHF enhancement) and then measuring the sizes of the nanoparticles over time. Large increases in the size of the nanoparticles would indicate nanoparticle agglomeration and thus an unstable nanofluid. The summarized results given in Table IV show that the changes in the nanoparticle size are within the experimental uncertainty (± 20 nm) of the dynamic-light-scattering particle measurement device chosen for these measurements. These results indicate that upon dilution little agglomeration occurs and the nanofluid remains stable. The details of this experiment are included in section B.1 of Appendix B.

Table IV: Mean Alumina Nanoparticle Diameter after Dilution

Time after dilution (hr)	Concentration		
	20% (by weight)	0.01% (by volume)	0.001% (by volume)
0	37.8 nm	N/A	N/A
1	N/A	42.6 nm	52.3 nm
6	N/A	32.6 nm	33.4 nm
24	N/A	46.7 nm	46.7 nm

[5] Maintaining the quality of and delivering the nanoparticles is much simplified if they are in concentrated colloidal suspension form as opposed to powder form.
[6] This calculation is shown in section A.1 of the Appendix.

In addition to investigating the changes in the sizes of the particles, measuring changes in nanoparticle concentration can also be used to evaluate the effects of dilution on nanofluid stability. This experiment consisted of diluting concentrated alumina nanofluid to lower concentrations and then measuring the concentrations of the nanoparticles over time. Any decrease in the nanoparticle concentration would indicate nanoparticle agglomeration and thus an unstable nanofluid. Table V shows the percentage differences of the actual, measured concentrations compared to the predicted concentrations if all the nanoparticles were to remain in solution. These results also indicate that upon dilution little agglomeration occurs and the nanofluid remains stable. The details of this experiment are included in section B.2 of Appendix B.

Table V: Actual Nanoparticle Concentration Difference after Dilution

Time after dilution (hr)	Concentration		
	20% (by weight)	0.01% (by volume)	0.001% (by volume)
0	-3.9%	N/A	N/A
1	N/A	3.6%	-6.0%
6	N/A	1.9%	2.2%
24	N/A	13.9%	18.2%

These experiments indicate that alumina nanofluid may be a good candidate for use in this nanofluid injection system. Alumina nanofluid is manufactured by several companies, notably Nyacol Nano Technologies, Inc. Table VI includes manufacturer-specified properties of commercially sold alumina nanofluid [15].

Table VI: Alumina Nanofluid Properties

Composition	Aluminum Hydroxide Oxide (20-25% by weight), Nitric Acid (<1% by weight), Water (75-79% by weight)
pH	4
Density	1200 kg/m^3
Boiling Point	100° C
Freezing Point	0° C

Other factors that need to be considered before making a final selection of a nanofluid are: (1) the response of the nanofluid to the dose of radiation it would be exposed to during IVR and (2) the response of the nanofluid to the coolant chemistry of it would encounter in the reactor cavity. Preliminary results of experiments conducted at MIT suggest that alumina nanofluid manufactured by Nyacol Nano Technologies, Inc. is stable when exposed to doses of radiation it would encounter in IVR but unstable when combined with trisodium phosphate [16]. This is an area that will require further investigation.

4.1.2.2 Concentrated Nanofluid Storage Tank Specifications

The required volume of concentrated nanofluid and thus the required capacity of the storage tanks can be determined by the volume of the fluid that it takes to flood the reactor cavity. In the Westinghouse AP1000 the volume of the flooded reactor cavity is 2503 m^3 [17].[7] The sizing of the storage tanks is based on a alumina nanofluid with a base fluid of water because it is one of the most widely available, stable, and affordable nanofluids. The concentration that is needed to attain the desired CHF enhancement is 0.001% alumina by volume [2]. Given that the nanofluid needs to fill the entire flooded reactor cavity, a total of 25.03 L of alumina is required[8], which using a density of 3970 kg/m^3 for alumina [18] results in a required mass of 99.37 kg of alumina. A typical maximum concentration for alumina nanofluids is a loading of 20% alumina by mass.[9] At a 20% mass loading, conservatively assuming a density of water in the tank at saturated conditions and 2 atm, the minimum required volume of concentrated nanofluid is 447 L.[10]

The material that a nanofluid storage tank should be constructed of depends on the conditions that the tank will operate under and the chemical composition of the contents of the tank. The operating conditions for the tank are a temperature close to the normal containment temperature of 295 K (70° F) [13] and a pressure of slightly above atmospheric pressure (resulting in a pressure gradient no greater than 2.5 atm in all relevant accident scenarios [13]). Concentrated alumina nanofluid with a 20% mass loading has a pH of 4 and contains low concentrations of nitric acid [15]. Similar tanks in nuclear reactors typically are constructed of annealed Stainless Steel 316 [19]. Although annealed Stainless Steel has "broad applicability" to nitric acid service [20], Titanium Grade 2 is a better option as it "used in applications where in which stainless steels have experienced significant uniform or intergranular attack" as it has "excellent resistance over the full concentration range at subboiling temperatures" [20].

The tank is designed to deliver all of its contents to the reactor cavity; however, because a minimal amount of fluid will accumulate on the walls of the tank and the pipes, the design capacity of the tank should be slightly higher than the minimum volume that needs to be delivered. Therefore, the design capacity of a tank is ~500 L, which corresponds to a cylindrical tank with dimensions of ~100 cm (diameter) and ~64 cm (height). Given the operating conditions, the thickness of the tank would not need to exceed the standard tank thicknesses of 0.125 in for the shell and 0.1875 in for the head (0.32 cm for the shell and 0.48 cm for the head) [21]. Additionally, the tank would require an N-stamp certification to be part of a safety system in a nuclear power plant.

The tank specifications are summarized in Table VII.

---

[7] 5,200,000 lb saturated water at 2 atm = (5,200,000 lb)(0.017 ft^3/lb) = 88400 ft^3 = 2503 m^3.

[8] (2503 m^3)·(0.001%) = 0.02503 m^3 = 25.03 L

[9] As prepared by Nyacol Nano Technologies for its AL20 nanofluid

[10] Volume of water = (99.37 kg alumina)/20% - 99.37 kg alumina = 397.48 kg water·(1 m^3/942.6 kg) = 0.422 m^3 water; total volume = 0.422 m^3 + 0.02503 m^3 = 0.447 m^3 = 447 L

Table VII: Tank Specifications

Material	Titanium Grade 2
Certification	N-stamp
Design Pressure	2.5 atm
Design Temperature	300 K
Capacity	~500 L
Dimensions	~100 cm (diameter), ~64 cm (height)
Thickness	0.32 cm (shell), 0.48 cm (head)
Nozzles	2.5-cm diameter nozzle on top (1), 2.5-cm diameter on bottom (1)
Supports	Vertical supports (2)

The tanks would need to be located above the IRWST to ensure that the nanofluid could be passively injected by gravity into the reactor cavity. A general location for the tanks is proposed in Figure 20.

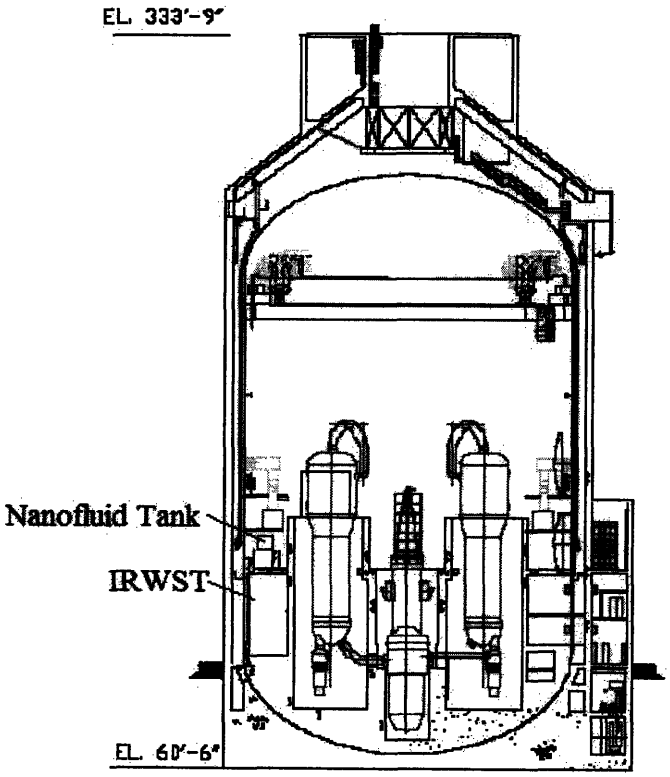

Figure 20: Proposed Location of Nanofluid Storage Tanks[11]

[11] Adapted from [22].

4.1.2.3 Initial Design Option Details

The nanofluid storage tanks need to be arranged in a configuration such that their contents can be mixed with water from the normal reactor safety systems and delivered into the reactor cavity within the time required by the IVR severe accident mitigation strategy. Three initial design options were considered.

Design Option #1: Nanofluid tanks inject directly into the reactor cavity

The first design option involves the injection of the concentrated nanofluid directly into the reactor cavity. The two nanofluid storage tanks are redundant, with each tank containing a sufficient amount of nanoparticles to provide the desired CHF enhancement when diluted by the water from the RCS and IRWST. Each tank is also equipped with one injection line and a gas accumulator. The accumulator on each tank provides a slight overpressure to aid the nanofluid injection. Each injection line is equipped with a motor-operated valve. The injection lines from the two tanks are cross-tied close to the injection points. The cross-tie line ensures that in the event of the failure of one of the injection lines the nanofluid will still be injected through all of the injection points. The injection lines also have spargers at their injection points to facilitate mixing. In this design, the injection line valves will open following a severe accident and nanofluid will be injected directly into the partially flooded cavity. The concentrated nanofluid will mix with the water in the cavity from the RCS and the IRWST. The diluted nanofluid will flow via natural circulation and remove heat from the outside of the reactor vessel with enhanced CHF capabilities. Design Option #1 is shown in Figure 21.

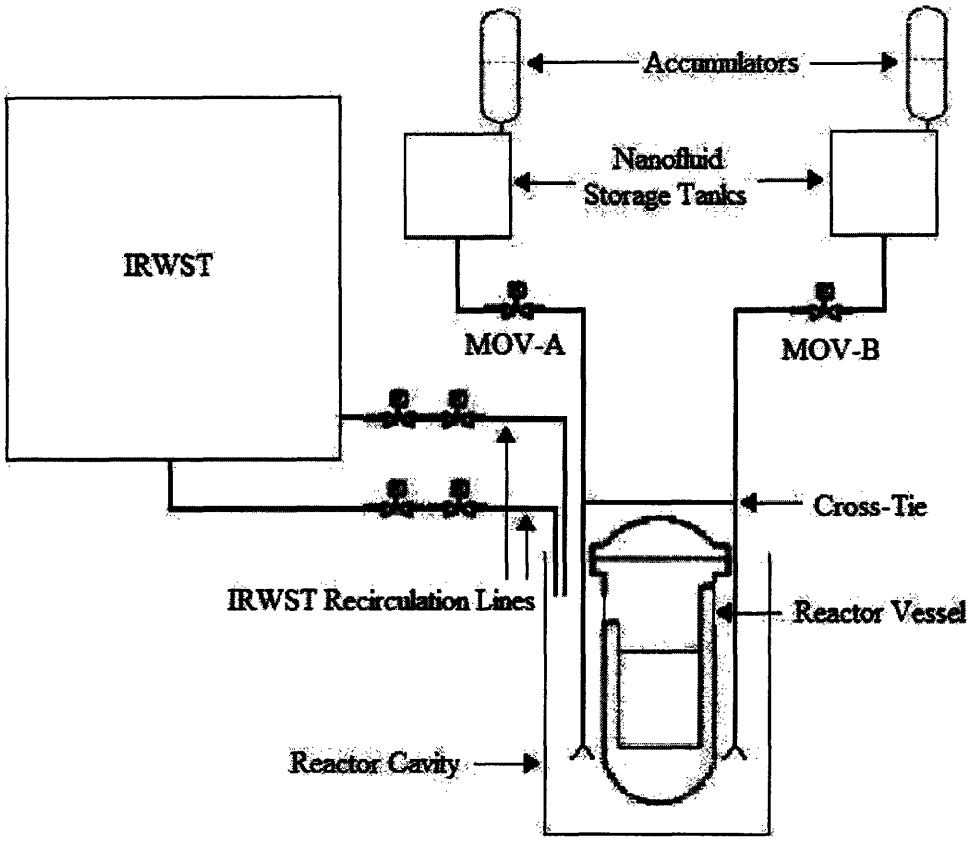

Figure 21: Nanofluid Tanks Inject directly into the Reactor Cavity (Design Option #1)

Design Option #2: Nanofluid tanks inject into the IRWST recirculation lines

The second design option is similar to the first except the nanofluid tank injection lines are connected to the IRWST recirculation lines that are used to manually flood the reactor cavity. The nanofluid tank injection lines connect to the IRWST recirculation lines below both the squib and motor-operated valves on the IRWST lines. In this design the concentrated nanofluid will mix with the water flowing from the IRWST into the reactor cavity. This mixture of concentrated nanofluid and water from the IRWST will then mix with the water from the RCS already in the cavity. The fully-diluted nanofluid will then remove the heat from the reactor vessel via natural circulation. Design Option #2 is shown in Figure 22.

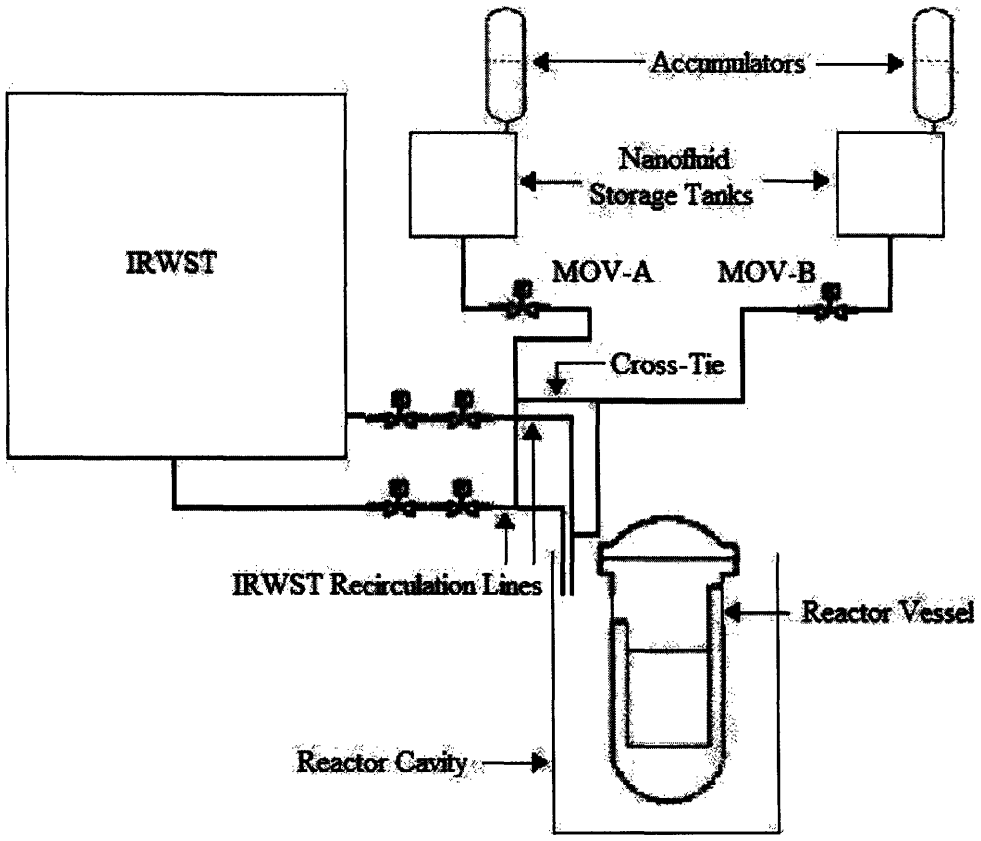

Figure 22: Nanofluid Tanks Inject into the IRWST Recirculation Lines (Design Option #2)

Design Option #3: Nanofluid tanks inject into the IRWST

The third initial design option injects concentrated nanofluid from the nanofluid storage tanks into the IRWST. In this design the concentrated nanofluid will mix with the water in the IRWST as they flow through the IRWST recirculation lines into the cavity. This mixture will then mix with the RCS water that is already present in the cavity and the fully-diluted nanofluid will cool the reactor vessel. Design Option #3 is shown in Figure 23.

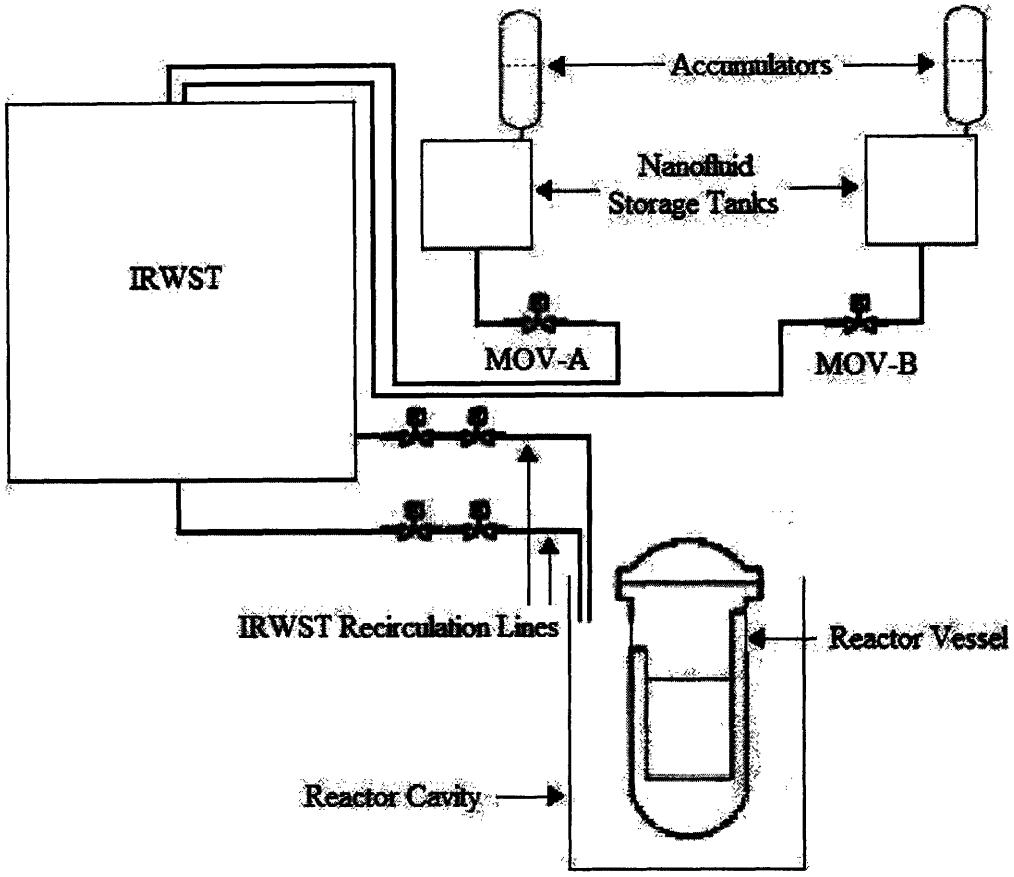

Figure 23: Nanofluid Tanks Inject into the IRWST (Design Option #3)

4.1.2.4 Cost Estimate

Because this nanofluid injection system is designed to be implemented in a commercial nuclear power plant, it is important to determine if the system will be prohibitively expensive and thus unfeasible for commercial use.

Each of the three designs consists of two nanofluid storage tanks, two accumulators, and two motor-operated valves with identical specifications. The injections lines are also identically sized in all three designs. The length of the lines, the presence of spargers, and the implementation costs could vary between the designs. Any variance, however, is likely to be small compared to the uncertainties in the analysis; therefore, a single cost estimate will suffice for all the designs.

The major factors in determining the total cost of the injection system are the costs of: the nanofluid storage tanks, the valves, the accumulators, the injection lines, the nanofluid, implementation, and maintenance. The nanofluid storage tanks constructed to the specifications in Table VII are estimated to cost roughly $35,000 each [21]. The valves,

accumulators, injection lines, and nanofluid are estimated to cost roughly $70,000,[12] resulting in a total system material cost of $140,000. The maintenance costs for the system should be minimal. Although periodically the valves will need to be checked and the nanofluid will need to be sampled and analyzed, these maintenance activities can be easily integrated into the existing maintenance schedule consisting of similar tasks, to be performed during outages. Based on this simple cost analysis, it is concluded that the cost of adding a nanofluid injection system could be very low.

4.2 Detailed Design Considerations

The three initial design options are similar in that they all contain the same number of nanofluid storage tanks, the same number of injection lines, and the same number of valves. The differences between the designs are more subtle and require an in-depth investigation of the safety systems that the nanofluid injection system will be interfacing with under the accident sequences that lead to the need for IVR.

4.2.1 Accident Sequences Leading to the Need for IVR

Accident sequences are grouped together into accident classes based upon their general characteristics and the final damage states that can result. The accident classes that will impact the design of the nanofluid injection system are all those accident classes containing sequences that require IVR to mitigate their damage states. The AP1000 PRA identifies six such accident classes: 3BE, 3BL, 3C, 3BR, 1D, and 3D [13].

4.2.1.1 Accident Class Definitions

Accident Class 3BE

Accident class 3BE includes fully depressurized accident sequences with failure of gravity injection. The gravity injection failure results in core damage. The initiating event for accident sequences in this accident class may be a reactor coolant system pipe break, spurious actuation of the automatic depressurization system (ADS), or a direct vessel injection line break. A small loss-of-coolant accident (LOCA) or spurious actuation of the ADS with failure of gravity injection will not result in the reflooding of the reactor vessel and core damage will result. A direct vessel injection line break could result in reactor vessel reflooding but the reflooding will not occur quickly enough to prevent core damage [13].

[12] Nanofluid ($5,000) [23] + Valves ($45,000) [24] + Injection lines ($18,000) [25] + Accumulators ($2,000) [26] = $70,000.

Accident Class 3BL

Accident class 3BL includes accident sequences in which gravity recirculation fails (after successful gravity injection). The core will eventually be uncovered and core damage will occur because failed recirculation after injection results in no available water to flood the core [13].

Accident Class 3BR

Accident class 3BR includes accident sequences that result from a large LOCA and a failure of accumulator core reflood. Neither the core makeup tank (CMT) nor the IRWST is able to inject into the reactor vessel quickly enough to prevent core damage [13].

Accident Class 3C

Accident class 3C includes accident sequences that are initiated by a large failure of the reactor vessel below the top of the core. ADS and gravity injection are successful, but core damage will occur because the core will not be fully reflooded before the reactor cavity fills with water above the level of the core [13].

Accident Classes 3D and 1D

Accident classes 3D and 1D include accident sequences that are only partially depressurized such that sufficient gravity injection fails, resulting in core damage [13].

4.2.1.2 Requirements for Reactor Cavity Flooding

The reactor cavity is flooded either through the progression of the accident sequence or by manually draining the IRWST. In the 3BE, 3D, and 1D accident classes gravity injection fails and thus the cavity will not be completely flooded as a result of the accident sequence. These accident classes require that the IRWST to be manually drained in order to flood the reactor cavity to a sufficient level for IVR. In contrast, the 3BL, 3BR, and 3C accident classes do not require any manual action to flood the reactor cavity as the cavity will be flooded as a result of the accident progression. In accident class 3BL, recirculation fails after successful injection so water will be in the cavity in these accident sequences. In accident class 3BR, the IRWST injects but not rapidly enough to prevent core damage so the cavity will have to be flooded if IVR is needed later in the accident sequence. In accident class 3C, the rupture of the reactor vessel will ensure that the water from the successful gravity injection will be in the reactor cavity if IVR is needed later in the accident sequence. The cavity flooding requirements for the accident classes that could lead to the need for IVR are summarized in Table VIII.

Table VIII: Reactor Cavity Flooding Requirements for Core Relocation Accident Classes

Accident Class	Cavity Flooding	Action to Flood
3BE	Required	Manual
3BL	Required	None
3BR	Required	None
3C	Required	None
3D/1D	Required	Manual

4.2.2 System Integration

The nanofluid injection system will most critically need to integrate with the existing IRWST design. Additionally, the design of the system will also need to take the RCS inventory and the current IVR strategy into consideration.

4.2.2.1 IRWST Design Details

The major functions of the IRWST are to "provide flooding of the refueling cavity for normal refueling, post-loss-of-coolant accident (LOCA) flooding of the containment to establish long-term reactor coolant system (RCS) cooling, and to support the passive residual heat removal (PRHR) heat exchangers (HXs) operation" [13].

In the accident classes that do not require manual action to flood the reactor cavity (3BL, 3BR, and 3C), the water from IRWST is injected into the reactor cavity prior to IVR. In the accident classes that do require manual action to flood the reactor cavity (3BE, 3D, and 1D), the IRWST must be drained in order to flood the reactor cavity to a sufficient level for IVR. The IRWST contains two 20.3-cm (8") diameter recirculation lines that provide paths for gravity draining (shown in Figure 21) [27]. Each recirculation line contains one squib valve and one normally-open motor-operated valve in series [13]. The IRWST is drained by manually opening the squib valves on the recirculation lines (actuated from the control room). The recirculation lines inject into the recirculation sumps at 90' (27.4 m) elevation [27].

4.2.2.2 RCS Inventory

Under normal operation, the RCS removes heat from the reactor core. In all the accident scenarios that lead to the need for IVR, the RCS is assumed to be depressurized, resulting in the containment (and thus the reactor cavity) being flooded up to at least the 83' elevation with water from the RCS.

4.2.2.3 IVR Strategy Details

The IVR strategy entails preventing core melt from penetrating the reactor vessel by passively removing heat from the outer surface of the reactor vessel with coolant in the reactor cavity. In order for the IVR strategy to be employed the RCS must be depressurized and the reactor cavity must be flooded to a sufficient level within a certain timeframe.

The Emergency Response Guideline AFR.C-1 determines the functional restoration guideline for the operator action to flood the reactor cavity. The specific operator procedures are detailed in the REN-MAN03 operator action. One of the cavity flooding lines is more restrictive than the other, so the worst case that is considered is the failure of the less restrictive line, leaving only the more restrictive line to inject. In this case, the cavity is flooded up to minimum level needed for IVR (98' elevation) within 65 minutes of opening the valves. For IVR to be successful, the cavity must be flooded to this minimum level within 70 minutes of a core-exit thermocouple reading of 1200° F (648.9° C).[13] Therefore, in order to guarantee that the reactor cavity will flood quickly enough, the operator must open at least one of the two cavity flooding lines within five minutes of a core-exit thermocouple reading of 1200° F [13]. The flooding timeline decision tree is shown in Figure 24.

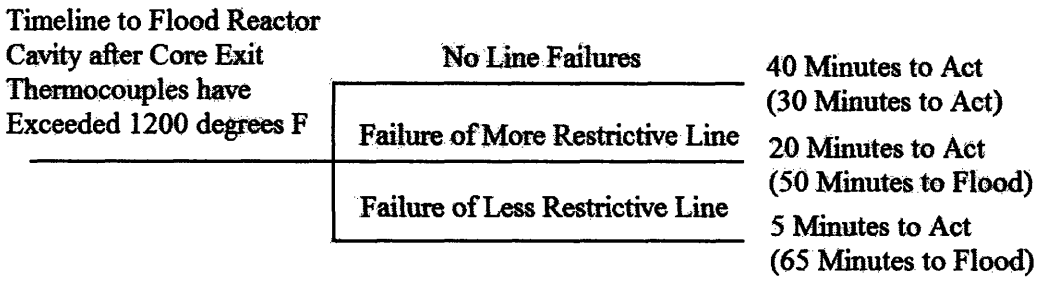

Figure 24: Flooding Timeline Decision Tree

A timeline of a typical core relocation event [13] requiring IVR and operator action is shown in Figure 25. Included in the timeline is a general placement of the time when the nanofluid valves must be opened. This time is dependent on how long the injection will take and how long the concentrated nanofluid will take to mix with the water in the cavity, as discussed next.

[13] Such a temperature reading signals the onset of core damage and can be viewed as the start of the severe accident.

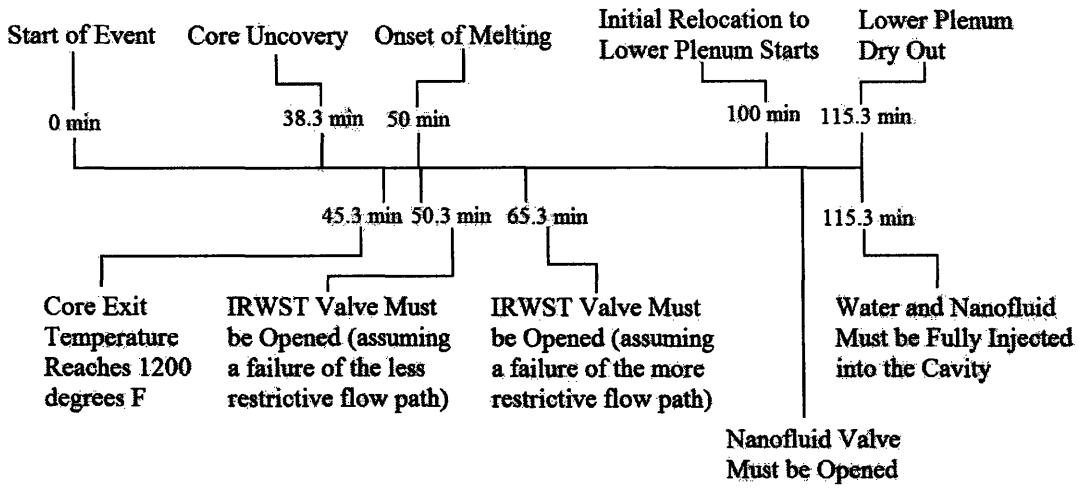

Figure 25: Accident Timeline for a Typical Core Relocation Event Requiring Operator Action

4.2.3 Design Comparison

Based upon the detailed system functions, the initial three design options described in Section 4.1.2.3 can be compared in detail in three different areas: the time it takes to inject the nanofluid, the promotion of mixing of the concentrated nanofluid with the reactor cavity water, and the space limitation within containment.

4.2.3.1 Time Required to Inject the Nanofluid

In order to employ IVR successfully the coolant must be in the flooded reactor cavity within 70 minutes after the core-exit thermocouples reach 1200° F. The nanofluid must thus be in the flooded reactor cavity, in the vicinity of the reactor vessel lower head and the insulation flow path[14] within this time frame. Each of the design options has a different flow path from the nanofluid tanks to the reactor vessel lower head. The most direct and quickest flow path is from the direct cavity injection (design option #1) in which the concentrated nanofluid is injected at the desired location. The design that injects the nanofluid into the IRWST recirculation lines (design option #2) is roughly the same as the recirculation lines inject at the 90' elevation. The insulation flow path is located between the 77' (23.5 m) elevation[15] and the 98' elevation [13], so the direct cavity injection would inject in roughly the same vicinity. The design that injects the nanofluid into the IRWST has the potential to take much longer to inject into the cavity. If operator action is not required to drain the IRWST (accident classes 3BL, 3BR, and 3C), then the flow path will be longer but the IRWST would be empty so the nanofluid

[14] The flow path is defined in Section 2.1.
[15] 98' elevation minus 6.14 m downcomer height given in Table I.

injection should occur in roughly the same timeframe as the other design options. If operator action to flood the IRWST is required (accident classes 3BE, 3D, and 1D), then the IRWST will be full and the tank could take up to 65 minutes to drain enough such that the minimum flooding level for IVR (98' elevation) is reached. In the worst-case the complete draining of the IRWST can take more than 100 minutes [13]. In the accident scenarios that require operator action to drain the IRWST, nanofluid injection into the IRWST will not result in the nanofluid being delivered to the reactor cavity in sufficient time.

4.2.3.2 Nanofluid Mixing in the Reactor Cavity

In order to employ IVR successfully, the concentrated nanofluid must not only be injected in sufficient time, but also must be sufficiently mixed with the water from the RCS and IRWST to form the desired nanofluid concentration through the coolant in the reactor cavity. Direct nanofluid injection into the cavity (design option #1) provides the best mixing of the three design options because the injection line is equipped with spargers at the injection point in the vicinity of the reactor vessel lower head. In addition the injection point can be located in a location that promotes mixing. Determination of the exact location that is optimal for mixing is beyond the scope the present study, but could be examined with a computational fluid dynamic (CFD) approach in future work. Injection into the IRWST recirculation lines (design option #2) is less effective because the injection occurs into the recirculation sump at the 90' elevation. Injection into the IRWST (design option #3) is equally effective at promoting mixing as the second design option in accident scenarios that do not require the operator action to drain the IRWST. This design option is less effective at promoting sufficient mixing in accident scenarios that do require operator action to drain the IRWST as concentrated nanofluid will not make it into the reactor cavity to mix with the RCS water in sufficient time.

4.2.3.3 Space Limitations within Containment

The containment in the AP1000 does have space limitations for the addition and integration of additional equipment. In particular, the space between the outside of the reactor vessel insulation and the reactor cavity wall is quite physically confined (*i.e.*, roughly 10 cm). The design that injects the nanofluid directly into the cavity (design option #1) is most restrained by the space limitations as the injection line and the spargers will need to be placed between the outside of the reactor vessel insulation and the reactor cavity wall. The design that injects the nanofluid into the IRWST recirculation lines below the recirculation line valves (design option #2) is less restrained by space limitations as the lines do not need to be placed between the outside of the reactor vessel insulation and the reactor cavity wall. The design that injects the nanofluid into the IRWST (design option #3) is the least constrained by the space limitations as the nanofluid tanks and the IRWST are located above the crowded areas in the containment.

4.2.4 Design Selection

Table IX summarizes the advantages and disadvantages of each design option.

Table IX: Comparison of Design Options

	Space Requirements	Time to Inject	Nanofluid Cavity Mixing
Direct Cavity Injection (Design Option #1)	Most restrictive space requirements (injection line located between vessel insulation and cavity wall)	Fastest nanofluid injection time	Promotes mixing in the cavity the best (due to spargers and injection point location)
IRWST Recirculation Line Injection (Design Option #2)	Somewhat restricted space requirements (nanofluid injection line must be connect downstream of recirculation valves)	Fast nanofluid injection time (only slightly slower than direct cavity injection)	Promotes mixing in the cavity worse than direct cavity injection (nanofluid injects into sump at 90' elevation)
IRWST Injection (Design Option #3)	Least restrictive space requirements	Fast injection time if IRWST is empty prior to nanofluid injection; slow injection time if IRWST is manually drained (too slow for successful IVR)	Promotes mixing in the cavity as well as IRWST recirculation line injection if IRWST is empty prior to nanofluid injection; poor mixing in cavity if IRWST is manually drained

Clearly nanofluid injection into the IRWST (design option #3) is eliminated because in the accident sequences that require operator action to drain the IRWST, the concentrated nanofluid will not be delivered to the reactor cavity in sufficient time to have successful IVR. Injecting the nanofluid directly into the cavity (design option #1) is preferred to injecting the nanofluid into the IRWST recirculation lines (design option #2) in terms of promoting nanofluid mixing, but does have more restrictive space requirements for the placement of the nanofluid injection line. Although the space limitations make implementation of the direct cavity nanofluid injection more difficult, this design option is preferred mainly because it is better at delivering the concentrated nanofluid close to the reactor vessel lower head and promoting nanofluid mixing in the cavity.

4.3 Calculation of System Failure Probabilities

The reliability of the nanofluid injection system can be determined by analyzing how the individual components of the system are connected and how the components will fail through fault trees. Event trees elucidate the connections between the individual components during different accident scenarios, while fault trees examine the factors that lead to component failure and assign appropriate probabilities.

4.3.1 Event Trees

The event trees that involve nanofluid injection for IVR can be simplified and divided into two categories: those for the accident sequences that require operator action to flood the reactor cavity and those for the ones that do not.

4.3.1.1 Accident Sequences that require Operator Action to Flood

The accident sequences that require operator action to flood are in the accident classes 3B, 3D, and 1D. A simplified event tree for accident class 3BE is shown in Figure 26 and accident class 3D/1D is shown in Figure 27. These event trees show that if the operator fails to recognize the need to flood then the reactor cavity will not flood sufficiently and the nanofluid will not inject effectively because both of these actions require an operator action for these accident sequences. The nanofluid injection system is design such that the operator action to flood the reactor cavity with water will be tied to the operator action to inject the nanofluid either procedurally or electronically. The failure of the operator to recognize the need to flood will lead to a likely vessel breach. This end-state is labeled as a "likely vessel breach" because although core damage will occur, it is possible for the water in the core and any water in the reactor cavity to prevent the core from relocating and breaching the vessel, respectively. Similarly, if the reactor cavity fails to flood sufficiently a vessel breach is likely. If the reactor cavity is sufficiently flooded but the nanofluid is not effectively injected then natural circulation heat removal through the vessel insulation flow path will occur with water as the coolant. These event trees assume that the AP1000 has been uprated to take advantage of the enhanced CHF properties of the nanofluid; therefore, heat removal with water as the coolant would not be able to ensure that the vessel would not be breached, thus the end-state labeled "possible vessel breach." The uprated AP1000 would require the successful injection of nanofluid (because the nanofluid would need to be the coolant) to ensure that the vessel would not be breached.

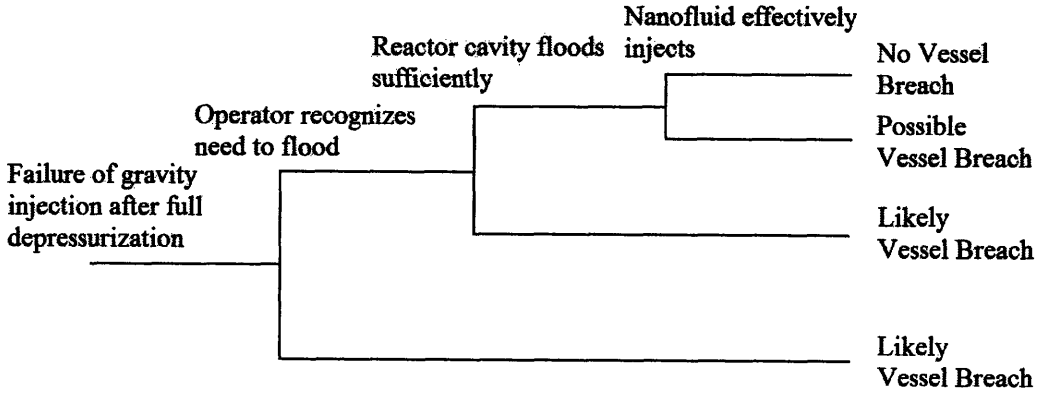

Figure 26: Simplified Event Tree for Accident Class 3BE

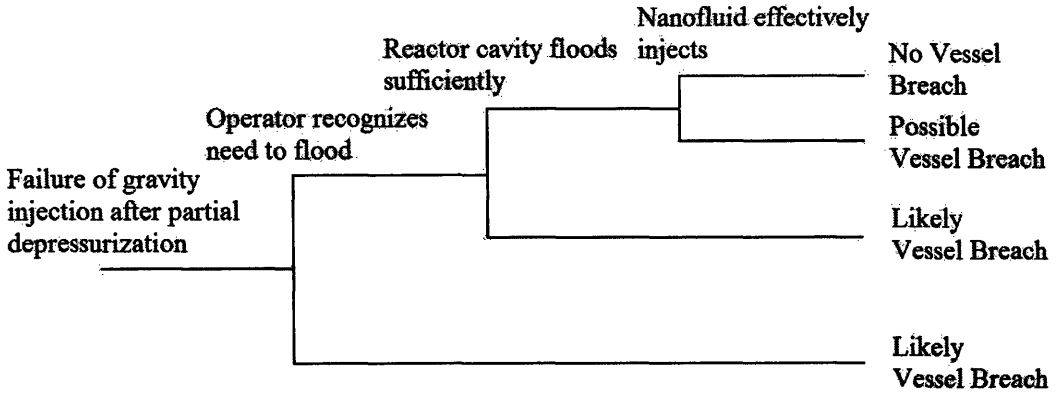

Figure 27: Simplified Event Tree for Accident Class 3D/1D

4.3.1.2 Accident Sequences that do not require Operator Action to Flood

The accident sequences that do not require operator action to flood are in the accident classes 3BL, 3BR, and 3C. A simplified event tree for accident class 3BL is shown in Figure 28, accident class 3BR is shown in Figure 29, and accident class 3C is shown in Figure 30. These event trees assume that even if the operator does not recognize the need to flood, the progression of the accident will result in the flooding of the cavity and natural circulation heat removal through the vessel insulation flow path will occur with water as the coolant. Because these event trees assume an uprated design of the AP1000, this sequence could result in a vessel breach. In order to ensure that the vessel is not breached, the operator must recognize the need to inject the nanofluid and the nanofluid must be effectively injected into the reactor cavity.

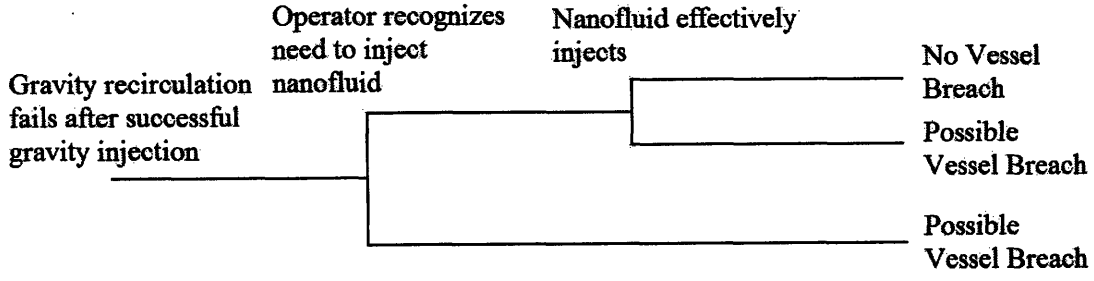

Figure 28: Simplified Event Tree for Accident Class 3BL

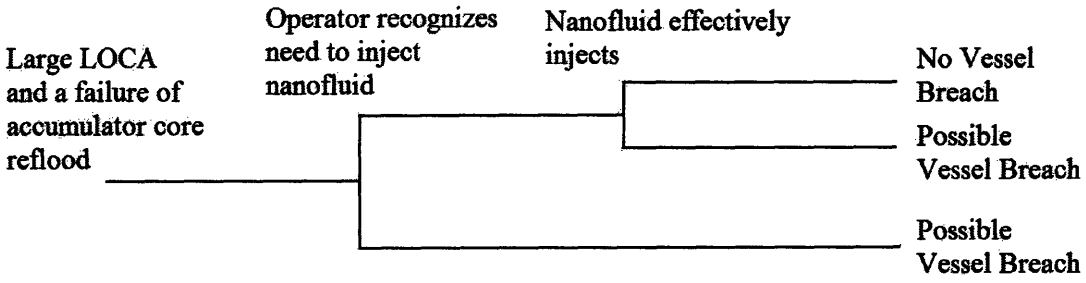

Figure 29: Simplified Event Tree for Accident Class 3BR

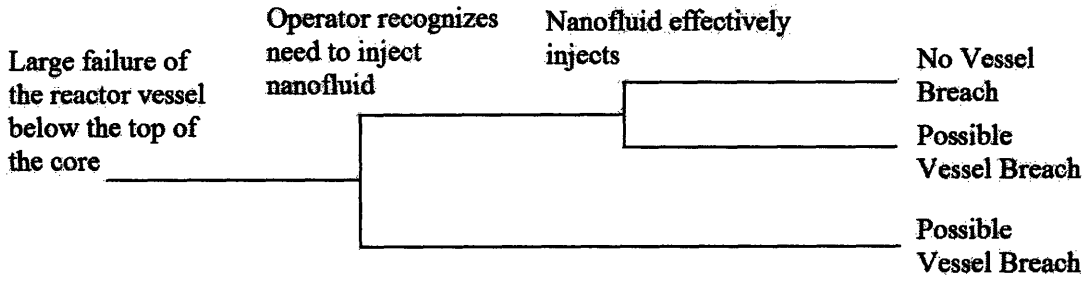

Figure 30: Simplified Event Tree for Accident Class 3C

4.3.2 Fault Trees

The fault trees are used to determine the probabilities of the different events in the event trees.

4.3.2.1 Sufficient Reactor Cavity Flooding

After the operator recognizes the need to inject and attempts to open the squib valves on the IRWST recirculation lines, the successful flooding of the reactor cavity depends on at least one of the two valves opening. The operator is assumed to have successfully recognized the need to flood quickly enough such that opening either of the two lines will result in sufficient reactor cavity flooding. From the AP1000 Probabilistic Risk Assessment (AP1000 PRA), the failure probability of sufficient reactor cavity flooding can be calculated.[16]

[16] Taken from the IWF Fault Tree (Recirculation MOVs fail to open following core damage) [13]: ("Sufficient reactor cavity flooding" failure probability) = ("Recirculation MOVs fail to open following core damage" failure probability) – ("Failure to open recirculation MOVs" failure probability).

4.3.2.2 Effective Nanofluid Injection

In order for the nanofluid to be effectively injected into the reactor cavity, the nanofluid must be delivered into reactor cavity and sufficiently mixed with the IRWST and RCS water without the nanoparticles agglomerating. The fault tree is shown in Figure 31.

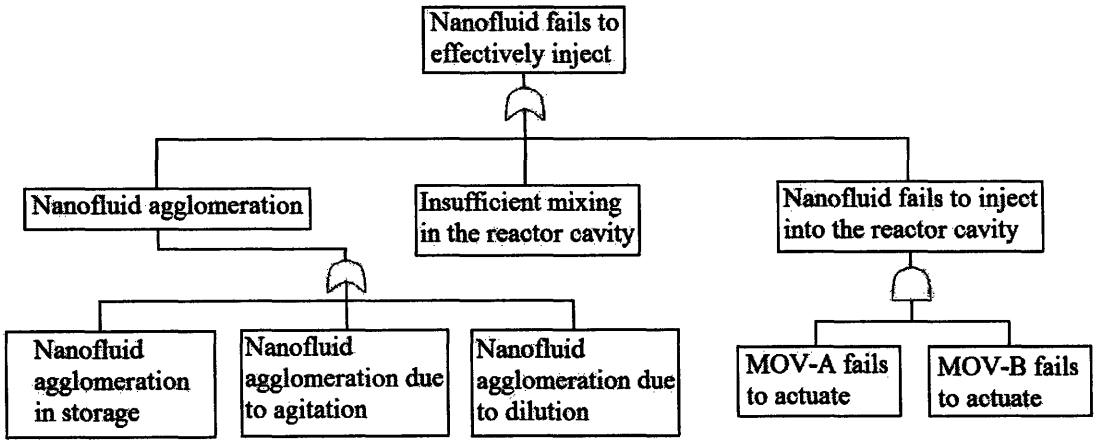

Figure 31: Effective Nanofluid Injection Fault Tree

However, the design of the nanofluid injection system is such that sufficient mixing in the reactor cavity will occur. In addition, the nanofluid is selected such that it will not agglomerate in storage or upon being injected and diluted. The simplified fault tree shown in Figure 32 also factors in the potential for a common cause failure.

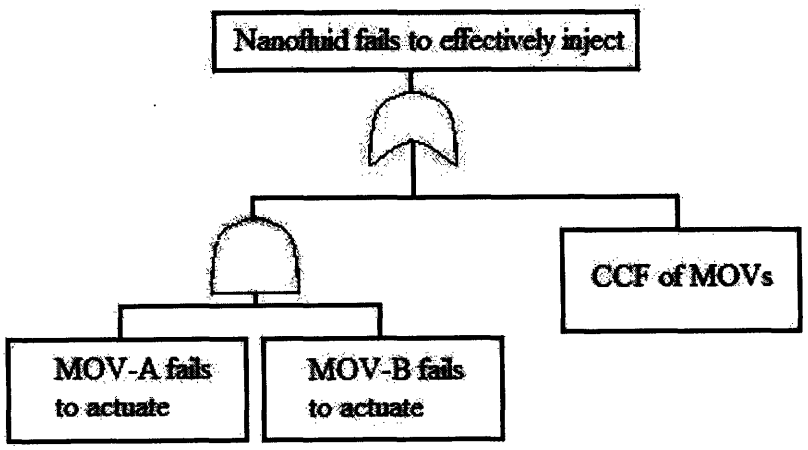

Figure 32: Simplified Effective Nanofluid Injection Fault Tree

4.3.3 Calculations

The probability of the reactor cavity failing to flood sufficiently is calculated to be $4.5x10^{-3}$.[17] The probability of the nanofluid failing to effectively inject is calculated to be to be $4.4x10^{-3}$ as shown in Figure 33. The valve failure probabilities for the valves used to manually flood the reactor cavity with water are assumed in the AP1000 PRA to be $5.00x10^{-4}$ [13]. The common cause failure probability of those valves is assumed in the AP1000 PRA to be $4.4x10^{-3}$ [13]. The failure and common cause failure probabilities for the nanofluid injection valves were assumed to be the same as manual flood failure probabilities because the valves will have similar design and operating characteristics.

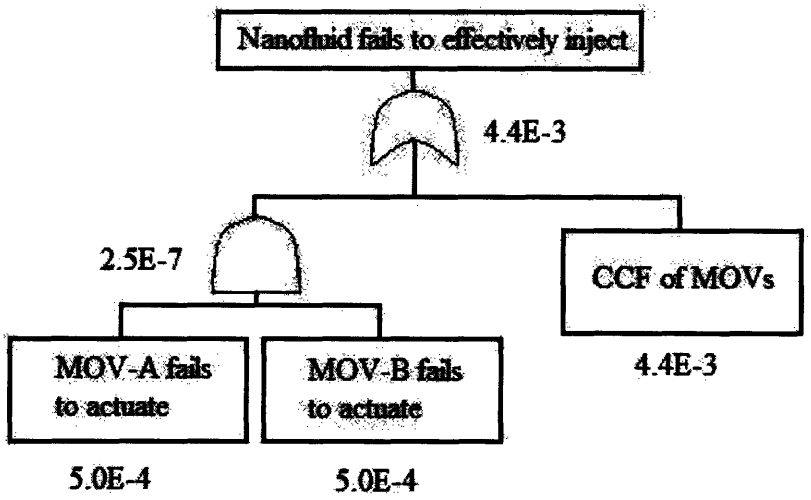

Figure 33: Failure Probability of the Effective Injection of the Nanofluid into the Reactor Cavity

The failure probability of the operator recognizing the need to flood the reactor cavity by draining the IRWST is given by the probability assigned to the REN-MAN03 Operator Action, which is $3.40x10^{-3}$ [13]. The failure probability of the operator recognizing the need to inject the nanofluid into the reactor cavity when the IRWST does not need to be manually drained is estimated as $3.40x10^{-3}$. The basis for this estimate is that the operator will be required to respond in a similar manner to recognizing the need to manually flood the cavity (the valve configurations and timeframe are similar).

Given these probabilities, the event success probabilities given an initiating event associated with a core relocation severe accident are calculated to be 0.99 for both categories of accident sequences. Figure 34 and Figure 35 show the calculation of these failure probabilities for accident class requiring and not requiring operator action to flood the reactor cavity, respectively. These success probabilities assume that the power of the reactor has been uprated.

[17] "Recirculation MOVs fail to open following core damage" failure probability = $7.9x10^{-3}$ [13] and "Failure to open recirculation MOVs" failure probability = $3.4x10^{-3}$ [13], therefore "Sufficient reactor cavity flooding" failure probability = $7.9x10^{-3} - 3.4x10^{-3} = 4.5x10^{-3}$.

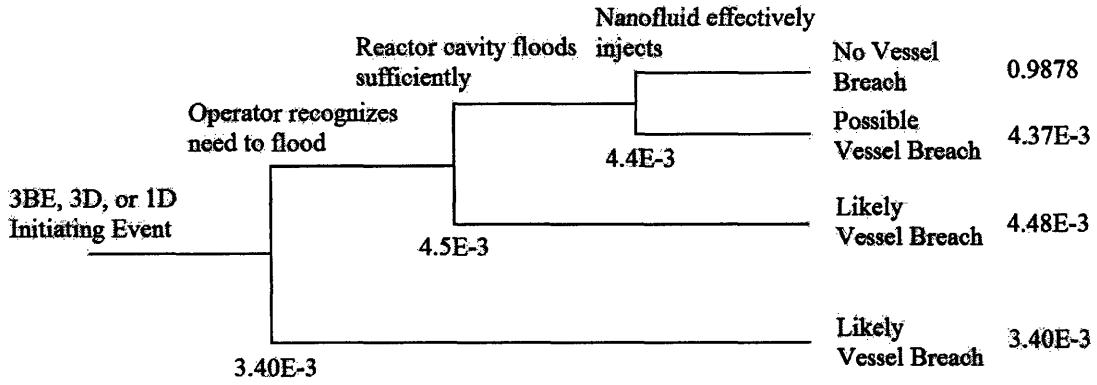

Figure 34: Event Failure Probability when Operator Action to Flood is required

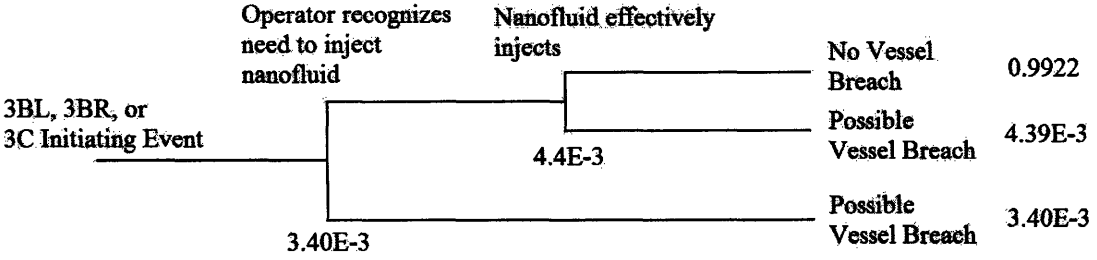

Figure 35: Event Failure Probability when Operator Action to Flood is not required

These success probabilities can be compared to the success probabilities of IVR just using water. In the accident classes that require operator action to flood, the success probability is 0.9921[18] compared to 0.9878. In the accident classes that do not require operator action to flood, the success probability is 1.0 compared to 0.9922. These probabilities are summarized in Table X.

Table X: Success Probability Comparison

	Prior Success Probability	Success Probability with Nanofluid Injection System
Manual Flooding Required	0.9921	0.9878
Manual Flooding Not Required	1.0	0.9922

Adding the nanofluid injection system does not lead to a significant decrease in the success probabilities for accident classes that do require manual flooding. This decrease in the success probabilities is considered insignificant because in order get the overall accident probability, the associated system failure probability[19] would have to be multiplied by the probability of an accident progressing to the point that IVR is required (a very small probability). However, adding the nanofluid injection system does lead to a

[18] (1-3.4*10-4)*(1-4.5*10-3) = 0.9921

[19] The associated system failure probabilities are equal to one minus the system success probability (listed in Table X).

new failure mode for accident classes that do not require manual flooding (for an uprated power reactor).

4.4 Summary of the Nanofluid Injection System Design

The proposed nanofluid injection system would take advantage of the enhanced CHF properties of the nanofluid in order to provide a higher safety margin than the current IVR strategy or, for given margin, enable IVR at higher core power. The preferred injection system design consists of injecting a concentrated nanofluid from two nanofluid storage tanks directly into the reactor cavity between the outside of the reactor vessel insulation and the reactor cavity wall. This injection system would be able to integrate into the AP1000's current systems without interfering with the current system functions. In addition, this injection system has a reasonably high success rate of 0.99, comparable to the success rate without the injection system. Finally, this system would not be prohibitively expensive, with the materials costs being roughly $140,000.

Finding #2: The proposed nanofluid injection system can be implemented with only a slight decrease in the overall PRA success probability.

5. REGULATORY IMPACT OF USING NANOFLUIDS IN IN-VESSEL RETENTION

This chapter investigates the regulatory impact of using nanofluids in an ALWR as part of the in-vessel retention severe accident mitigation strategy (IVR). Because the enhancement properties of nanofluids currently contain atypically large uncertainties, this chapter addresses: (1) what must be demonstrated to the NRC before a nanofluid injection system can be approved as part of a severe accident mitigation strategy and (2) how the NRC deals with large uncertainties when approving a new technology as part of a severe accident mitigation strategy. This chapter also addresses (3) the issue of the potential adverse health and environmental effects associated with the use of nanofluids in IVR and (4) the adequacy of the current regulatory regimes for ensuring that the implementation of the proposed nanofluid injection system will not endanger public health or safety.

5.1 NRC Severe Accident Current Practices

When implementing a new technology in a nuclear power plant, the current practices of the NRC are the primary source of information on what will be required for such an implementation to be realized.

5.1.1 NRC Severe Accident Requirements

Severe accidents are defined as postulated accidents beyond the design basis of the plant and were first addressed by the NRC as a response to the Three Mile Island Nuclear Power Plant accident in 1979.

The NRC has developed guidance and goals for preventing and/or mitigating events that are beyond the design basis of the plant. In order for a new nuclear power plant to adequately address severe accident concerns, the NRC staff must review the design and conclude that it is sufficiently safe, placing no undue risk to public health and safety. This review is to use an approach that stresses deterministic engineering analyses and judgment and is complemented with PRA [28]. The use of PRA is required for both the design basis and severe accident analyses [29].

In addressing severe accidents, the NRC issued two qualitative safety goals and two associated quantitative objectives. The two safety goals that were established are: (1) individual members of the public should be provided a level of protection from the consequences of nuclear power plant operation such that individuals bear no additional risk to life and health and (2) societal risks to life and health from nuclear power plant operation should be comparable to or less than the risks of generating electricity by viable competing technologies and should not be a significant addition to other societal risks.

The two associated quantitative objectives are: (1) the risk to an average individual in the vicinity of a nuclear power plant of a prompt fatality that might result from reactor accidents should not exceed 0.1 percent of the sum of prompt fatality risks resulting from other accidents to which members of the United States population are generally exposed and (2) the risk to the population in the area near a nuclear power plant of cancer fatalities that might result from nuclear power plant operation should not exceed 0.1 percent of the sum of cancer fatality risks resulting from all other causes [30].

5.1.2 NRC IVR Assessment

The NRC has reviewed the IVR analysis for both the AP600 design and its successor, the AP1000 design. In both of these designs, water from the IRWST is used as the reactor vessel coolant. The IVR analysis for the current AP1000 design, the substance of which has been approved by the NRC, provides a baseline for what the NRC views as a sufficient demonstration of safety for IVR.

5.1.2.1 AP1000 Design Documents

An analysis of IVR is contained in the AP1000 design documents that Westinghouse Electric Company has submitted to the NRC for review. These design documents include the AP1000 Probabilistic Risk Assessment (AP1000 PRA), the AP1000 Design Control Document (AP1000 DCD), and the AP1000 Final Safety Evaluation Report (AP1000 FSER).

This analysis provides a safety margin that the NRC found acceptable for IVR when using water as the coolant. In addition this analysis includes calculations of the core melt progression and the structural integrity of the reactor vessel and insulation.

5.1.2.2 Severe Accident Management Guidelines

Severe Accident Management Guidelines (SAMGs) are also required by the NRC. SAMGs contain the procedures that operators rely on in the case of a severe accident. The AP1000 Emergency Response Guidelines contain these procedures. These procedures would be largely unchanged with the proposed addition of a nanofluid injection system. An instruction to ensure nanofluid injection would need to be included with the instruction to manually flood the reactor cavity (REN-MAN03). In addition, for the accident sequences that do not require a manual flood of the reactor cavity, an instruction to inject the nanofluid would have to be added.

5.1.2.3 Uncertainties Associated with the Use of Nanofluids

The IVR analysis using water as the coolant is not entirely applicable to IVR using a nanofluid as the coolant. The properties of a nanofluid are not as stable and well-known as the properties of water; the use of nanofluids in IVR contains significantly larger uncertainties. Although PRA can be employed in a similar fashion with a nanofluid coolant analysis as with a water coolant analysis (as was done in Section 4.3), more deterministic assumptions underlie the nanofluid-based analysis.

The three key uncertainties that apply to the use of nanofluids in IVR that do not apply to the water-based analysis are: (1) the amount of CHF enhancement the nanofluid can provide in the IVR geometry and environment, (2) the stability of the nanofluid when used in the proposed nanofluid injection system, and (3) the manner in which the concentrated nanofluid mixes with the water in the flooded reactor cavity, and (4) the properties of the nanofluids (*i.e.*, particle size, shape, and loading).

These uncertainties need to be greatly reduced before a nanofluid coolant IVR system could be considered as reliable as a water coolant IVR system. A successful demonstration on par with the UCSB facility experiments (described in Chapter 2), but using nanofluids, would address the first key uncertainty. In order to address the second and third key uncertainties, additional features would have to be added to the experiment. The nanofluid would have to be injected into water with the actual chemical composition that would exist in the flooded reactor cavity. In addition, experiments would have to be run for a longer amount of time than in the UCSB facility experiments. These features would address the second key uncertainty. To address the third key uncertainty, more than just a hemispherical slice as a test section as in the UCSB facility would be required. The reactor cavity would have to be simulated and at least a half-hemisphere test section would likely be needed to properly capture the nanofluid mixing effects. A computation fluid dynamic model would aid in the design and reduce the third key uncertainty, but not to the degree that direct experimental verification would.

Recommendation #1: Nanofluid CHF enhancement must be experimentally verified for prototypical IVR geometry and conditions.

The fourth key uncertainty is somewhat different from the previous three key uncertainties in that the uncertainties can be reduced by practices taken after installation of the nanofluid injection system, as opposed to by experimental verifications conducted prior to installation. The properties of the nanofluid in the storage tanks can be ensured to be in the proper ranges such that CHF enhancement will be possible after injection through periodic sampling of the nanofluid. Nanofluid properties have been observed to remain constant over a period of months. Given that most nuclear power plants shut down to refuel every 18 months, it is proposed that the nanofluid in the nanofluid storage tanks be sampled during every refueling outage. These samples would then be used to measure the properties of nanofluid in the nanofluid storage tank in order to ensure that

the properties are in the appropriate ranges. This sampling could be incorporated into the maintenance procedures of the plant.

Recommendation #2: Sample and measure the properties of the nanofluid in the storage tanks at least during every refueling outage.

5.1.3 NRC Case Studies

These case studies illustrate the policies and actions of the NRC when the NRC was previously faced with the implementation of a new technology in a nuclear power plant. From these past actions one can predict to an extent how the NRC will treat the implementation of another new technology such as using nanofluids in IVR.

5.1.3.1 Replacement of Analog Technologies with Digital Technologies in Nuclear Power Plants

Background

The original nuclear power plant designs approved by the NRC contained all analog systems. As the plants aged and digital technology advanced, interest in digital technologies increased: "the age-related degradation of some earlier analog electronic systems and the difficulties in obtaining qualified replacement components for those systems, as well as a desire for enhanced features such as automatic self-test and diagnostics, greater flexibility, and increased data availability have prompted some operating reactor licensees to replace existing analog systems with digital systems" [31].

Replacing analog systems with digital ones raised concerns with the NRC staff:

> "The concerns of the staff stem from the design characteristics specific to the new digital electronics that could result in failure modes and system malfunctions that either were not considered during the initial plant design or may not have been evaluated in sufficient detail in the safety analysis report. These concerns include potential common mode failures due to (1) the use of common software in redundant channels, (2) increased sensitivity to the effects of electromagnetic interference, (3) the improper use and control of equipment used to control and modify software and hardware configurations, (4) the effect that some digital designs have on diverse trip functions, (5) improper system integration, and (6) inappropriate commercial dedication of digital electronics" [31].

With the increased use of PRA in NRC decision-making, the NRC staff later raised additional concerns with the proper way to model digital systems in PRAs.

NRC Actions and Policies

In light of the pending necessity of analog-to-digital upgrades in nuclear power plants, the NRC commissioned Lawrence Livermore National Laboratory to produce the report, "The Programmable Logic Controller and Its Application in Nuclear Reactor Systems [33]," which was issued in 1993. The initial NRC policy issued in a 1992 draft generic letter published in the Federal Register[20] was to review virtually all digital upgrades as "essentially all safety-related digital replacements result in an unreviewed safety question because of the possibility of the creation of a different type of malfunction than those evaluated previously in the safety analysis report" [31].

In 1994, the NRC's Advisory Committee on Reactor Safeguards recommended that the NRC commission a study to investigate the use of digital systems in nuclear power plants. Subsequently the NRC commissioned a study by the National Academy of Science (NAS) to investigate this subject [34]. Concurrently with the development of the NAS study, the NRC reviewed the findings of available reports and revised its policy, allowing the use of a 1993 NUMARC/EPRI Report [35] "as acceptable guidance for determining when an analog-to-digital replacement can be performed without prior NRC staff approval under the requirements of Section 50.59 of Title 10 of the Code of Federal Regulations (10 CFR 50.59)" [31]. In addition, the NRC initiated a revision of Chapter 7 (Instrumentation & Controls) of the Standard Review Plan [34].

In 1995, the NRC issued the policy statement encouraging greater use of PRA to "improve safety decision making and improve regulatory efficiency" [34]. In response to this emphasis on PRA, the NRC commissioned Ohio State University to produce the report, "Current State of Reliability Modeling Methodologies for Digital Systems and Their Acceptance Criteria for Nuclear Power Plant Assessments" [34], which was issued in 2006. This report was intended "to provide technical support for the development of regulatory guidance for risk-informing digital systems and guidance on the best approaches for the development of a tool to support independent evaluation of the risk associated with the use of digital systems in commercial nuclear power plants" [34].

General Applicability of this Case Study

It should be noted that digital systems are used (1) in normal plant operation, (2) to mitigate design-basis accidents, and (3) to mitigate severe accidents. Most of the listed NRC actions and policies were implemented for the first two uses of digital systems; however, general lessons are still applicable to severe accident mitigation. This case study illustrates that the NRC is very conservative when approving design changes that contain significant uncertainties. It also illustrates that once relevant reports have been developed and reviewed, the NRC will change its policies accordingly.

[20] This draft generic letter was issued for public comment in the Federal Register (57FR36680) on August 14, 1992 [34].

5.1.3.2 Assessment of Active and Passive Systems in Nuclear Power Plants

Background

Passive systems and components are defined as those systems or components that do not require external input and especially energy to operate [34]. Passive systems can be divided into four categories: (1) physical barriers and static structures (*e.g.*, structural through material selection, condition, design and geometrical arrangement), (2) moving working fluids (*e.g.*, by fluid/gas movement, by phase changes, by chemical reactions and/or by neutron flux effects), (3) moving mechanical parts (*e.g.*, spring loaded check-valves opening based on pressure difference), and (4) external signals and stored energy (*e.g.*, passive execution / active actuation) [37].

ALWR designs rely significantly more on passive systems than previous reactor designs. Passive systems have been implemented because of their perceived increased safety and their perceived lower cost [36]. The aim of passive systems is to increase safety by reducing human error and active component malfunctions [37]. Passive systems based on thermal hydraulics typically contain large uncertainties that are "difficult to quantify due to the fact that not all important factors may have been identified and there is no common agreement about calculating principles" [37].

NRC Actions and Policies

The underlying NRC policy regarding the assessment of passive safety systems in the licensing of new reactors is contained in Title 10, Part 52 of the Code of Federal Regulations (CFR) [28]. This section of the CFR states that passive safety systems will be approved if:

> (1) The performance of each safety feature of the design has been demonstrated through either analysis, appropriate test programs, experience, or a combination thereof;
>
> (2) Interdependent effects among the safety features of the design have been found acceptable by analysis, appropriate test programs, experience, or a combination thereof;
>
> (3) Sufficient data exist on the safety features of the design to assess the analytical tools used for safety analyses over a sufficient range of normal operating conditions, transient conditions, and specified accident sequences, including equilibrium core conditions; and
>
> (4) The scope of the design is complete except for site-specific elements such as the service water intake structure and the ultimate heat sink [28].

Alternatively, passive safety systems can be approved if "there has been acceptable testing of an appropriately sited, full-size, prototype of the design over a sufficient range

of normal operating conditions, transient conditions, and specified accident sequences, including equilibrium core conditions" [28].

How these standards have been employed in practice for severe accidents can be seen in what the NRC found acceptable in the Westinghouse AP1000 design. For the passive features used as part of IVR, analysis and experimental results (but not of a full-size design) were used. These features were generally not assigned failure probabilities as active components were, but instead were analyzed in a deterministic fashion with an appropriate safety margin. Additionally, many passive safety systems are not required to be tested as active components are, simply because such testing of passive systems is either not applicable or not feasible. For example, natural circulation loops used to mitigate severe accidents cannot be tested after installation the same way that MOVs can be tested.

General Applicability of this Case Study

This case study illustrates that when assessing passive safety systems the NRC typically requires in-depth analysis and experimental verification (if reasonably possible) before it will have enough confidence to integrate these systems into the overall design PRA. Furthermore, the NRC requires a larger safety margin for passive safety systems, the larger uncertainties present, preferring to err of the side of precaution. The NRC attempts to reduce any uncertainties associated with passive safety systems upfront, as they generally cannot be tested after installation in the manner that active systems can be.

5.2 Nanofluid Health and Environmental Hazards

In addition to investigating the potential adverse effects of using a nanofluid as a coolant in IVR, the potential adverse health and environmental effects resulting directly from the nanofluid need to be investigated.

5.2.1 Regulation of Nanofluids

Currently nanofluids and other nanomaterials are not specifically regulated for safety by the federal government. Nanomaterials are regulated based upon the properties of their bulk constituents even though it is the details of their composition that make them more useful and potentially more hazardous. As a result, occupational regulations are typically set for larger size particles and are too lax for nanoparticles [39]. It is also unclear how nanomaterials will ultimately be regulated. The two federal acts that will have jurisdiction over nanomaterials are the Toxic Substances Control Act (TSCA) and the Occupational Safety and Health Act of 1970 (OSHAct), with the Environmental Protection Agency (EPA) and the Occupational Health and Safety Administration (OSHA) being the primary regulators.

5.2.1.1 The Toxic Substances Control Act

If nanomaterials are new chemicals then they would have to meet the definition of a "chemical substance" as defined in TSCA [40]. Section 2 of TSCA states that EPA can regulate "chemical substances and mixtures which present an unreasonable risk of injury to health or the environment" [40]. Section 3 of TSCA defines a "chemical substance" as "any organic or inorganic substance of a particular molecular identity" [40]. A "mixture" is defined as "any combination of two or more chemical substances if the combination does not occur in nature and is not, in whole or in part, the result of a chemical reaction" [40]. EPA under section 6(a) of TSCA clearly could regulate nanofluids either as a "chemical substance" or a "mixture" if they presented "an unreasonable risk of injury to health or the environment."

Section 5(a) of TSCA requires a manufacturer to file a Premanufacture Notification (PMN) with EPA if the "chemical substance" is "new" or is put to a "significant new use" [40]. A PMN allows EPA to review the health and environmental risks of a "chemical substance" before manufacturing begins. However, "if a company has no toxicity data for a given chemical, the manufacturer is only required to submit data that already exists elsewhere, or may simply rely on information for chemicals that are structurally analogous to the one being reviewed" [41]. Nanomaterials are generally considered by manufacturers to be variations of the bulk material (and thus not a "new chemical substance") and thus manufacturers have not been submitting a PMN to EPA. Even if the manufacturer does deem that a nanomaterial is "new" or that it is being put to a "significant new use," currently "no mechanism exists to prevent a manufacturer from simply extrapolating toxicity information from the bulk-sized toxicity data on file" [41] when filing a PMN. Thus, a potentially hazardous nanoparticle with a safe bulk material would not be safely regulated through the PMN requirement.[21]

While a PMN does not require the manufacturer to conduct toxicity tests, section 4 of TSCA allows EPA to "require that manufacturers generate new test data in the face of unreasonable risk or substantial human exposure" [41]. If in the future tests began to show that nanomaterials were toxic, further toxicity testing could be required by EPA under section 4 of TSCA.

5.2.1.2 The Occupational Safety and Health Act of 1970

The "general duty clause" contained in section 5(a) of the OSHAct states that each employer "furnish to each of his employees employment and a place of employment which are free from recognized hazards that are causing or are likely to cause death or serious physical harm to his employees" and that each employer "shall comply with occupational safety and health standards promulgated under this Act" [42]. Section 6(b) of the OSHAct states that standards promulgated under the OSHAct should assure that "no employee will suffer material impairment of health or functional capacity" [42]. If

[21] See Section 5.2.2.1 for examples.

nanomaterials become a "recognized hazard" then they clearly can be regulated by OSHA under the OSHAct. To date, however, OSHA has not promulgated any nanomaterial-specfic rules or Permissible Exposure Limits (PELs) [41].

The Hazard Communication Standard (HCS) is an important standard promulgated by OSHA under the OSHAct that while not specific to nanomaterials does apply to them. The HCS ensures "that the hazards of all chemicals produced or imported are evaluated, and that information concerning their hazards is transmitted to employers and employees" [41]. A full transmittal of hazard information is to be accomplished by "labeling, a Material Safety Data Sheet (MSDS), and employee training" [41]. The hazard information for nanomaterials, however, is currently still based on the bulk material if it is available at all. For example, the MSDS for Nyacol alumina nanofluid lists all toxicological and ecological information as either "not available" or "none reported" [15].

5.2.1.3 Safety Guidelines

The National Institute for Occupational Safety and Health (NIOSH), a branch of the United States Department of Health and Human Services, has issued only general safety guidelines:

> Workers within nanotechnology-related industries have the potential to be exposed to uniquely engineered materials with novel sizes, shapes and physical and chemical properties, at levels far exceeding ambient concentrations. To understand the impact of these exposures on health, and how best to devise appropriate exposure monitoring and control strategies, much research is still needed. Until a clearer picture emerges, the limited evidence available would suggest caution when potential exposures to nanoparticles may occur [43].

Safety guidelines issued by smaller non-governmental organizations are not any more specific. For example, the MIT Environment, Health, and Safety Office states:

> There are currently no government occupational exposure standards for nanomaterials. When they are eventually developed, different standards for different types of nanomaterials will be needed. One should also be aware that Material Safety Data Sheets may not have accurate information at this point in time [44].

5.2.2 Health and Environmental Risk Assessment

Risk assessment is a useful tool for evaluating health and environmental hazards, even when large uncertainties allow for only a qualitative assessment. A basic framework that is commonly used for risk assessment was developed in a study by the United States National Academy of Sciences [45]. The four stages of this framework are: (1) hazard

identification, (2) dose-response assessment, (3) exposure assessment, and (4) risk characterization.

5.2.2.1 Hazard Identification

The first stage of analysis is hazard identification, which is the process of determining if a substance is "casually linked to particular health effects" [46]. Hazard identification is used the environmental context to identify if a substance casually linked to adverse environmental effects.

Health

The causal links to adverse health effects are determined by examining the toxicological properties of the substance, usually focusing on test results in animals or other test organisms. In general, a toxic substance can enter the body via any of three pathways: through inhalation, by ingestion, or by contact with the skin [46]. Of the three pathways into the body, the inhalation and dermal (contact with skin) pathways are likely of most concern for the handling of nanofluids.

The Health and Safety Commission in the United Kingdom (UK HSC) issued a report in 2004 stating:

> There is some evidence that dermal exposure to nanoparticles may lead to direct penetration of nanoparticles into the epidermis and possibly beyond into the blood stream. Therefore, it may be necessary to introduce control to exclude or limit the level of dermal exposure likely to occur.
>
> No published literature has been identified which has investigated the effectiveness of skin protective equipment (suits and gloves) effectiveness to prevent dermal exposure. It is unlikely that it will be more effective against nanoparticles than against larger particles. It is conceivable that for many current forms of skin protective equipment, nanoparticles could penetrate directly under certain conditions [47].

Additionally, the UK HSC warns that "if there is retention in hair follicles, there could be an enhanced potential for systemic availability of leachates from nanoparticles compared with micrometer particles" [47].

Once in the body, either by contact with the skin or more directly by inhalation, nanoparticles can readily enter the bloodstream and may be able to pass through the blood-brain barrier or blood placenta barrier" [39,48,49]. Once in the bloodstream nanoparticles have the potential to have adverse effects on humans that would not occur with chemically identical substances made up of larger particles. A report by Swiss Reinsurance Company, the global reinsurance and risk management firm, notes that "as size decreases and reactivity increases, harmful effects may be intensified, and normally

harmless substances may assume hazardous characteristics" [39]. The potentially harmful effects of nanoparticles speculated based on the nanoparticle's increased reactivity (due to the larger surface area per unit volume) and the nanoparticle's accessibility to regions of the body that larger particles are excluded from. Although nanoparticle toxicity is not well-studied, there are some studies that suggest potential adverse health effects. For example, "nanoparticles such as metals and metal oxides (Cu, Co, TiO_2, and SiO_2) have also been shown to have inflammatory [50,51] and toxic [52] effects on cells" [53]. Another study found that Teflon inhalation "correlated well with surface area per mass," with the Teflon nanoparticle inhalation being much more toxic than inhalation of larger particles [54]. There has been little research conducted on the carcinogenicity of nanoparticles to date, but this type of research is vital to characterizing the hazard that nanofluids pose as it is believed that for carcinogens there may be "no threshold dose below which the risk is zero" [46]. The latent effect problem further complicates matters by making evidence for carcinogenicity difficult to obtain for new substances.

The personal protective equipment (PPE) that workers are currently required to wear in containment (where the exposure to nanofluids would occur) typically includes coveralls, shoe covers, gloves, and masks. When handling penetrating radioactive nuclear species (*e.g.*, tritium), supplied-air respirators and supplied-air suits are often worn [55]. Wearing the proper PPE would appear to be sufficient to greatly reduce the amount of (if not prevent) inhalation and dermal exposure. The nanofluid would additionally be contained in sealed tanks during normal operation of the plant further reducing any chance of contact. It must be noted that casual linkages between nanofluids and adverse health effects are largely speculative at this time due to the lack of scientific data.

Environment

Nanoparticles could also have adverse environmental effects, such as aiding the transport of pollutants by bonding with them [39]. Nanoparticles could also be absorbed by plants that are ingested by humans or other animals [39]. It must again be noted that casual linkages between nanofluids and adverse environmental effects are speculative at this time due to the lack of scientific data. These adverse environmental hazards are very unlikely to be significant for the use of nanofluids in IVR because of the containment structure. The fact that the proposed nanofluid injection system is located within containment will prevent any nanofluid from coming into contact with the outside environment.

5.2.2.2 Dose-Response Assessment

The second stage of analysis is dose-response assessment, which is "the process of characterizing the relationship between the dose of an agent administered or received and the incidence of an adverse health effect" [46]. Environmental effects are be similarly characterized in this stage of analysis.

Health

At this stage "risk assessors determine significant levels of concentration, such as the 'lowest observable adverse effect level' (LOAEL) and the 'no observable adverse effect level' (NOAEL) for health assessment" [56]. Other relationships that must be determined are "whether the response is carcinogenic (cancer causing) or non-carcinogenic and whether the experiment is a one-time acute test or a long-term chronic test" [46]. Determining the NOAEL and LOAEL for nanofluids is very difficult at this point because of the scarcity of testing on humans or animals and the possible latent adverse health effects. Again it should be noted that NOAEL is believed to be zero for carcinogens.

Environment

For environmental assessments the dose-response stage of analysis involves determining "the 'predicted no-effect concentration' (PNEC)" [56]. Determining the PNEC for nanofluids is also very difficult at this point because of the scarcity of testing. It should be noted, however, that for the postulated adverse environmental effect of aiding the transport of pollutants, the PNEC would have to be higher than the PNEC for absorption by plants because the former is a bulk process, while the latter is potentially subject such phenomena as bioaccumulation in the food chain [57].

5.2.2.3 Exposure Assessment

The third stage of analysis is the exposure assessment, in which an estimate is made of the "dose or concentration of the substance to which a population is or may be exposed and the size of the population exposed" [56]. The extent to which the environment is exposed to a substance is also estimated in this stage of analysis.

Health

The number of people exposed to nanofluids in IVR is very limited. The exposure is limited to the maintenance workers who fill and check the contents of the nanofluid storage tanks. Checking the contents of the tanks involves taking a small sample of the nanofluid for analysis and checking the tank level. This maintenance action would only need to be conducted during refueling outages, which occur approximately once every 18 months. The tanks would need to be filled less frequently than the maintenance actions. No exposure after the deployment of the nanofluid injection system (*i.e.*, cleanup) needs to be considered because in the case of a severe accident the containment structure would be permanently sealed off from the outside environment. Even in the exceedingly rare event of a large release of radioactive material from containment (with a frequency of 5×10^{-7} per reactor year [12]), the health and environmental consequences would be negligible compared to the consequences of the fission product release.

Environment

For environmental assessments, estimates are made of "the concentration of the substance that will eventually be found in the environment" [56]. This concentration is known as "the 'predicted environmental concentration' (PEC)" [56]. The PEC for nanofluids used in IVR should be negligible as they are to be used in relatively small quantities (*i.e.*, ~1000 *L* of 20% by weight alumina nanofluid per reactor) within the containment structure.

5.2.2.4 Risk Characterization

The fourth and final step of analysis is risk characterization. This determination involves estimating the "likelihood that the examined substance will adversely affect human health or the environment, and the severity of the anticipated negative effects" [56]. This determination is what "should be used as a basis for legal and policy decision-making" [56].

Health

Although there are large uncertainties in the extent of the hazard and the dose that would produce adverse health effects, the extremely small amount of exposure is much more certain. The very small fraction of the population that would be exposed, the very limited time that they would be exposed, and the fact that anyone exposed would be wearing PPE makes the potential health risks associated with the use of nanofluids extremely low even factoring in the large uncertainties. The one health hazard to be potentially concerned with at these low dose levels is carcinogenicity.

Environment

Because of the extremely small exposures associated with this proposed use of nanofluids and the fact that the nanofluids will remain within the containment structure, makes the environmental risk negligible.

5.2.3 Health and Environmental Risk Management

After the risk assessment is completed, the determinations from the risk characterization can be used to make recommendations for how to manage the health and environmental risks. The health and environmental risk characterization (Section 5.2.2.4), states that the despite significant uncertainties, the health and environmental risks remain low because of the low dose and exposure levels. However, because the amount of available health and environmental data will greatly increase with the large amount of research that is currently being conducted (as detailed in Section 5.2.4), unforeseen health and environmental concerns could emerge. Of particular concern are long-term latent and no-threshold risks, such as certain types of cancer. Due to these factors, a periodic review of

relevant nanomaterial research should be conducted to identify any heightened health or environmental concerns. A periodic review cycle of once every 12 months is proposed. This review frequency is consistent with the standard review frequency used in TSCA [40].

Recommendation #3: Health and environmental risks of the use of nanofluids in IVR should be reevaluated every 12 months.

5.2.4 Research on the Health and Environmental Effects of Nanomaterials

In order to reduce the uncertainties associated with the adverse health and environmental effects of nanoparticles, much research is currently being conducted. The 21st Century Nanotechnology Research and Development Act, passed by Congress in 2003, "formalized the preexisting bureaucratic arrangement under the less formal National Nanotechnology Initiative, established research centers, and appropriated the necessary funds" [41]. In fiscal year 2006, the funding request for nanotechnology research and development totaled $1.054 billion for 11 agencies, with approximately $81 million being allocated for research on the health and environmental aspects of nanomaterials [41]. For example, "the Department of Defense will spend $5.5 million developing a computer model that predicts whether nanostructures are toxic" [58], "EPA requested $5 million in 2005 to fund studies on the toxicity of nanomaterials and their reaction while in transport" [58], and "the National Toxicology Program launched a five-year $3 million project to assess the toxic and carcinogenic potential of nanoparticles" [58]. More generally, "additional toxicology testing is being funded or planned by the National Science Foundation (NSF), the National Toxicology Program, and other research organizations in the US and in Europe" [44].

Because the toxicity of nanomaterials is highly dependent on the bulk material, its structure, and the type of exposure, toxicity research on the specific nanomaterial in question will be the most applicable. Nanofluids of the type proposed for use in IVR are unlikely to generate much public agency interest in toxicity research because they are not nearly as widespread as other nanomaterials. As stated in the risk characterization (Section 5.2.2.4), despite the large associated uncertainties, the total health and environmental risks will be low. Unless the periodic review finds research indicating a heightened concern for the health or environmental risks at the low dose levels associated with nanofluids use in IVR, toxicity research specifically on nanofluids used in IVR does not seem necessary. However, if the periodic review does find a heightened health or environmental concern, then specific research should be conducted.

Recommendation #4: If the periodic review finds a heightened concern, specific research should be conducted on the health and/or environmental effects of nanofluids.

5.3 Frameworks for Managing Large Uncertainties

Most decisions must be made with some amount of uncertainty. Decisions made with large amounts of uncertainty are typically very difficult to make. In the face of such large uncertainties (such as those associated with the use of nanofluids in IVR), frameworks are useful in determining how best to manage these large uncertainties.

5.3.1 Precautionary Principle vs. Proof Before Action Framework

The first framework classifies risk management strategies into abiding by either the precautionary principle (PP) or by proof before action (PBA). When dealing with large uncertainties, two types of errors are possible. Figure 36 illustrates these competing risks, the classification of which was first developed to analyze the Food and Drug Administration's drug approval process [59].

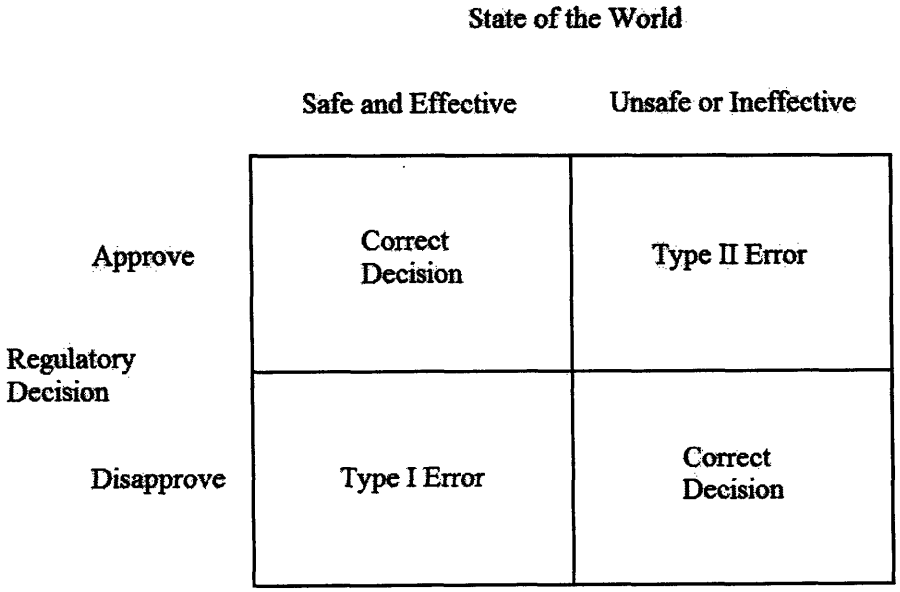

Figure 36: Regulatory Decision-Making under Uncertainty[22]

[22] Adapted from [59].

Figure 36 underlies this framework, with the PP proponents favoring the avoidance of Type II errors and PBA proponents favoring the avoidance of Type I errors. Type I errors can be described as avoiding false positives, while Type II errors can be described as avoiding false negatives.

5.3.1.1 Precautionary Principle

PP proponents argue that "the precautionary principle demands the proactive introduction of protective measures in the face of possible risks, which science at present – in the absence of knowledge – can neither confirm nor reject" [39]. Furthermore, risk should generally be shielded in order to correct for bias for under-protection. This bias, PP proponents argue, results from industry incentives for down-playing risks and the fact that the scientific review process leads to a bias for false negatives. This risk shielding serves to avoid the ultimate costs of irreversible harms [60]. Finally, PP proponents argue that more irreversible harm (caused directly by the action in question) will result from focusing on protecting against Type I errors than from focusing on protecting against Type II errors.

5.3.1.2 Proof Before Action

PBA proponents argue potentially unsafe activities should be regulated only after these activities have been proven to in fact be unsafe. Furthermore, risk should be shielded less in order to correct for the bias for over-protection. PBA proponents base their claim on the fact that retrospective studies have found exaggerated risks (such as food irradiation). This bias for over-protection is the result of the incentives for non-governmental organizations, courts, and the government to over-state risks and the fact that mass perceptions and fear create a bias for false positives. This risk management strategy avoids the direct and opportunity costs associated with regulation [61]. Finally, PBA proponents argue that more irreversible harm (caused by lock-in preventing a publicly beneficial action from being allowed) will result from focusing on protecting against Type II errors than from focusing on protecting against Type I errors.

5.3.1.3 Application of the PP vs. PBA Framework to Nanofluids

With regard to nanomaterials, some groups are invoking the use of PP by calling for a "moratorium [on the use of nanomaterials] until the scientific uncertainties surrounding the risks are clarified" [58]. However, currently the United States and most countries around the world are abiding by PBA, as nanomaterials are not specifically regulated by any federal agencies.

Whether the precautionary principle or proof before action should be applied is dependent on the details of the activity in consideration. When analyzing the use of

nanofluids in IVR, two risk categories emerge: (1) the risk of the nanofluid not mitigating a severe accident as designed and (2) the health and environmental risk from exposure to the nanofluid.

The first category involves a large irreversible potential consequence if allowed in its current knowledge state. If temporarily restricted, the potential for lock-in and the potential unrealized benefits are a much smaller and much more reversible consequence. Based on the relative reversibilities and consequences, the use of PP seems to be more prudent than PBA with the current state of knowledge for the first risk category. However, if the uncertainties associated with this risk category could be greatly reduced and the nanofluid injection system is still shown to be effective, then the benefits could outweigh the risks such that the using nanofluids in IVR would be more prudent.

The second category (health and environmental risk from exposure to nanofluids) involves a multitude of consequences, with varying levels of severity and reversibility. Most of the postulated potential health effects would not result in permanent damage and would thus be considered reversible. However, other postulated potential adverse health and environmental effects would be irreversible. Because of these potential irreversible adverse effects, use of PP seems more appropriate with the current state of knowledge.

5.3.2 Observability vs. Controllability Framework

M. Granger Morgan, the risk management expert and professor at Carnegie Mellon University, proposed another way to assess risk, based on where the risk falls on the observablity-controllablity matrix [62].

5.3.2.1 Observability-Controllability Matrix

With the observablity-controllablity matrix, risks are placed in one of four quadrants as shown in Figure 37.

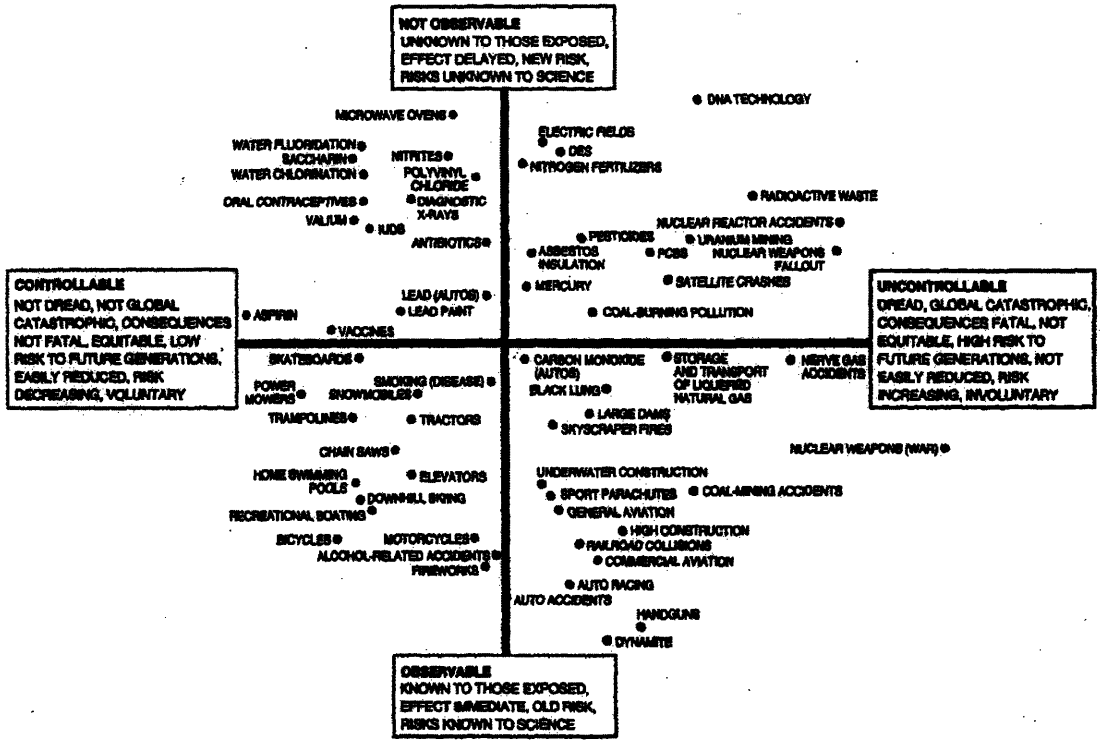

Figure 37: General Observablity-Controllablity Matrix[23]

Risks viewed as uncontrollable are more likely to be regulated than risks viewed as controllable. For example, the risks of using a trampoline are viewed as controllable primarily because using a trampoline is a voluntary activity, individuals can easily engage in safe practices that greatly reduce the risk, and the consequences of an accident are generally reversible. In contrast, the storage and transport of liquefied natural gas is viewed as uncontrollable as members of the public are involuntarily exposed to the consequences of an accident, individuals cannot easily reduce this risk through safe practices, and the consequences of an accident can be irreversible. Therefore, because of the greater risk controllability associated with the use of trampolines, the risks associated with the use of trampolines are less likely to be regulated than the risks associated with storage and transport of liquefied natural gas.

Risks that are viewed as not being observable are more likely to be regulated than risks viewed as observable. For example, the risks from riding a motorcycle are very well-known to both experts and the individuals exposed to the risk (*i.e.,* the rider). The consequences of the risk are also known immediately with strong causation. In contrast, the risks of pesticides are somewhat less well-known to experts, the consequences are not known immediately, and the causation is often fairly weak (*i.e.,* the long-term latent biological and ecological effects). The individuals exposed to this risk are also generally much less aware of their exposure and the potential consequences. Therefore, because of

[23] Taken from [62].

the greater risk observability associated with riding motorcycles, motorcycle risks are less likely to be regulated than pesticide risks.

In the observablity-controllablity matrix, the risks that are most likely to be regulated are in the upper-right quadrant (not observable and uncontrollable) and the risks that are least likely to be regulated are in the lower-left quadrant (observable and controllable) [60]. When dealing with large uncertainties, the quadrants that are of interest are the upper quadrants (not observable).

5.3.2.2 Application of the Observability vs. Controllability Framework to Nanofluids

Dividing the risks of using of nanofluids in IVR into the two categories used in Section 5.3.2.1, we can analyze each category using the observability vs. controllability framework. The placements of these two risks are shown in Figure 38. The risk of IVR failure with water as a coolant is also shown in Figure 38.

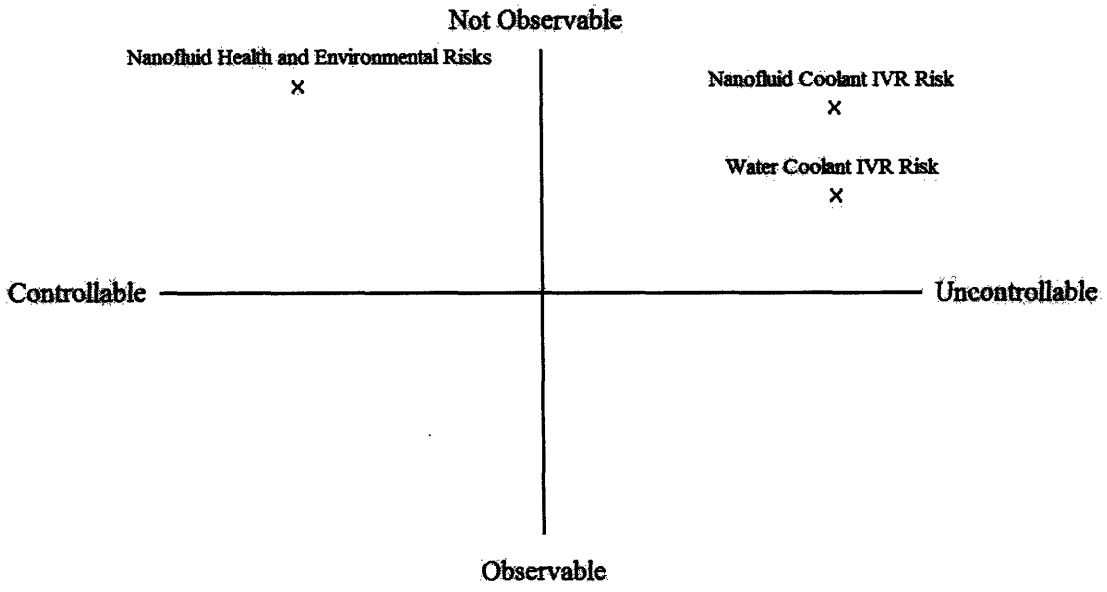

Figure 38: Nanofluid-specific Observablity-Controllablity Matrix

The nanofluid health and environmental risks are placed in the upper-left quadrant of the observablity-controllablity matrix because these risks, while fairly controllable are presently not observable. These risks are considered fairly controllable when used in IVR because exposure is limited to workers who enter containment and can be easily reduced by using the proper PPE. These risks, however, are not considered to be observable primarily because of the large uncertainties associated with their potential health and environmental hazards. Few, if any, relevant experiments have been conducted that accurately assess these potential hazards.

The nanofluid coolant IVR risk is placed high in the upper-right quadrant of the observablity-controllablity matrix because this risk is presently uncontrollable and not observable. This risk is considered to be uncontrollable because the failure of IVR could result in irreversible consequences, with some of those consequences being borne involuntarily. Again, the large uncertainties result in this risk not being observable. However, this risk is more observable than the nanofluid health and environmental risks because there is some relevant experimental evidence of the CHF enhancement properties of a nanofluid. The uncertainties are still much greater than when water is used as the coolant, justifying the placement of the water coolant IVR risk well below the nanofluid coolant IVR risk in the observablity-controllablity matrix.

Recommendations #1 and #2 would serve to move the nanofluid coolant IVR risk straight down in the observablity-controllablity matrix, ideally as close to the water coolant IVR risk as possible. Likewise, Recommendations #3 and #4 would serve to move the nanofluid health and environmental risks downwards in the observablity-controllablity matrix.

5.4 Adequacy of the Current Regulatory Regimes

Emerging technologies, including nanofluids, often do not fall readily into the existing regulatory regimes. This section analyzes how well the use of nanofluids in IVR falls into the existing regulatory regimes and makes recommendations for improving the adequacy of the current regulatory regimes.

5.4.1 Regulatory Adequacy of Severe Accident Mitigation

As discussed in Section 5.1, the NRC has extensive regulatory requirements in place to deal with the implementation of new technologies. Furthermore, taking the case study in Section 5.1.3 as an example, the NRC has dealt with the regulation of an uncertain technology before. NRC issues licenses to nuclear power plants after the NRC has reviewed the specific plant design. Any changes to this design must be reviewed by the NRC before implementation, giving the NRC ample opportunity to ensure continued public health and safety.

Using the frameworks discussed in Section 5.3, one can analyze some aspects of how the NRC treats uncertainty and assess the appropriateness of the approach. Taking the NRC policies and actions in the case study as the prime examples, one can clearly see that the NRC employs the precautionary principle, not approving the use of any new technology until research has been conducted to sufficiently reduce the associated uncertainties. Considering the high level of irreversible consequences associated with severe accident risks, the precautionary principle seems to be the appropriate approach. Additionally, considering that severe accident risks are in the upper-right quadrant of the observability-controllability matrix, this high level of regulation seems entirely appropriate.

5.4.2 Regulatory Adequacy of Health and Environmental Hazard Control

As discussed in Section 5.2.1, nanomaterials can be regulated under TSCA and the OSHAct, even though they have not been specifically regulated as nanomaterials to date. The control of the potential health and environmental hazards has thus followed the risk management strategy of proof before action. The health and environmental risks associated with using nanofluids in IVR are in the upper-left quadrant of the observability-controllability matrix. Because of the high level of controllability for this nanofluid application, the proof before action strategy that the current regulatory regimes implicitly utilize seems appropriate.[24] The one *caveat* that needs to be noted is the potential for irreversible health hazards to emerge in the future, shifting the health risk to the right in the observability-controllability matrix. If this were to occur, the current regulatory regimes might need to be changed.

Finding #3: The current regulatory regimes are adequate for ensuring that the implementation of the proposed nanofluid injection system will not endanger public health or safety.

[24] While the current regulatory regime may be appropriate for this particular application, this is not necessarily the case for other applications using nanomaterials.

6. SUMMARY, RECOMMENDATIONS, AND FUTURE WORK

The use of nanofluids as part of the IVR strategy in ALWRs presents both opportunities to increase the safety margin and/or increase the reactor power as well as potential difficulties with implementation in an actual nuclear power plant. These opportunities and potential difficulties were investigated in this thesis. The associated findings are summarized below.

Findings

1. **Using a nanofluid as the coolant in IVR could allow a ~40% increase in the power compared to using water as a coolant, while maintaining the same safety margin.**
2. **The proposed nanofluid injection system can be implemented with only a slight decrease in the overall PRA success probability.**
3. **The current regulatory regimes are adequate for ensuring that the implementation of the proposed nanofluid injection system will not endanger public health or safety.**

The first finding is the result of the model that simulated the two-phase flow and heat transfer on the reactor vessel outer surface and quantified the increase in residual power that can be removed using a nanofluid (detailed in Chapters 2 and 3). The second finding is the result of the analysis of the conceptual nanofluid injection system proposed in Chapter 4. The third finding is the general conclusion of the legal analysis, environmental and health risk assessment, uncertainty analysis, and case studies in Chapter 5.

In addition to the three findings, the four recommendations, reiterated below, seek to remedy some of the potential difficulties with using nanofluids in IVR.

Recommendations

1. **Nanofluid CHF enhancement must be experimentally verified for prototypical IVR geometry and conditions.**
2. **Sample and measure the properties of the nanofluid in the storage tanks at least during every refueling outage.**
3. **Health and environmental risks of the use of nanofluids in IVR should be reevaluated every 12 months.**
4. **If the periodic review finds a heightened concern, specific research should be conducted on the health and/or environmental effects of nanofluids.**

The first and second recommendations are aimed at significantly reducing the key uncertainties associated with using nanofluids in IVR. These uncertainties, if not addressed, would very likely prevent the NRC from approving the use of nanofluids in nuclear safety systems. The third and fourth recommendations seek to ensure that public health will not be endangered by the use of nanofluids in IVR by periodically reviewing the risks and conducting more research if necessary.

Related future work includes:

- Experimental verification of the CHF performance of nanofluids at prototypical IVR flow conditions and geometry
- Experimental study of the colloidal stability of nanofluids in the IVR chemical and radiation environment
- CFD analysis and experimental verification of the mixing of the concentrated nanofluid upon injection into the flooded reactor cavity
- Toxicity assessment of any nanofluids selected for use in IVR.

APPENDIX A: SUPPLEMENTAL PROOFS AND CALCULATIONS

A.1 Verification of Power-Flow Curve Shape in Natural Circulation

This proof assumes a very simplified version of the natural circulation loop that the model simulates. This simplified version has a height of H, a power into the system of $\dot{Q}$, and a form loss with a form loss coefficient of K in the riser as shown in Figure 39. The water is assumed to be saturated, with the riser in two-phase flow and the downcomer in single-phase liquid flow.

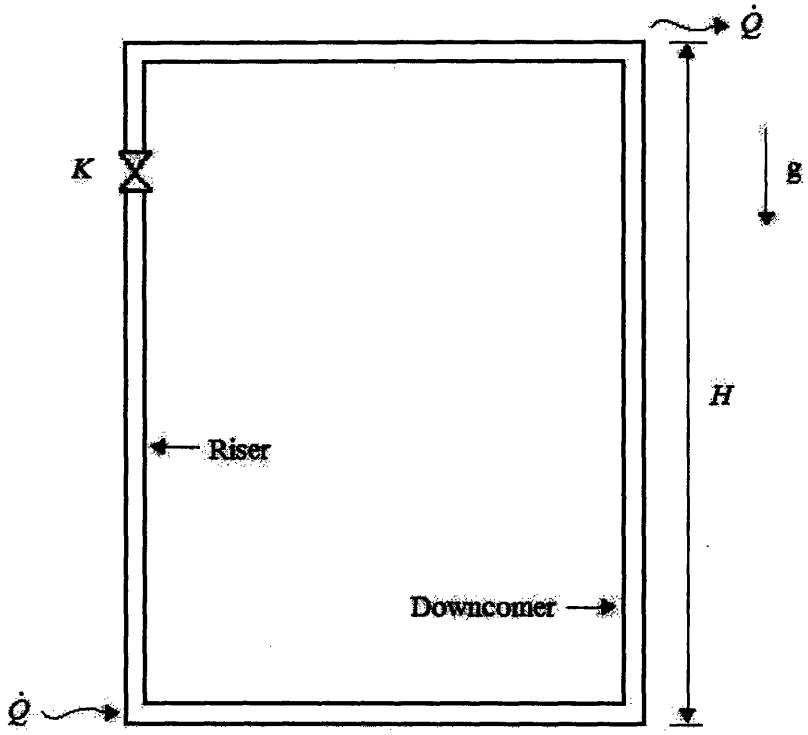

Figure 39: Simplified Natural Circulation Loop

First the pressure loss versus mass flow rate curve for the system will be plotted for different power levels. The form pressure loss, ΔP_{form}, is the only pressure loss in this system and is given by Equation (A.1) [3].

$$\Delta P_{form} = \frac{\Phi^2 \cdot K \cdot \dot{m}^2}{2 \cdot \rho_f \cdot A^2} \tag{A.1}$$

where: Φ^2 = two-phase friction multiplier, K = form loss coefficient, A = riser cross-sectional area

Since the water is assumed to be saturated throughout, the power of the system, $\dot{Q}$, is given by Equation (A.2).

$$\dot{Q} = \dot{m} \cdot h_{fg} \cdot x \tag{A.2}$$

By making the simplifying assumption that the flow is homogenous and in equilibrium throughout (HEM), the two-phase friction multiplier, Φ^2, is given by Equation (A.3) [3].

$$\Phi^2 \cong 1 + \frac{\rho_f}{\rho_g} \cdot x \tag{A.3}$$

Equations (A.1), (A.2), and (A.3) can be combined to give an expression for the system pressure loss, ΔP, shown in Equation (A.4).

$$\Delta P = \Delta P_{form} = \frac{K}{2\rho_f A^2} \cdot \left(\dot{m}^2 + \dot{m} \cdot \frac{\rho_f}{\rho_g} \cdot \frac{\dot{Q}}{h_{fg}} \right) \tag{A.4}$$

Equation (A.4) is plotted in Figure 40 for different power levels. Figure 40 illustrates that in this system there is no slope reversal in the pressure loss versus mass flow rate curve.

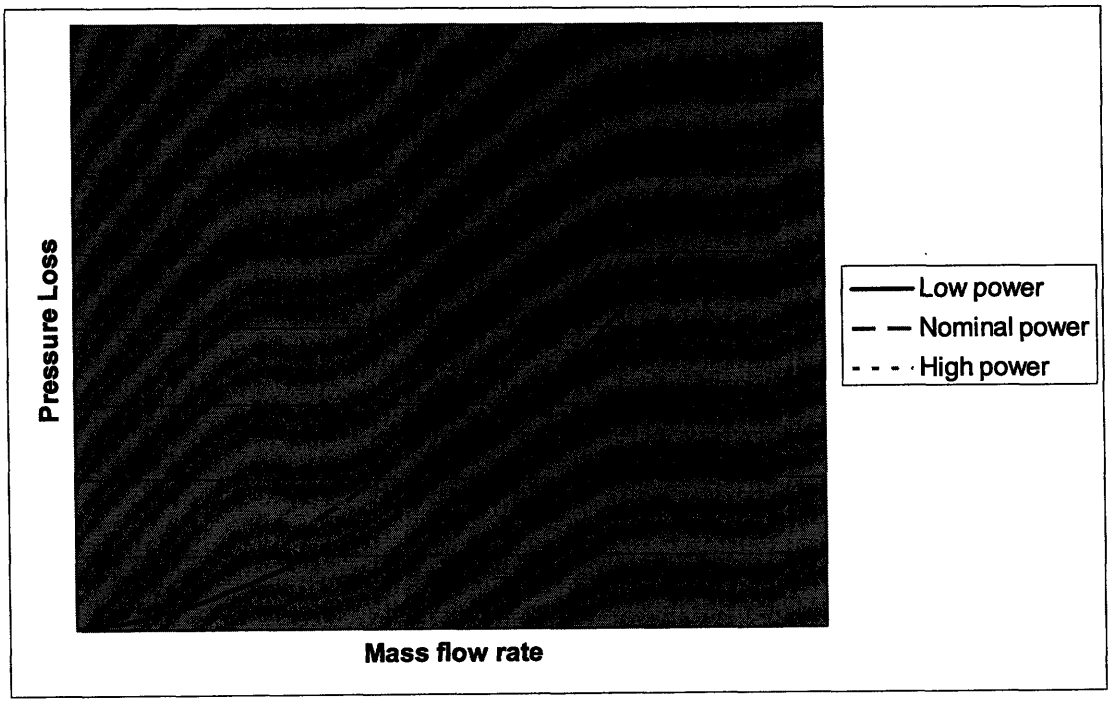

Figure 40: Pressure Loss versus Mass Flow Rate Curves

Next the mass flow rate versus power curve for the system will be plotted. The gravity pressure gains of the system, ΔP_{grav}, are given by Equation (A.5).

$$\Delta P_{grav} = (\rho_f - \rho_m) \cdot g \cdot H = \alpha \cdot \rho_f \cdot g \cdot H \tag{A.5}$$

where: ρ_m = mixture density, H = loop height

Assuming HEM, the void fraction, α, is given by Equation (A.6) [3].

$$\alpha = \frac{\rho_f \cdot x}{\rho_f \cdot x + (1-x) \cdot \rho_g} \tag{A.6}$$

Equating the pressure gain of gravity and the form pressure loss and combining Equations (A.4), (A.5), and (A.6), yields Equation (A.7).

$$\frac{\rho_g}{\rho_f} \cdot h_{fg} \cdot \dot{m}^3 + 2 \cdot \dot{Q} \cdot \dot{m}^2 + \frac{\rho_f}{\rho_g} \cdot \frac{\dot{Q}^2 \cdot \dot{m}}{h_{fg}} - \frac{\rho_f^2 \cdot g \cdot H \cdot A^2 \cdot \dot{Q}}{K} = 0 \tag{A.7}$$

Equation (A.7) can be expressed in terms of non-dimensional terms as shown in Equation (A.8).

$$\xi^3 + 2 \cdot \eta \cdot \xi^2 + \eta^2 \cdot \xi - \eta = 0 \tag{A.8}$$

where: $\xi = \dfrac{\dot{m}}{\sqrt{\dfrac{\rho_f^2 \cdot g \cdot H \cdot A^2}{K}}}, \eta = \dfrac{\dot{Q}}{h_{fg} \cdot \dfrac{\rho_g}{\rho_f} \cdot \sqrt{\dfrac{\rho_f^2 \cdot g \cdot H \cdot A^2}{K}}}$

Equation (A.8) is plotted in Figure 41.

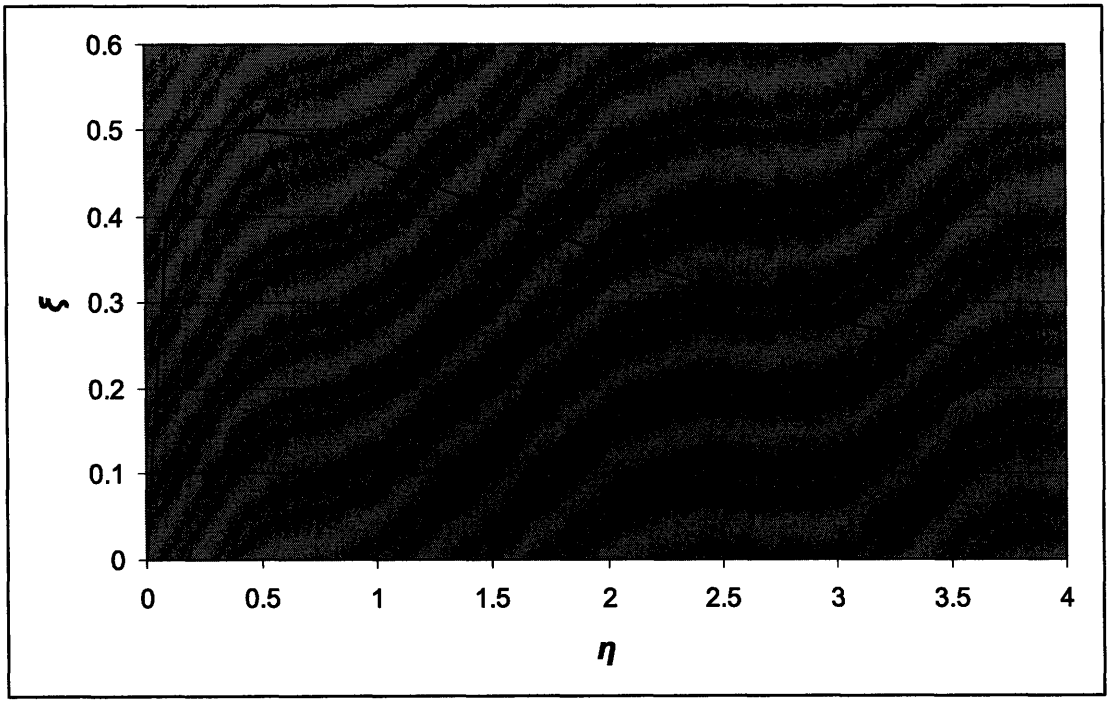

Figure 41: Non-dimensional Mass Flow Rate versus Power Curve

Figure 41 has a peak at $\eta = 0.5$ (ξ is proportional to mass flow rate and η is proportional to power); therefore, for this simplified natural circulation loop, there is a peak in the mass flow rate versus power curve without a slope reversal in the associated pressure loss versus mass flow rate curves. Physically, the peak arises from the competing effects of increasing riser-to-downcomer density difference and increasing hydraulic resistance of the form loss, as the power (thus the steam quality) increases.

A.2 Calculation of the Duration of Time that a Nanofluid Needs to be Effective for after Injection

The decay power as a function of the time after the reactor has shut down is given by Equation (A.9) [3].

$$P(t) = P_0 \cdot 0.066 \cdot t^{-0.2} \tag{A.9}$$

where: P = decay power, P_0 = reactor operating power, t = time after shutdown

From Chapter 3, nanofluids were found to remove 42% more decay power than water; therefore, water can remove 70.4% of the decay power that nanofluids can. This relationship is shown in Equation (A.10).

$$P(t = t_2) = 0.704 \cdot P(t = t_1) \tag{A.10}$$

where: t_1 = time to core relocation, t_2 = time in which water can remove the same amount of decay heat that nanofluids could at time to core relocation (t_1), $t_2 - t_1$ = time the nanofluid needs to be effective for

Given the time to core relocation (t_1), one can calculate the time the nanofluid needs to be effective for ($t_2 - t_1$) using Equation (A.9) and Equation (A.10). The worst-case time it takes for core relocation to occur is dependent on the accident sequence, but the general range is 1 to 3 hours [13]. Since IVR is based on removing the amount of heat in the worst case (decay power will be highest the faster it can melt and relocate), the time the nanofluid needs to be effective is likely biased towards the lower end of the range shown in Table XI, *i.e.*, about 5 hours.

Table XI: Sensitivity of Nanofluid Effectiveness Time to Core Relocation Time

Time to Core Relocation (hr)	Duration of Time that a Nanofluid Needs to Effective For (hr)
1.0	4.8
2.0	9.6
3.0	14.3

APPENDIX B: NANOFLUID AGGLOMERATION EXPERIMENTAL DETAILS

The stability of the nanofluid after it is significantly diluted is vital to the success of the proposed nanofluid injection system because an unstable nanofluid will not exhibit the enhanced CHF properties that this system utilizes. The stability of a nanofluid can be assessed by measuring the sizes and concentration of the nanoparticles in the nanofluid.

The nanofluid used in these experiments was an alumina nanofluid manufactured by Nyacol Nano Technologies, Inc. The concentrated form of this nanofluid as received from the manufacturer is 20% by weight, the concentration to be used in the nanofluid storage tanks. The diluted concentrations investigated in this experiment were 0.01% by volume (0.04% by weight) and 0.001% by volume (0.004% by weight). At these diluted concentrations the CHF enhancement has been experimentally observed.

For the severe accident scenarios that employ IVR, the nanofluid needs to be stable for a period of less than a day after it is diluted as a result of being injected into the reactor cavity (as calculated in section A.2 of Appendix A). The experimental parameters are summarized in Table XII.

Table XII: Summary of Nanofluid Agglomeration Experimental Parameters

Concentrations	20% by weight, 0.01% by volume (0.04% by weight), 0.001% by volume (0.004% by weight)
Measurement times	0 hr, 1 hr, 6 hr, 1 d

B.1 Variation of Nanoparticle Size with the Time after Dilution

This experiment consisted of diluting the concentrated nanofluid to concentrations sufficient to see the desired CHF enhancement and then measuring the sizes of the nanoparticles over time. Large increases in the size of the nanoparticles would indicate nanoparticle agglomeration and thus an unstable nanofluid.

The sizes of the nanoparticles were measured using a dynamic light scattering device. The data was analyzed using the EXPSAM algorithm (based exponential sampling, which is also known as the Pike/Ostrowski Method). The uncertainty in the nanoparticle size measurement is ± 20 nm.

Figure 42 shows the initial nanoparticle size distribution for the concentrated (20% by weight) nanofluid. This distribution has a mean nanoparticle diameter[25] of 37.75 nm.

[25] The mean nanoparticle diameter is the number-weighted nanoparticle diameter.

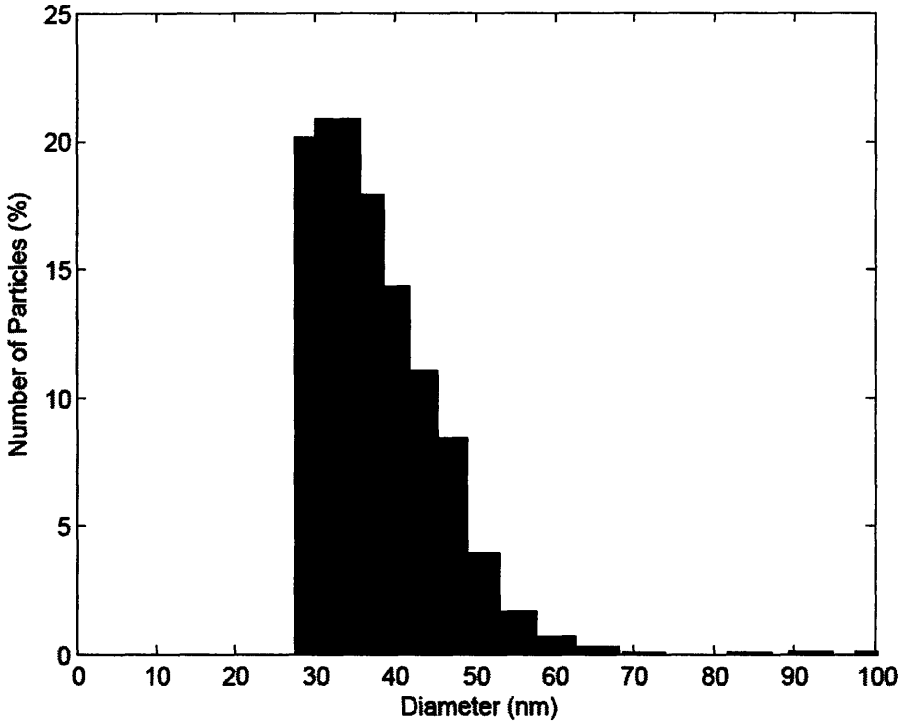

Figure 42: Initial Nanoparticle Size Distribution (20% by weight)

Figure 43 and Figure 44 show the nanoparticle size distributions 1 hour after dilution for the 0.01% and 0.001% by volume concentrations, respectively. At 1 hour the mean nanoparticle diameters for both of the concentrations (42.56 nm and 52.33 nm, respectively) are within the experimental uncertainty of the nanoparticle mean diameter of the concentrated nanofluid.

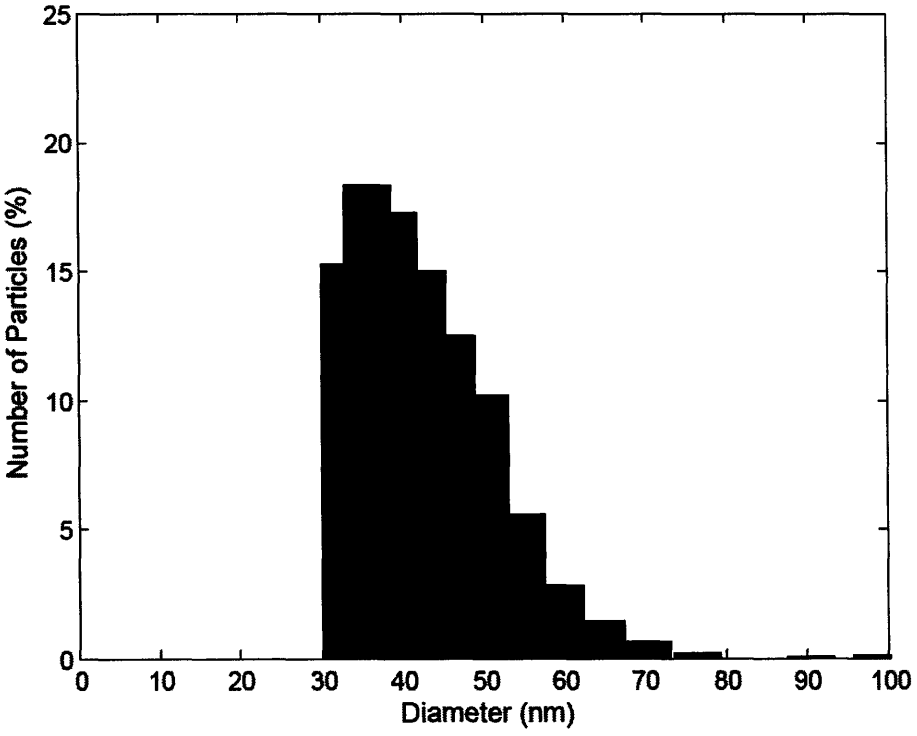

Figure 43: Nanoparticle Size Distribution after 1 hour (0.01% by volume)

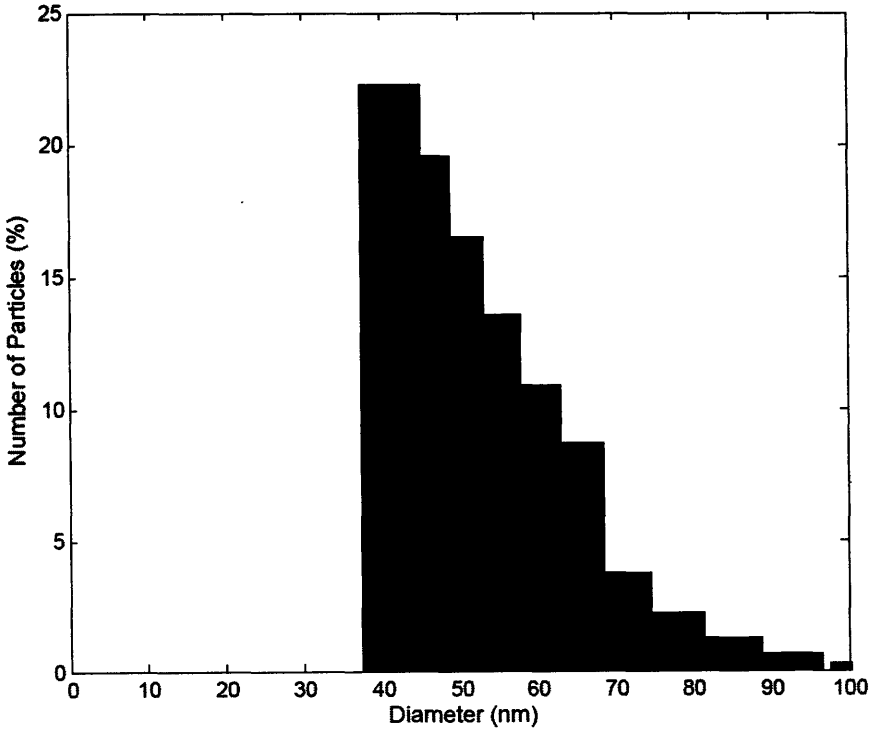

Figure 44: Nanoparticle Size Distribution after 1 hour (0.001% by volume)

Figure 45 and Figure 46 show the nanoparticle size distributions 6 hours after dilution for the 0.01% and 0.001% by volume concentrations, respectively. At 6 hours the mean nanoparticle diameters for both of the concentrations (32.64 nm and 33.36 nm, respectively) are still within the experimental uncertainty of the nanoparticle mean diameter of the concentrated nanofluid.

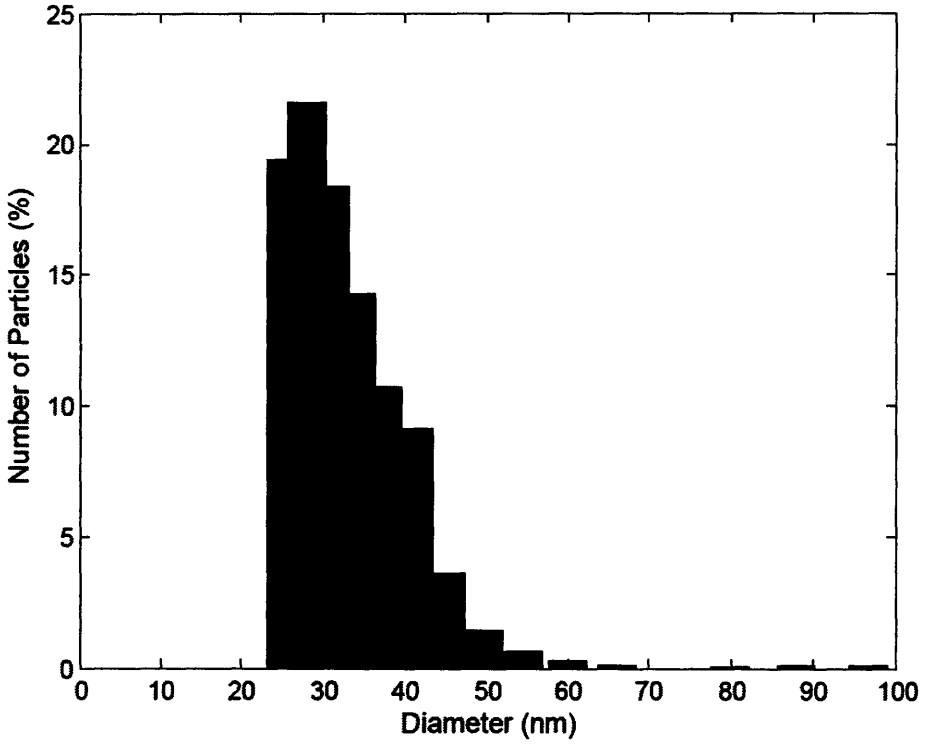

Figure 45: Nanoparticle Size Distribution after 6 hours (0.01% by volume)

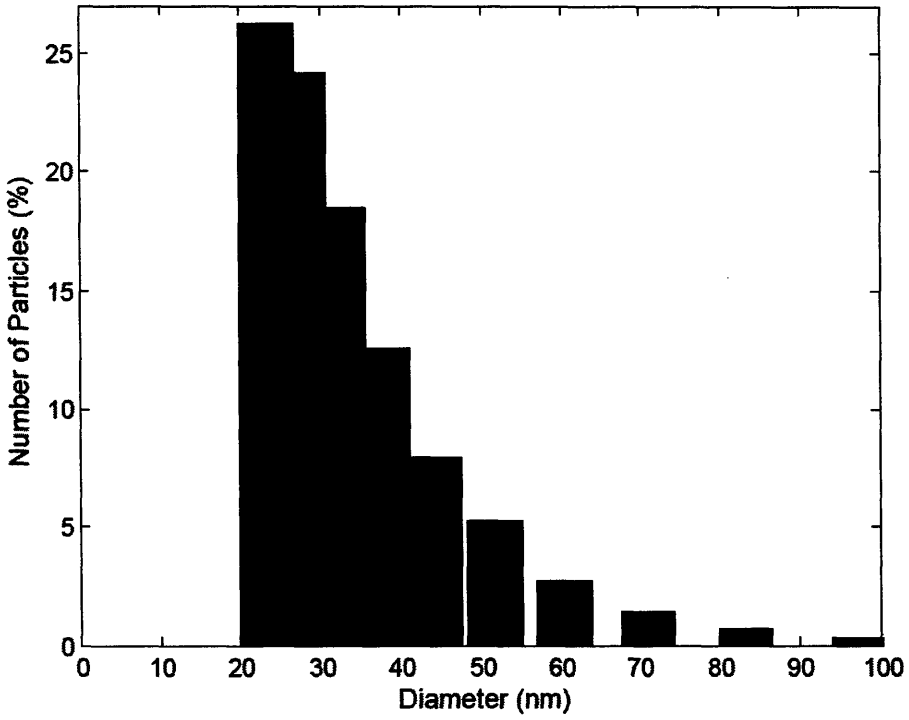

Figure 46: Nanoparticle Size Distribution after 6 hours (0.001% by volume)

Figure 47 and Figure 48 show the nanoparticle size distributions 1 day after dilution for the 0.01% and 0.001% by volume concentrations, respectively. The mean nanoparticle diameters for both of the concentrations (46.71 nm and 46.74 nm, respectively) appear to remain within the experimental uncertainty of the nanoparticle mean diameter of the concentrated nanofluid.

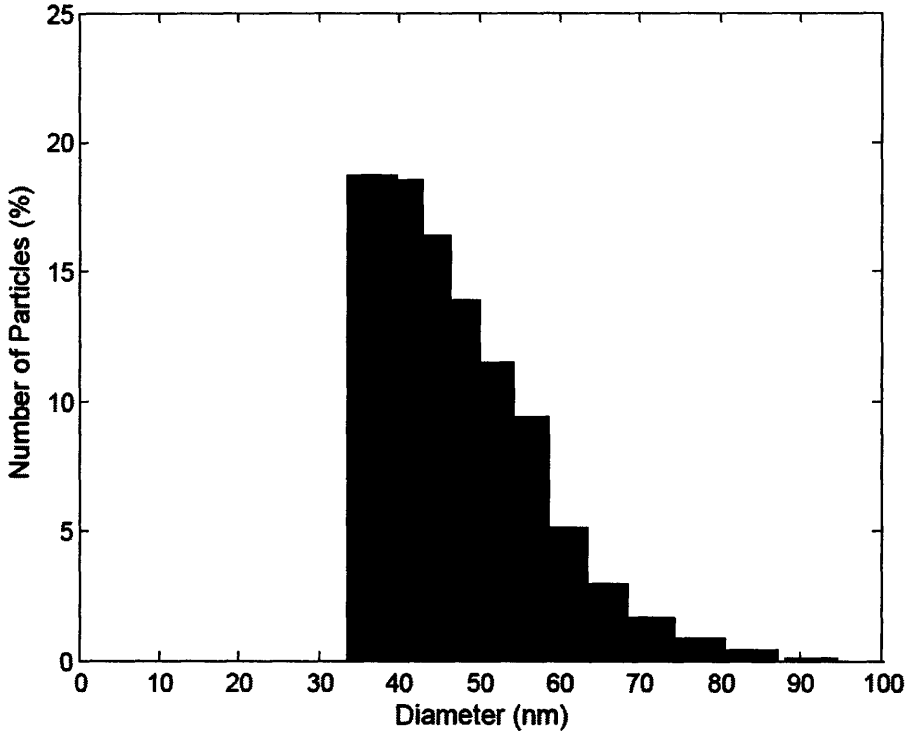

Figure 47: Nanoparticle Size Distribution after 1 day (0.01% by volume)

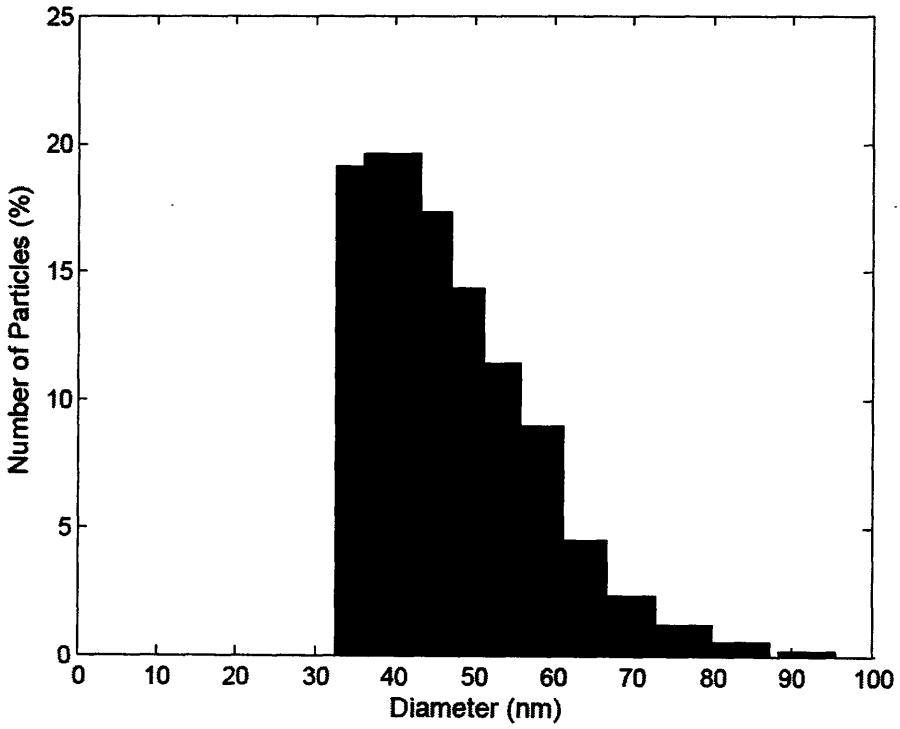

Figure 48: Nanoparticle Size Distribution after 1 day (0.001% by volume)

B.2 Variation of Concentration with the Time after Dilution

This experiment consisted of diluting the concentrated nanofluid to concentrations sufficient to see the desired CHF enhancement and then measuring the actual concentrations of the nanoparticles in solution over time. A large reduction in the concentration of the nanofluid would also indicate an unstable nanofluid.

The actual concentrations of the nanoparticles in solution were measured with an Inductively Coupled Plasma – Optical Emission Spectrometer (ICP-OES). Concentrated alumina nanofluid was first diluted from 20% by weight to the target concentrations (0.01% and 0.001% by volume). Seven samples were created at the specified times (at 0 hr, 1 hr, 6 hr, and 1 d) before a single set of measurements by the ICP-OES system were taken. The results are shown in Table XIII. This experiment confirms that the alumina nanofluids remain stable for at least 24 hours after initial dilution without significant settling of nanoparticles.

Table XIII: OES-ICP System Concentration Measurements

Sample #	Target Concentration (% by volume)	Time after initial dilution (hr)	Concentration without agglomeration (ppm of Al)	Measured Concentration (ppm of Al)	Percent Difference
1	N/A	0	2.064	1.984	-3.9%
2	0.01%	1	2.064	2.139	3.6%
3	0.001%	1	0.206	0.194	-6.0%
4	0.01%	6	2.064	2.103	1.9%
5	0.001%	6	0.206	0.211	2.2%
6	0.01%	24	2.064	2.352	13.9%
7	0.001%	24	0.206	0.244	18.2%

APPENDIX C: THERMAL HYDRAULIC MODEL SOURCE CODE

```
function [geo,dth,angle]=ap1000modinlet
dth=0.01;
i=1;
n1=floor((1.571-.149525)/dth);
n2=floor(3.826/(2.01*dth));
n=n1+n2;
geo=null(23,n);%meters
ri=2.01;
ro=2.086;
dh=dth*ri;
for i=[1:n]
   theta=(i-1)*dth+.149525;
   if theta<=1.57
      angle(i)=3.14159/2-theta;
   else
      angle(i)=0;
   end
   if i==1
      geo(1,1)=0;
      geo(2,1)=-ri;
      geo(3,1)=0;
      geo(4,1)=-2.31;
      geo(5,i)=ri*sin(theta);
      geo(6,i)=-ri*cos(theta);
      geo(7,i)=0.348;
      geo(8,i)=-2.31;
   else
      if theta<=0.29%.288674
         geo(1,i)=geo(5,i-1);
         geo(2,i)=geo(6,i-1);
         geo(3,i)=geo(7,i-1);
         geo(4,i)=geo(8,i-1);
         geo(5,i)=ri*sin(theta);
         geo(6,i)=-ri*cos(theta);
         geo(7,i)=2.31*tan(theta);
         geo(8,i)=-2.31;
      elseif theta<=0.34%0.335095
         geo(1,i)=geo(5,i-1);
         geo(2,i)=geo(6,i-1);
         geo(3,i)=geo(7,i-1);
         geo(4,i)=geo(8,i-1);
         geo(5,i)=ri*sin(theta);
         geo(6,i)=-ri*cos(theta);
         geo(7,i)=0.686;
         geo(8,i)=-0.686/tan(theta);
      elseif theta<=1.57%1.5708
         geo(1,i)=geo(5,i-1);
         geo(2,i)=geo(6,i-1);
         geo(3,i)=geo(7,i-1);
         geo(4,i)=geo(8,i-1);
```

```
        geo(5,i)=ri*sin(theta);
        geo(6,i)=-ri*cos(theta);
        geo(7,i)=ro*sin(theta);
        geo(8,i)=-ro*cos(theta);
      else
        geo(1,i)=geo(5,i-1);
        geo(2,i)=geo(6,i-1);
        geo(3,i)=geo(7,i-1);
        geo(4,i)=geo(8,i-1);
        geo(5,i)=2.01;
        geo(6,i)=(i-n1)*dh;
        geo(7,i)=2.086;
        geo(8,i)=(i-n1)*dh;
      end
    end
end
for i=[1:n]
   geo(9,i)=(geo(1,i)+geo(3,i)+geo(5,i)+geo(7,i))/4;%centroid x-coordinate
   geo(10,i)=(geo(2,i)+geo(4,i)+geo(6,i)+geo(8,i))/4;%centroid y-coordinate
   geo(11,i)=0.5*abs((geo(1,i)*geo(4,i)-geo(3,i)*geo(2,i))+(geo(3,i)*geo(8,i)-
geo(7,i)*geo(4,i))+(geo(7,i)*geo(6,i)-geo(5,i)*geo(8,i))+(geo(5,i)*geo(2,i)-geo(1,i)*geo(6,i)));%area
   geo(12,i)=geo(11,i)*6.28319*geo(9,1);%volume [m^3]
   geo(13,i)=((geo(1,i)-geo(5,i))^2+(geo(2,i)-geo(6,i))^2)^0.5;%interior length
   geo(14,i)=((geo(3,i)-geo(7,i))^2+(geo(4,i)-geo(8,i))^2)^0.5;%exterior length
   geo(15,i)=0.5*((geo(1,i)+geo(5,i)))*2*3.14159*geo(13,i);%interior area
   geo(16,i)=0.5*((geo(3,i)+geo(7,i)))*2*3.14159*geo(14,i);%exterior area
   geo(17,i)=0.5*((geo(1,i)+geo(5,i)));%interior x midpoint
   geo(18,i)=0.5*((geo(3,i)+geo(7,i)));%exterior x midpoint
   geo(19,i)=0.5*((geo(2,i)+geo(6,i)));%interior y midpoint
   geo(20,i)=0.5*((geo(4,i)+geo(8,i)));%exterior y midpoint
   geo(21,i)=((geo(17,i)-geo(18,i))^2+(geo(19,i)-geo(20,i))^2)^0.5;%hydraulic diameter, De-Di
   geo(22,i)=2*3.14159*geo(9,i)*((geo(17,i)-geo(18,i))^2+(geo(19,i)-geo(20,i))^2)^0.5;%flow area
   geo(23,i)=0.5*(geo(13,i)+geo(14,i));%characteristic length
end

%Non-Homogenous flow EPRI model (centerline entry) with acceleration term
%and AP1000 critical heat flux (T48A) with subcoooled boiling
function [flow]=flow6001(geo,mdot,dth,angle,uprate)
[rn,cn]=size(geo);
n=cn;
flow=null(7,cn);
mdot=mdot;%mass flow rate [kg/s]
multiplier=1;%nanolfluid multiplier
for j=[1:n]
   theta(j)=(j-1)*dth+.149525;
   phi(j)=(3.14159-theta(j));
   if theta(j)<=15*3.14159/180
      qdot(j)=(0.0065+(0.0160-0.0065)*(theta(j)-
5*3.14159/180)/(10*3.14159/180))*uprate;%[MW/m^2]
   elseif theta(j)<=25*3.14159/180
      qdot(j)=(0.0160+(0.0704-0.0160)*(theta(j)-
15*3.14159/180)/(10*3.14159/180))*uprate;%[MW/m^2]
   elseif theta(j)<=35*3.14159/180
      qdot(j)=(0.0704+(0.1520-0.0704)*(theta(j)-
25*3.14159/180)/(10*3.14159/180))*uprate;%[MW/m^2]
   elseif theta(j)<=45*3.14159/180
```

```
      qdot(j)=(0.1520+(0.3060-0.1520)*(theta(j)-
35*3.14159/180)/(10*3.14159/180))*uprate;%[MW/m^2]
   elseif theta(j)<=55*3.14159/180
      qdot(j)=(0.3060+(0.6050-0.3060)*(theta(j)-
45*3.14159/180)/(10*3.14159/180))*uprate;%[MW/m^2]
   elseif theta(j)<=65*3.14159/180
      qdot(j)=(0.6050+(0.8500-0.6050)*(theta(j)-
55*3.14159/180)/(10*3.14159/180))*uprate;%[MW/m^2]
   elseif theta(j)<=75*3.14159/180
      qdot(j)=(0.8500+(1.1880-0.8500)*(theta(j)-
65*3.14159/180)/(10*3.14159/180))*uprate;%[MW/m^2]
   elseif theta(j)<=85*3.14159/180
      qdot(j)=(1.1880+(1.4700-1.1880)*(theta(j)-
75*3.14159/180)/(10*3.14159/180))*uprate;%[MW/m^2]
   elseif theta(j)<=90*3.14159/180
      qdot(j)=(1.4700+(1.4700-1.1880)*(theta(j)-
85*3.14159/180)/(10*3.14159/180))*uprate;%[MW/m^2]
   else
      qdot(j)=0;
   end
   flow(27,j)=qdot(j);
end
phase=0;
walltemp(1)=373;%initial wall temperature [K]
temp(1)=373;%initial bulk temperature (of subcooled liquid) [K]
num=1;
while phase==0
   if num==1

enthalpy(num)=hf(100)*1000+qdot(num)*10^6*geo(13,num)*2*3.14159*geo(17,num)/mdot;%enth
alpy [J/kg], initial enthalpy at 373 K, 152810 Pa
      P(num)=1/vf(373-273)*9.81*(3.826-geo(10,num))+101325-0.5*mdot^2*vf(373-
273)/2/0.145209;%initial pressure in Pa minus form inlet (k=0.5)
      Dh(num)=geo(21,num);%hydraulic diameter [m], Dh=Do-Di
      hf1=461300;%saturated liquid enthalpy at 1.4 atm [J/kg]
      hfg1=2230200;%heat of vaporization at 1.4 atm [J/kg]
      tf(num)=381.865+(P(num)-137169)/(152810-137169)*(385.086-381.865);%saturated liquid
temperature [K]
      xe(num)=(enthalpy(num)-hf1)/hfg1;%equilibrium quality
      temp(num)=xe(num)*(hfg1)/4183+385;%bulk temperature of subcooled liquid [K]
      rhol(num)=998-(temp(num)-293)/80*(998-958.313);%subcooled liquid density [kg/m3]
      rhog(num)=0.59773+(P(num)-101400)/(143300-101400)*(0.82645-0.59773);
      Pr(num)=6-(temp(num)-293)/80*(6-1.76);%Prandtl number
      k(num)=0.606+(temp(num)-293)/80*(0.68-.606);%liquid conductivity
      %k(num)=Kf(temp(num)-273);%liquid conductivity
      area(num)=geo(22,num);%flow area
      Resub(num)=mdot*Dh(num)/area(num)/(279*10^-6);%Reynolds number
      h(num)=k(num)/Dh(num)*0.023*(Resub(num))^0.8*(Pr(num))^0.4;%heat transfer coefficient,
Dittus-Boelter
      walltemp(num)=qdot(num)*10^6/h(num)+temp(num);
      flow(1,num)=enthalpy(num);
      flow(2,num)=0;%quality
      flow(3,num)=0;%void fraction
      flow(4,num)=rhol(num);
      flow(6,num)=Resub(num);%Reynolds Number
```

```
flow(7,num)=0.184/(flow(6,num))^0.2*geo(23,num)/geo(21,num)*mdot^2/(2*flow(4,num)*(geo(22,
num))^2);%pressure loss
    accout(num)=0;
    accin(num)=0;
    flow(9,num)=accout(num)-accin(num);%acceleration term
    flow(20,num)=xe(num);
    flow(21,num)=temp(num);%bulk temperature
    flow(22,num)=qdot(num)*10^6*geo(13,num)*2*3.14159*geo(17,num);%power
    if theta(num)>=(3.14159/2)
      theta(num)=(3.14159/2);
      phi(num)=(3.14159/2);
    end
    SA0=(0.65444)+(-1.2018)*(Dh(num)/2)*log(mdot/geo(22,num))+(-
0.008388)/(P(num)/10^6)^2+(0.000179)*(mdot/geo(22,num))+(1.36899)*(Dh(num)/2)/(P(num)/10
^6)+(-
0.077415)*(Dh(num)/2)/(P(num)/10^6)^2+(0.024967)*(P(num)/10^6)*(log(mdot/geo(22,num)))^2;
    SA1=(-0.086511)*(log(mdot/geo(22,num)))^2+(-
4.49425)*(Dh(num)/2)*log(mdot/geo(22,num));
    SA2=(9.28489)*(Dh(num)/2);
    SA3=(-
0.0066169)*(log(mdot/geo(22,num)))^2+(11.62546)*(Dh(num)/2)*(P(num)/10^6)+(0.855759)*xe(n
um)*log(mdot/geo(22,num));
    SA4=(-1.74177)*(P(num)/10^6)+(0.182895)*log(mdot/geo(22,num))+(-
1.8898)*xe(num)+(2.2636)*(Dh(num)/2);

flow(23,num)=(SA0+SA1*xe(num)+SA2*(xe(num))^2+SA3*theta(num)+SA4*(theta(num))^2)*10^
6;%critical heat flux
    if phi(num)>=150/180*(3.14159)
        flow(25,num)=(4.8*flow(23,num))*multiplier;%nanofluid critical heat flux (multiplier% of
graph)
    elseif phi(num)>135/180*(3.14159)
        flow(25,num)=((3+(phi(num)-135/180*(3.14159))/(15/180*(3.14159))*(4.8-
3))*flow(23,num))*multiplier;
    elseif phi(num)>120/180*(3.14159)
        flow(25,num)=((2.5+(phi(num)-120/180*(3.14159))/(15/180*(3.14159))*(3-
2.5))*flow(23,num))*multiplier;
    elseif phi(num)>90/180*(3.14159)
        flow(25,num)=((2.1+(phi(num)-90/180*(3.14159))/(30/180*(3.14159))*(2.5-
2.1))*flow(23,num))*multiplier;
    else
    end
    flow(24,num)=flow(23,num)/(qdot(num)*10^6);%dnbr
    flow(26,num)=flow(25,num)/(qdot(num)*10^6);%nanofluid dnbr
    num=num+1;
  else
    enthalpy(num)=flow(1,num-
1)+qdot(num)*10^6*geo(13,num)*2*3.14159*geo(17,num)/mdot;%enthalpy [J/kg]
    P(num)=P(num-1)-flow(7,num-1)-flow(9,num-1)-1/vf(temp(num-1)-273)*9.81*(geo(10,num)-
geo(10,num-1));
    Dh(num)=geo(21,num);%hydraulic diameter [m], Dh=Do-Di
    hf1=461300;%saturated liquid enthalpy at 1.4 atm [J/kg]
    hfg1=2230200;%heat of vaporization at 1.4 atm [J/kg]
    tf(num)=381.865+(P(num)-137169)/(152810-137169)*(385.086-381.865);%saturated liquid
temperature [K]
    xe(num)=(enthalpy(num)-(hf1))/(hfg1);%equilibrium quality
```

```
    temp(num)=xe(num)*(hfg1)/4183+385;%bulk temperature of subcooled liquid [K]
    rhol(num)=998-(temp(num)-293)/80*(998-958.313);%subcooled liquid density [kg/m3]
    rhog(num)=0.59773+(P(num)-101400)/(143300-101400)*(0.82645-0.59773);
    Pr(num)=6-(temp(num)-293)/80*(6-1.76);%Prandtl number
    k(num)=0.606+(temp(num)-293)/80*(0.68-.606);%liquid conductivity
    area(num)=geo(22,num);%flow area
    Resub(num)=mdot*Dh(num)/area(num)/(279*10^-6);%Reynolds number
    h(num)=k(num)/Dh(num)*0.023*(Resub(num))^0.8*(Pr(num))^0.4;%heat transfer coefficient,
Dittus-Boelter
    walltemp(num)=qdot(num)*10^6/h(num)+temp(num);
    flow(1,num)=enthalpy(num);
    flow(2,num)=0;%quality
    flow(3,num)=0;%void fraction
    flow(4,num)=rhol(num);
    flow(6,num)=Resub(num);%Reynolds Number

flow(7,num)=0.184/(flow(6,num))^0.2*geo(23,num)/geo(21,num)*mdot^2/(2*flow(4,num)*(geo(22,
num))^2);%pressure loss
    if flow(3,num)==0
        accout(num)=2*mdot^2/(geo(22,num)+geo(22,num-
1))*(1/(rhol(num)*geo(22,num)));%acceleration out term
        accin(num)=accout(num-1);%acceleration in term
        flow(19,num)=rhol(num);
    else
        accout(num)=2*mdot^2/(geo(22,num)+geo(22,num-
1))*((flow(2,num))^2/(flow(3,num)*0.88)+(1-flow(2,num))^2/((1-
flow(3,num))*950))/geo(22,num);%acceleration out term
        accin(num)=accout(num-1);%acceleration in term
        rhop(num)=((flow(2,num))^2/(flow(3,num)*0.88)+(1-flow(2,num))^2/((1-
flow(3,num))*950))^-1;
        flow(19,num)=rhop(num);
    end
    flow(9,num)=accout(num)-accin(num);%acceleration term
    flow(20,num)=xe(num);
    flow(21,num)=temp(num);%bulk temperature
    flow(22,num)=qdot(num)*10^6*geo(13,num)*2*3.14159*geo(17,num);%power
    if theta(num)>=(3.14159/2)
      theta(num)=(3.14159/2);
      phi(num)=(3.14159/2);
    end
    SA0=(0.65444)+(-1.2018)*(Dh(num)/2)*log(mdot/geo(22,num))+(-
0.008388)/(P(num)/10^6)^2+(0.000179)*(mdot/geo(22,num))+(1.36899)*(Dh(num)/2)/(P(num)/10
^6)+(-
0.077415)*(Dh(num)/2)/(P(num)/10^6)^2+(0.024967)*(P(num)/10^6)*(log(mdot/geo(22,num)))^2;
    SA1=(-0.086511)*(log(mdot/geo(22,num)))^2+(-
4.49425)*(Dh(num)/2)*log(mdot/geo(22,num));
    SA2=(9.28489)*(Dh(num)/2);
    SA3=(-
0.0066169)*(log(mdot/geo(22,num)))^2+(11.62546)*(Dh(num)/2)*(P(num)/10^6)+(0.855759)*xe(n
um)*log(mdot/geo(22,num));
    SA4=(-1.74177)*(P(num)/10^6)+(0.182895)*log(mdot/geo(22,num))+(-
1.8898)*xe(num)+(2.2636)*(Dh(num)/2);

flow(23,num)=(SA0+SA1*xe(num)+SA2*(xe(num))^2+SA3*theta(num)+SA4*(theta(num))^2)*10^
6;%critical heat flux
    if phi(num)>=150/180*(3.14159)
```

```
        flow(25,num)=(4.8*flow(23,num))*multiplier;%nanofluid critical heat flux
    elseif phi(num)>135/180*(3.14159)
        flow(25,num)=((3+(phi(num)-135/180*(3.14159))/(15/180*(3.14159))*(4.8-
3))*flow(23,num))*multiplier;
    elseif phi(num)>120/180*(3.14159)
        flow(25,num)=((2.5+(phi(num)-120/180*(3.14159))/(15/180*(3.14159))*(3-
2.5))*flow(23,num))*multiplier;
    elseif phi(num)>90/180*(3.14159)
        flow(25,num)=((2.1+(phi(num)-90/180*(3.14159))/(30/180*(3.14159))*(2.5-
2.1))*flow(23,num))*multiplier;
    else
    end
    flow(24,num)=flow(23,num)/(qdot(num)*10^6);%dnbr
    flow(26,num)=flow(25,num)/(qdot(num)*10^6);%nanofluid dnbr
    if walltemp(num)>=tf%saturated liquid temperature at 1.5 atm [385 K]
      phase=1;
      xc=geo(9,num);
      yc=geo(10,num);
      hlonb=enthalpy(num);
      xeonb=xe(num);
    else
    end
    num=num+1;
  end
end
  for i=[num:n]
      if flow(1,i-1)<=2676100%below bulk boiling
        flow(1,i)=flow(1,i-1)+qdot(i)*10^6*geo(13,i)*2*3.14159*geo(17,i)/mdot;%enthalpy [J/kg]
        xe(i)=(flow(1,i)-hf1)/hfg1;
        Dh(i)=geo(21,i);%hydraulic diameter [m], Dh=Do-Di
        P(i)=P(i-1)-flow(7,i-1)-flow(9,i-1)-rhol(i-1)*9.81*(geo(10,i)-geo(10,i-1));
        tsat(i)=373.15+(P(i)-101400)/(152330-101400)*(385-373.15);
        tsat(num-1)=373.15+(P(num-1)-101400)/(152330-101400)*(385-373.15);
        temp(i)=xe(i)*hfg1/4183+385;%bulk temperature of subcooled liquid [K]
        if temp(i)>=tsat(i)
          temp(i)=tsat(i);
        else
        end
        rhol(i)=998-(temp(i)-293)/80*(998-958.313);%subcooled liquid density [kg/m3]
        Pr(i)=6-(temp(i)-293)/80*(6-1.76);%Prandtl number
        k(i)=0.606+(temp(i)-293)/80*(0.68-.606);%liquid conductivity
        area(i)=geo(22,i);%flow area
        Re(i)=mdot*Dh(i)/area(i)/(279*10^-6);%(1-flow(2,i-1));%Reynolds number
        h(i)=k(i)/Dh(i)*0.023*(Re(i))^0.8*(Pr(i))^0.4;%heat transfer coefficient, Dittus-Boelter
        walltemp(i)=qdot(i)*10^6/h(i)+temp(i);
        flow(3,num-1)=0;
        alphabub(num-1)=flow(3,num-2);
        alphabub(i)=flow(3,i-1);
        tlc(num-1)=tsat(num-1)-(4183*(tsat(num-1)-temp(num-1))+hfg1*flow(2,num-
1))/(4183*(1-flow(2,num-1)));
        tl(num-1)=tlc(num-1);
        dz(num-1)=geo(23,num-1);
        dz(i)=geo(23,i);
        if alphabub(num-1)<10^-5
          F4(num-1)=flow(3,num-2)*10^5;
          alphabub(num-1)=10^-5;
```

```
        else
          F4(num-1)=1;
        end
        F3(num-1)=F4(num-1);
        if alphabub(i)<10^-5
          F4(i)=flow(3,i-1)*10^5;
          alphabub(i)=10^-5;
        else
          F4(i)=1;
        end
        F3(i)=F4(i);
        rhof=955;%saturated liquid density
        rhog(i)=0.59773+(P(i)-101400)/(143300-101400)*(0.82645-0.59773);
        if alphabub(num-1)<0.25
          vflux(num-1)=mdot/rhol(num-1)/area(num-1)/(1-flow(2,num-2));
          if abs(vflux(num-1))>0.61
            phihif(num-1)=(1.639344*abs(vflux(num-1)))^0.47;
          else
            phihif(num-1)=1;
          end
          C(num-1)=65-(5.69*10^-5)*(P(num-1)-10^5);
          F5(num-1)=1.8*phihif(num-1)*C(num-1)*exp(-45*alphabub(num-1))+0.075;
        else
          F5(num-1)=0.075;
        end
        Hif(num-1)=(F3(num-1)*F5(num-1)*hfg1*rhog(num-1)*rhof*alphabub(num-1))/(rhof-
rhog(num-1));
        if alphabub(i)<0.25
          vflux(i)=mdot/rhol(i)/area(i)/(1-flow(2,i-1));
          if abs(vflux(i))>0.61
            phihif(i)=(1.639344*abs(vflux(i)))^0.47;
          else
            phihif(i)=1;
          end
          C(i)=65-(5.69*10^-5)*(P(i)-10^5);
          F5(i)=1.8*phihif(i)*C(i)*exp(-45*alphabub(i))+0.075;
        else
          F5(i)=0.075;
        end
        Hif(i)=(F3(i)*F5(i)*hfg1*rhog(i)*rhof*alphabub(i))/(rhof-rhog(i));
        if qdot(i)==0
          if tl(i-1)>=temp(i-1)
            tl(i)=tl(i-1);
            flow(2,i)=flow(2,i-1);
          else
            tl(i)=tl(i-1)+(Hif(i-1)*(tsat(i-1)-tl(i-1))*area(i-1)*dz(i-1))/((1-flow(2,i-1))*mdot*4183);
            collapse=300;
            flow(2,i)=flow(2,i-1)-(Hif(i-1)*(tsat(i-1)-tl(i-1))*collapse*area(i-1)*dz(i-
1))/(mdot*hfg1);
            if flow(2,i)<=0
              flow(2,i)=0;
            else
            end
          end
        else
          tl(i)=tlc(i-1);
```

```
    flow(2,i)=xe(i)-xeonb*exp((xe(i)/xeonb)-1);%quality, Levy Model
  end
  hf2(i)=(419.04+(tsat(i)-373)/10*(461.30-419.04))*1000;
  hfg2(i)=(2257+(tsat(i)-373)/10*(2230.2-2257))*1000;
  if hf2(i)<=flow(1,i)
      flow(2,i)=(flow(1,i)-hf2(i))/(hfg2(i));
  else
  end
  onephvis=0.000281832;%one phase viscosity
  onephden(i)=rhol(i);%one phase density
  onephre(i)=mdot*geo(21,i)/(geo(22,i)*onephvis);%one phase Re
  [flow(3,i),jg(i),jf(i),c0(i)]=epri(flow(2,i),mdot,geo(22,i),angle(i),geo(21,i));
  flow(4,i)=flow(3,i)*rhog(i)+(1-flow(3,i))*onephden(i);%density [kg/m^3]
  flow(5,i)=flow(3,i)*0.000012+(1-flow(3,i))*0.000281832;%viscosity [N*s/m^2]
  flow(6,i)=mdot*geo(21,i)/(geo(22,i)*flow(5,i));%Reynolds Number
  flow(8,i)=onephre(i);
  if flow(3,i)==0
    flow(10,i)=100000;
  else
    flow(10,i)=jg(i)/jf(i)*(1-flow(3,i))/flow(3,i);%slip ratio
  end
  flow(11,i)=jg(i);
  flow(12,i)=jf(i);
  flow(13,i)=jg(i)/jf(i);
  flow(16,i)=[1+flow(2,i)*(onephden(i)/.59773-1)];
  rhobar=(flow(2,i)/rhog(i)+(1-flow(2,i))/onephden(i))^-1;
  We=mdot^2*geo(21,i)/((geo(22,i))^2*rhobar*0.0589);
  Fr=mdot^2/(9.81*geo(21,i)*(rhobar)^2*(geo(22,i))^2);
  A1=(1-flow(2,i))^2+((flow(2,i))^2)*(onephden(i)/0.59773)*(0.0000012/0.000281832)^0.2;
  A2=(flow(2,i))^0.78*(1-flow(2,i))^0.224;
  A3=(onephden(i)/rhog(i))^0.91*(0.0000012/0.000281832)^0.19*(1-
0.0000012/0.000281832)^0.7;
  flow(18,i)=A1+3.24*A2*A3/(Fr^0.045*We^0.035);%two phase flow friction factor Friedel
correlation

flow(7,i)=0.184/onephre(i)^0.2*geo(23,i)/geo(21,i)*mdot^2/(2*onephden(i)*(geo(22,i))^2)*flow(18,i)
;%pressure loss
  if flow(3,i)==0
    accout(i)=2*mdot^2/(geo(22,i)+geo(22,i-
1))*(1/(onephden(i)*geo(22,i)));%acceleration out term
    accin(i)=accout(i-1);%acceleration in term
    flow(19,i)=rhol(i);
  else
    accout(i)=2*mdot^2/(geo(22,i)+geo(22,i-1))*((flow(2,i))^2/(flow(3,i)*rhog(i))+(1-
flow(2,i))^2/((1-flow(3,i))*onephden(i)))/geo(22,i);%acceleration out term
    accin(i)=accout(i-1);%acceleration in term
    rhop(i)=((flow(2,i))^2/(flow(3,i)*rhog(i))+(1-flow(2,i))^2/((1-flow(3,i))*onephden(i)))^-1;
    flow(19,i)=rhop(i);
  end
  flow(9,i)=accout(i)-accin(i);%acceleration pressure loss
  flow(20,i)=xe(i);
  if flow(20,i)<=0
    flow(21,i)=temp(i);%bulk temperature
  else
    flow(21,i)=373;
  end
```

```
            flow(22,i)=qdot(i)*10^6*geo(13,i)*2*3.14159*geo(17,i);%power
            tlc(i)=tsat(i)-(4183*(tsat(i)-temp(i))+hfg1*flow(2,i))/(4183*(1-flow(2,i)));
            if theta(i)>=(3.14159/2)
               theta(i)=(3.14159/2);
               phi(i)=(3.14159/2);
            end
            SA0=(0.65444)+(-1.2018)*(Dh(i)/2)*log(mdot/geo(22,i))+(-
0.008388)/(P(i)/10^6)^2+(0.000179)*(mdot/geo(22,i))+(1.36899)*(Dh(i)/2)/(P(i)/10^6)+(-
0.077415)*(Dh(i)/2)/(P(i)/10^6)^2+(0.024967)*(P(i)/10^6)*(log(mdot/geo(22,i)))^2;
            SA1=(-0.086511)*(log(mdot/geo(22,i)))^2+(-4.49425)*(Dh(i)/2)*log(mdot/geo(22,i));
            SA2=(9.28489)*(Dh(i)/2);
            SA3=(-
0.0066169)*(log(mdot/geo(22,i)))^2+(11.62546)*(Dh(i)/2)*(P(i)/10^6)+(0.855759)*xe(i)*log(mdot/g
eo(22,i));
            SA4=(-1.74177)*(P(i)/10^6)+(0.182895)*log(mdot/geo(22,i))+(-
1.8898)*xe(i)+(2.2636)*(Dh(i)/2);

flow(23,i)=(SA0+SA1*xe(i)+SA2*(flow(2,i))^2+SA3*xe(i)+SA4*(theta(i))^2)*10^6;%critical heat flux
            if phi(i)>=150/180*(3.14159)
               flow(25,i)=(4.8*flow(23,i))*multiplier;%nanofluid critical heat flux
            elseif phi(i)>135/180*(3.14159)
               flow(25,i)=((3+(phi(i)-135/180*(3.14159))/(15/180*(3.14159))*(4.8-
3))*flow(23,i))*multiplier;
            elseif phi(i)>120/180*(3.14159)
               flow(25,i)=((2.5+(phi(i)-120/180*(3.14159))/(15/180*(3.14159))*(3-
2.5))*flow(23,i))*multiplier;
            elseif phi(i)>90/180*(3.14159)
               flow(25,i)=((2.1+(phi(i)-90/180*(3.14159))/(30/180*(3.14159))*(2.5-
2.1))*flow(23,i))*multiplier;
            else
            end
            if qdot(i)==0
               flow(24,i)=25;
               flow(26,i)=25;
            else
               flow(24,i)=flow(23,i)/(qdot(i)*10^6);%dnbr
               flow(26,i)=flow(25,i)/(qdot(i)*10^6);%nanofluid dnbr
            end
         else
            bulkboiling=1
         end
      end
flow(14,:)=geo(22,:);
flow(15,:)=c0;
flow(17,1)=cn;

%Non-Homogenous flow EPRI model (centerline entry) with acceleration term
%and AP1000 critical heat flux (T40B) with subcoooled boiling
function [flow]=flow6002(geo,mdot,dth,angle,uprate)
[rn,cn]=size(geo);
n=cn;
flow=null(7,cn);
mdot=mdot;%mass flow rate [kg/s]
multiplier=1;%nanolfluid multiplier
for j=[1:n]
   theta(j)=(j-1)*dth+.149525;
```

```
  phi(j)=(3.14159-theta(j));
  if theta(j)<=15*3.14159/180
     qdot(j)=(0.65*.02+(0.80*.05-0.65*.02)*(theta(j)-
5*3.14159/180)/(10*3.14159/180))*uprate;%[MW/m^2]
  elseif theta(j)<=25*3.14159/180
     qdot(j)=(0.80*.05+(0.88*.13-0.80*.05)*(theta(j)-
15*3.14159/180)/(10*3.14159/180))*uprate;%[MW/m^2]
  elseif theta(j)<=35*3.14159/180
     qdot(j)=(0.88*.13+(0.95*.25-0.88*.13)*(theta(j)-
25*3.14159/180)/(10*3.14159/180))*uprate;%[MW/m^2]
  elseif theta(j)<=45*3.14159/180
     qdot(j)=(0.95*.25+(1.02*.57-0.95*.25)*(theta(j)-
35*3.14159/180)/(10*3.14159/180))*uprate;%[MW/m^2]
  elseif theta(j)<=55*3.14159/180
     qdot(j)=(1.02*.57+(1.1*.72-1.02*.57)*(theta(j)-
45*3.14159/180)/(10*3.14159/180))*uprate;%[MW/m^2]
  elseif theta(j)<=65*3.14159/180
     qdot(j)=(1.1*.72+(1.25*.85-1.1*.72)*(theta(j)-
55*3.14159/180)/(10*3.14159/180))*uprate;%[MW/m^2]
  elseif theta(j)<=75*3.14159/180
     qdot(j)=(1.25*.85+(1.35*.70-1.25*.85)*(theta(j)-
65*3.14159/180)/(10*3.14159/180))*uprate;%[MW/m^2]
  elseif theta(j)<=85*3.14159/180
     qdot(j)=(1.35*.70+(1.47*.72-1.35*.70)*(theta(j)-
75*3.14159/180)/(10*3.14159/180))*uprate;%[MW/m^2]
  elseif theta(j)<=90*3.14159/180
     qdot(j)=(1.47*.72+(1.47*.72-1.35*.70)*(theta(j)-
85*3.14159/180)/(10*3.14159/180))*uprate;%[MW/m^2]
  else
     qdot(j)=0*uprate;
  end
  flow(27,j)=qdot(j);
end
phase=0;
walltemp(1)=373;%initial wall temperature [K]
temp(1)=373;%initial bulk temperature (of subcooled liquid) [K]
num=1;
while phase==0
  if num==1

enthalpy(num)=hf(100)*1000+qdot(num)*10^6*geo(13,num)*2*3.14159*geo(17,num)/mdot;%enth
alpy [J/kg], initial enthalpy at 373 K, 152810 Pa
     P(num)=1/vf(373-273)*9.81*(3.826-geo(10,num))+101325-0.5*mdot^2*vf(373-
273)/2/0.145209;%initial pressure in Pa minus form inlet (k=0.5)
     Dh(num)=geo(21,num);%hydraulic diameter [m], Dh=Do-Di
     hf1=461300;%saturated liquid enthalpy at 1.4 atm [J/kg]
     hfg1=2230200;%heat of vaporization at 1.4 atm [J/kg]
     tf(num)=381.865+(P(num)-137169)/(152810-137169)*(385.086-381.865);%saturated liquid
temperature [K]
     xe(num)=(enthalpy(num)-hf1)/hfg1;%equilibrium quality
     temp(num)=xe(num)*(hfg1)/4183+385;%bulk temperature of subcooled liquid [K]
     rhol(num)=998-(temp(num)-293)/80*(998-958.313);%subcooled liquid density [kg/m3]
     rhog(num)=0.59773+(P(num)-101400)/(143300-101400)*(0.82645-0.59773);
     Pr(num)=6-(temp(num)-293)/80*(6-1.76);%Prandtl number
     k(num)=0.606+(temp(num)-293)/80*(0.68-.606);%liquid conductivity
     %k(num)=Kf(temp(num)-273);%liquid conductivity
```

```
      area(num)=geo(22,num);%flow area
      Resub(num)=mdot*Dh(num)/area(num)/(279*10^-6);%Reynolds number
      h(num)=k(num)/Dh(num)*0.023*(Resub(num))^0.8*(Pr(num))^0.4;%heat transfer coefficient,
Dittus-Boelter
      walltemp(num)=qdot(num)*10^6/h(num)+temp(num);
      flow(1,num)=enthalpy(num);
      flow(2,num)=0;%quality
      flow(3,num)=0;%void fraction
      flow(4,num)=rhol(num);
      flow(6,num)=Resub(num);%Reynolds Number

flow(7,num)=0.184/(flow(6,num))^0.2*geo(23,num)/geo(21,num)*mdot^2/(2*flow(4,num)*(geo(22,
num))^2);%pressure loss
      accout(num)=0;
      accin(num)=0;
      flow(9,num)=accout(num)-accin(num);%acceleration term
      flow(20,num)=xe(num);
      flow(21,num)=temp(num);%bulk temperature
      flow(22,num)=qdot(num)*10^6*geo(13,num)*2*3.14159*geo(17,num);%power
      if theta(num)>=(3.14159/2)
         theta(num)=(3.14159/2);
         phi(num)=(3.14159/2);
      end
      SA0=(0.65444)+(-1.2018)*0.076*log(mdot/geo(22,num))+(-
0.008388)/(0.1)^2+(0.000179)*(mdot/geo(22,num))+(1.36899)*0.076/0.1+(-
0.077415)*0.076/(0.1)^2+(0.024967)*0.1*(log(mdot/geo(22,num)))^2;
      SA1=(-0.086511)*(log(mdot/geo(22,num)))^2+(-4.49425)*0.076*log(mdot/geo(22,num));
      SA2=(9.28489)*0.076;
      SA3=(-
0.0066169)*(log(mdot/geo(22,num)))^2+(11.62546)*0.076*0.1+(0.855759)*xe(num)*log(mdot/geo
(22,num));
      SA4=(-1.74177)*0.1+(0.182895)*log(mdot/geo(22,num))+(-
1.8898)*xe(num)+(2.2636)*0.076;

flow(23,num)=(SA0+SA1*xe(num)+SA2*(xe(num))^2+SA3*theta(num)+SA4*(theta(num))^2)*10^
6;%critical heat flux
      if phi(num)>=150/180*(3.14159)
           flow(25,num)=(4.8*flow(23,num))*multiplier;%nanofluid critical heat flux (multiplier% of
graph)
      elseif phi(num)>135/180*(3.14159)
           flow(25,num)=((3+(phi(num)-135/180*(3.14159))/(15/180*(3.14159))*(4.8-
3))*flow(23,num))*multiplier;
      elseif phi(num)>120/180*(3.14159)
           flow(25,num)=((2.5+(phi(num)-120/180*(3.14159))/(15/180*(3.14159))*(3-
2.5))*flow(23,num))*multiplier;
      elseif phi(num)>90/180*(3.14159)
           flow(25,num)=((2.1+(phi(num)-90/180*(3.14159))/(30/180*(3.14159))*(2.5-
2.1))*flow(23,num))*multiplier;
      else
      end
      flow(24,num)=flow(23,num)/(qdot(num)*10^6);%dnbr
      flow(26,num)=flow(25,num)/(qdot(num)*10^6);%nanofluid dnbr
      num=num+1;
   else
      enthalpy(num)=flow(1,num-
1)+qdot(num)*10^6*geo(13,num)*2*3.14159*geo(17,num)/mdot;%enthalpy [J/kg]
```

```
    P(num)=P(num-1)-flow(7,num-1)-flow(9,num-1)-1/vf(temp(num-1)-273)*9.81*(geo(10,num)-
geo(10,num-1));
    %P(num)=P(num-1)-1/vf(temp(num-1)-273)*9.81*(geo(10,num)-geo(10,num-1));
    Dh(num)=geo(21,num);%hydraulic diameter [m], Dh=Do-Di
    hf1=461300;%saturated liquid enthalpy at 1.4 atm [J/kg]
    hfg1=2230200;%heat of vaporization at 1.4 atm [J/kg]
    tf(num)=381.865+(P(num)-137169)/(152810-137169)*(385.086-381.865);%saturated liquid
temperature [K]
    xe(num)=(enthalpy(num)-(hf1))/(hfg1);%equilibrium quality
    temp(num)=xe(num)*(hfg1)/4183+385;%bulk temperature of subcooled liquid [K]
    rhol(num)=998-(temp(num)-293)/80*(998-958.313);%subcooled liquid density [kg/m3]
    rhog(num)=0.59773+(P(num)-101400)/(143300-101400)*(0.82645-0.59773);
    Pr(num)=6-(temp(num)-293)/80*(6-1.76);%Prandtl number
    k(num)=0.606+(temp(num)-293)/80*(0.68-.606);%liquid conductivity
    %k(num)=Kf(temp(num)-273);%liquid conductivity
    area(num)=geo(22,num);%flow area
    Resub(num)=mdot*Dh(num)/area(num)/(279*10^-6);%Reynolds number
    h(num)=k(num)/Dh(num)*0.023*(Resub(num))^0.8*(Pr(num))^0.4;%heat transfer coefficient,
Dittus-Boelter
    walltemp(num)=qdot(num)*10^6/h(num)+temp(num);
    flow(1,num)=enthalpy(num);
    flow(2,num)=0;%quality
    flow(3,num)=0;%void fraction
    flow(4,num)=rhol(num);
    flow(6,num)=Resub(num);%Reynolds Number

flow(7,num)=0.184/(flow(6,num))^0.2*geo(23,num)/geo(21,num)*mdot^2/(2*flow(4,num)*(geo(22,
num))^2);%pressure loss
    if flow(3,num)==0
        accout(num)=2*mdot^2/(geo(22,num)+geo(22,num-
1))*(1/(rhol(num)*geo(22,num)));%acceleration out term
        accin(num)=accout(num-1);%acceleration in term
        flow(19,num)=rhol(num);
    else
        accout(num)=2*mdot^2/(geo(22,num)+geo(22,num-
1))*((flow(2,num))^2/(flow(3,num)*0.88)+(1-flow(2,num))^2/((1-
flow(3,num))*950))/geo(22,num);%acceleration out term
        accin(num)=accout(num-1);%acceleration in term
        rhop(num)=((flow(2,num))^2/(flow(3,num)*0.88)+(1-flow(2,num))^2/((1-
flow(3,num))*950))^-1;
        flow(19,num)=rhop(num);
    end
    flow(9,num)=accout(num)-accin(num);%acceleration term
    flow(20,num)=xe(num);
    flow(21,num)=temp(num);%bulk temperature
    flow(22,num)=qdot(num)*10^6*geo(13,num)*2*3.14159*geo(17,num);%power
    if theta(num)>=(3.14159/2)
      theta(num)=(3.14159/2);
      phi(num)=(3.14159/2);
    end
    SA0=(0.65444)+(-1.2018)*0.076*log(mdot/geo(22,num))+(-
0.008388)/(0.1)^2+(0.000179)*(mdot/geo(22,num))+(1.36899)*0.076/0.1+(-
0.077415)*0.076/(0.1)^2+(0.024967)*0.1*(log(mdot/geo(22,num)))^2;
    SA1=(-0.086511)*(log(mdot/geo(22,num)))^2+(-4.49425)*0.076*log(mdot/geo(22,num));
    SA2=(9.28489)*0.076;
```

```
    SA3=(-
0.0066169)*(log(mdot/geo(22,num)))^2+(11.62546)*0.076*0.1+(0.855759)*xe(num)*log(mdot/geo
(22,num));
    SA4=(-1.74177)*0.1+(0.182895)*log(mdot/geo(22,num))+(-
1.8898)*xe(num)+(2.2636)*0.076;

flow(23,num)=(SA0+SA1*xe(num)+SA2*(xe(num))^2+SA3*theta(num)+SA4*(theta(num))^2)*10^
6;%critical heat flux
    if phi(num)>=150/180*(3.14159)
        flow(25,num)=(4.8*flow(23,num))*multiplier;%nanofluid critical heat flux
    elseif phi(num)>135/180*(3.14159)
        flow(25,num)=((3+(phi(num)-135/180*(3.14159))/(15/180*(3.14159))*(4.8-
3))*flow(23,num))*multiplier;
    elseif phi(num)>120/180*(3.14159)
        flow(25,num)=((2.5+(phi(num)-120/180*(3.14159))/(15/180*(3.14159))*(3-
2.5))*flow(23,num))*multiplier;
    elseif phi(num)>90/180*(3.14159)
        flow(25,num)=((2.1+(phi(num)-90/180*(3.14159))/(30/180*(3.14159))*(2.5-
2.1))*flow(23,num))*multiplier;
    else
    end
    flow(24,num)=flow(23,num)/(qdot(num)*10^6);%dnbr
    flow(26,num)=flow(25,num)/(qdot(num)*10^6);%nanofluid dnbr
    if walltemp(num)>=tf%saturated liquid temperature at 1.5 atm [385 K]
      phase=1;
      xc=geo(9,num);
      yc=geo(10,num);
      hlonb=enthalpy(num);
      xeonb=xe(num);
    else
    end
    num=num+1;
  end
end
  for i=[num:n]
      if flow(1,i-1)<=2676100%below bulk boiling
        flow(1,i)=flow(1,i-1)+qdot(i)*10^6*geo(13,i)*2*3.14159*geo(17,i)/mdot;%enthalpy [J/kg]
        xe(i)=(flow(1,i)-hf1)/hfg1;
        Dh(i)=geo(21,i);%hydraulic diameter [m], Dh=Do-Di
        P(i)=P(i-1)-flow(7,i-1)-flow(9,i-1)-rhol(i-1)*9.81*(geo(10,i)-geo(10,i-1));
        tsat(i)=373.15+(P(i)-101400)/(152330-101400)*(385-373.15);
        tsat(num-1)=373.15+(P(num-1)-101400)/(152330-101400)*(385-373.15);
        temp(i)=xe(i)*hfg1/4183+385;%bulk temperature of subcooled liquid [K]
        if temp(i)>=tsat(i)
          temp(i)=tsat(i);
        else
        end
        rhol(i)=998-(temp(i)-293)/80*(998-958.313);%subcooled liquid density [kg/m3]
        Pr(i)=6-(temp(i)-293)/80*(6-1.76);%Prandtl number
        k(i)=0.606+(temp(i)-293)/80*(0.68-.606);%liquid conductivity
        area(i)=geo(22,i);%flow area
        Re(i)=mdot*Dh(i)/area(i)/(279*10^-6);%(1-flow(2,i-1));%Reynolds number
        h(i)=k(i)/Dh(i)*0.023*(Re(i))^0.8*(Pr(i))^0.4;%heat transfer coefficient, Dittus-Boelter
        walltemp(i)=qdot(i)*10^6/h(i)+temp(i);
        flow(3,num-1)=0;
        alphabub(num-1)=flow(3,num-2);
```

```
            alphabub(i)=flow(3,i-1);
            tlc(num-1)=tsat(num-1)-(4183*(tsat(num-1)-temp(num-1))+hfg1*flow(2,num-
1))/(4183*(1-flow(2,num-1)));
            tl(num-1)=tlc(num-1);
            dz(num-1)=geo(23,num-1);
            dz(i)=geo(23,i);
            if alphabub(num-1)<10^-5
               F4(num-1)=flow(3,num-2)*10^5;
               alphabub(num-1)=10^-5;
            else
               F4(num-1)=1;
            end
            F3(num-1)=F4(num-1);
            if alphabub(i)<10^-5
               F4(i)=flow(3,i-1)*10^5;
               alphabub(i)=10^-5;
            else
               F4(i)=1;
            end
            F3(i)=F4(i);
            rhof=955;%saturated liquid density
            rhog(i)=0.59773+(P(i)-101400)/(143300-101400)*(0.82645-0.59773);
            if alphabub(num-1)<0.25
               vflux(num-1)=mdot/rhol(num-1)/area(num-1)/(1-flow(2,num-2));
               if abs(vflux(num-1))>0.61
                  phihif(num-1)=(1.639344*abs(vflux(num-1)))^0.47;
               else
                  phihif(num-1)=1;
               end
               C(num-1)=65-(5.69*10^-5)*(P(num-1)-10^5);
               F5(num-1)=1.8*phihif(num-1)*C(num-1)*exp(-45*alphabub(num-1))+0.075;
            else
               F5(num-1)=0.075;
            end
            Hif(num-1)=(F3(num-1)*F5(num-1)*hfg1*rhog(num-1)*rhof*alphabub(num-1))/(rhof-
rhog(num-1));
            if alphabub(i)<0.25
               vflux(i)=mdot/rhol(i)/area(i)/(1-flow(2,i-1));
               if abs(vflux(i))>0.61
                  phihif(i)=(1.639344*abs(vflux(i)))^0.47;
               else
                  phihif(i)=1;
               end
               C(i)=65-(5.69*10^-5)*(P(i)-10^5);
               F5(i)=1.8*phihif(i)*C(i)*exp(-45*alphabub(i))+0.075;
            else
               F5(i)=0.075;
            end
            Hif(i)=(F3(i)*F5(i)*hfg1*rhog(i)*rhof*alphabub(i))/(rhof-rhog(i));
            if qdot(i)==0
               if tl(i-1)>=temp(i-1)
                  tl(i)=tl(i-1);
                  flow(2,i)=flow(2,i-1);
               else
                  tl(i)=tl(i-1)+(Hif(i-1)*(tsat(i-1)-tl(i-1))*area(i-1)*dz(i-1))/((1-flow(2,i-1))*mdot*4183);
                  collapse=300;
```

```
                flow(2,i)=flow(2,i-1)-(Hif(i-1)*(tsat(i-1)-tl(i-1))*collapse*area(i-1)*dz(i-
1))/(mdot*hfg1);
                if flow(2,i)<=0
                   flow(2,i)=0;
                else
                end
             end
          else
             tl(i)=tlc(i-1);
             flow(2,i)=xe(i)-xeonb*exp((xe(i)/xeonb)-1);%quality, Levy Model
          end
          hf2(i)=(419.04+(tsat(i)-373)/10*(461.30-419.04))*1000;
          hfg2(i)=(2257+(tsat(i)-373)/10*(2230.2-2257))*1000;
          if hf2(i)<=flow(1,i)
               flow(2,i)=(flow(1,i)-hf2(i))/(hfg2(i));
          else
          end
          onephvis=0.000281832;%one phase viscosity
          onephden(i)=rhol(i);%one phase density
          onephre(i)=mdot*geo(21,i)/(geo(22,i)*onephvis);%one phase Re
          [flow(3,i),jg(i),jf(i),c0(i)]=epri(flow(2,i),mdot,geo(22,i),angle(i),geo(21,i));
          flow(4,i)=flow(3,i)*rhog(i)+(1-flow(3,i))*onephden(i);%density [kg/m^3]
          flow(5,i)=flow(3,i)*0.000012+(1-flow(3,i))*0.000281832;%viscosity [N*s/m^2]
          flow(6,i)=mdot*geo(21,i)/(geo(22,i)*flow(5,i));%Reynolds Number
          flow(8,i)=onephre(i);
          if flow(3,i)==0
             flow(10,i)=100000;
          else
             flow(10,i)=jg(i)/jf(i)*(1-flow(3,i))/flow(3,i);%slip ratio
          end
          flow(11,i)=jg(i);
          flow(12,i)=jf(i);
          flow(13,i)=jg(i)/jf(i);
          flow(16,i)=[1+flow(2,i)*(onephden(i)/.59773-1)];
          rhobar=(flow(2,i)/0.59773+(1-flow(2,i))/onephden(i))^-1;
          We=mdot^2*geo(21,i)/((geo(22,i))^2*rhobar*0.0589);
          Fr=mdot^2/(9.81*geo(21,i)*(rhobar)^2*(geo(22,i))^2);
          A1=(1-flow(2,i))^2+((flow(2,i))^2)*(onephden(i)/0.59773)*(0.0000012/0.000281832)^0.2;
          A2=(flow(2,i))^0.78*(1-flow(2,i))^0.224;
          A3=(onephden(i)/0.59773)^0.91*(0.0000012/0.000281832)^0.19*(1-
0.0000012/0.000281832)^0.7;
          flow(18,i)=A1+3.24*A2*A3/(Fr^0.045*We^0.035);%two phase flow friction factor Friedel
correlation

flow(7,i)=0.184/onephre(i)^0.2*geo(23,i)/geo(21,i)*mdot^2/(2*onephden(i)*(geo(22,i))^2)*flow(18,i)
;%pressure loss
          if flow(3,i)==0
             accout(i)=2*mdot^2/(geo(22,i)+geo(22,i-
1))*(1/(onephden(i)*geo(22,i)));%acceleration out term
             accin(i)=accout(i-1);%acceleration in term
             flow(19,i)=rhol(i);
          else
             accout(i)=2*mdot^2/(geo(22,i)+geo(22,i-1))*((flow(2,i))^2/(flow(3,i)*rhog(i))+(1-
flow(2,i))^2/((1-flow(3,i))*onephden(i)))/geo(22,i);%acceleration out term
             accin(i)=accout(i-1);%acceleration in term
             rhop(i)=((flow(2,i))^2/(flow(3,i)*rhog(i))+(1-flow(2,i))^2/((1-flow(3,i))*onephden(i)))^-1;
```

```
            flow(19,i)=rhop(i);
          end
          flow(9,i)=accout(i)-accin(i);%acceleration pressure loss
          flow(20,i)=xe(i);
          if flow(20,i)<=0
            flow(21,i)=temp(i);%bulk temperature
          else
            flow(21,i)=373;
          end
          flow(22,i)=qdot(i)*10^6*geo(13,i)*2*3.14159*geo(17,i);%power
          tlc(i)=tsat(i)-(4183*(tsat(i)-temp(i))+hfg1*flow(2,i))/(4183*(1-flow(2,i)));
          if theta(i)>=(3.14159/2)
            theta(i)=(3.14159/2);
            phi(i)=(3.14159/2);
          end
          SA0=(0.65444)+(-1.2018)*0.076*log(mdot/geo(22,i))+(-
0.008388)/(0.1)^2+(0.000179)*(mdot/geo(22,i))+(1.36899)*0.076/0.1+(-
0.077415)*0.076/(0.1)^2+(0.024967)*0.1*(log(mdot/geo(22,i)))^2;
          SA1=(-0.086511)*(log(mdot/geo(22,i)))^2+(-4.49425)*0.076*log(mdot/geo(22,i));
          SA2=(9.28489)*0.076;
          SA3=(-
0.0066169)*(log(mdot/geo(22,i)))^2+(11.62546)*0.076*0.1+(0.855759)*xe(i)*log(mdot/geo(22,i));
          SA4=(-1.74177)*0.1+(0.182895)*log(mdot/geo(22,i))+(-1.8898)*xe(i)+(2.2636)*0.076;
          flow(23,i)=(SA0+SA1*xe(i)+SA2*(xe(i))^2+SA3*theta(i)+SA4*(theta(i))^2)*10^6;%critical
heat flux
          if phi(i)>=150/180*(3.14159)
            flow(25,i)=(4.8*flow(23,i))*multiplier;%nanofluid critical heat flux
          elseif phi(i)>135/180*(3.14159)
            flow(25,i)=((3+(phi(i)-135/180*(3.14159))/(15/180*(3.14159))*(4.8-
3))*flow(23,i))*multiplier;
          elseif phi(i)>120/180*(3.14159)
            flow(25,i)=((2.5+(phi(i)-120/180*(3.14159))/(15/180*(3.14159))*(3-
2.5))*flow(23,i))*multiplier;
          elseif phi(i)>90/180*(3.14159)
            flow(25,i)=((2.1+(phi(i)-90/180*(3.14159))/(30/180*(3.14159))*(2.5-
2.1))*flow(23,i))*multiplier;
          else
          end
          if qdot(i)==0
            flow(24,i)=25;
            flow(26,i)=25;
          else
            flow(24,i)=flow(23,i)/(qdot(i)*10^6);%dnbr
            flow(26,i)=flow(25,i)/(qdot(i)*10^6);%nanofluid dnbr
          end
        else
          bulkboiling=1
        end
      end
flow(14,:)=geo(22,:);
flow(15,:)=c0;
flow(17,1)=cn;

%Non-Homogenous flow EPRI model (centerline entry) with acceleration term
%and AP1000 critical heat flux (T40D) with subcoooled boiling
function [flow]=flow6003(geo,mdot,dth,angle,uprate)
```

```
[rn,cn]=size(geo);
n=cn;
flow=null(7,cn);
mdot=mdot;%mass flow rate [kg/s]
multiplier=1;%nanolfluid multiplier
for j=[1:n]
   theta(j)=(j-1)*dth+.149525;
   phi(j)=(3.14159-theta(j));
   if theta(j)<=15*3.14159/180
      qdot(j)=(0.65*.02+(0.80*.05-0.65*.02)*(theta(j)-
5*3.14159/180)/(10*3.14159/180))*uprate;%[MW/m^2]
   elseif theta(j)<=25*3.14159/180
      qdot(j)=(0.80*.05+(0.88*.13-0.80*.05)*(theta(j)-
15*3.14159/180)/(10*3.14159/180))*uprate;%[MW/m^2]
   elseif theta(j)<=35*3.14159/180
      qdot(j)=(0.88*.13+(0.95*.25-0.88*.13)*(theta(j)-
25*3.14159/180)/(10*3.14159/180))*uprate;%[MW/m^2]
   elseif theta(j)<=45*3.14159/180
      qdot(j)=(0.95*.25+(1.02*.57-0.95*.25)*(theta(j)-
35*3.14159/180)/(10*3.14159/180))*uprate;%[MW/m^2]
   elseif theta(j)<=55*3.14159/180
      qdot(j)=(1.02*.57+(1.1*.72-1.02*.57)*(theta(j)-
45*3.14159/180)/(10*3.14159/180))*uprate;%[MW/m^2]
   elseif theta(j)<=65*3.14159/180
      qdot(j)=(1.1*.72+(1.25*.85-1.1*.72)*(theta(j)-
55*3.14159/180)/(10*3.14159/180))*uprate;%[MW/m^2]
   elseif theta(j)<=70*3.14159/180
      qdot(j)=(1.3*1)*uprate;%[MW/m^2]
   else
      qdot(j)=0*uprate;
   end
   flow(27,j)=qdot(j);
end
phase=0;
walltemp(1)=373;%initial wall temperature [K]
temp(1)=373;%initial bulk temperature (of subcooled liquid) [K]
num=1;
while phase==0
   if num==1

enthalpy(num)=hf(100)*1000+qdot(num)*10^6*geo(13,num)*2*3.14159*geo(17,num)/mdot;%enth
alpy [J/kg], initial enthalpy at 373 K, 152810 Pa
      P(num)=1/vf(373-273)*9.81*(3.826-geo(10,num))+101325-0.5*mdot^2*vf(373-
273)/2/0.145209;%initial pressure in Pa minus form inlet (k=0.5)
      Dh(num)=geo(21,num);%hydraulic diameter [m], Dh=Do-Di
      hf1=461300;%saturated liquid enthalpy at 1.4 atm [J/kg]
      hfg1=2230200;%heat of vaporization at 1.4 atm [J/kg]
      tf(num)=381.865+(P(num)-137169)/(152810-137169)*(385.086-381.865);%saturated liquid
temperature [K]
      xe(num)=(enthalpy(num)-hf1)/hfg1;%equilibrium quality
      temp(num)=xe(num)*(hfg1)/4183+385;%bulk temperature of subcooled liquid [K]
      rhol(num)=998-(temp(num)-293)/80*(998-958.313);%subcooled liquid density [kg/m3]
      rhog(num)=0.59773+(P(num)-101400)/(143300-101400)*(0.82645-0.59773);
      Pr(num)=6-(temp(num)-293)/80*(6-1.76);%Prandtl number
      k(num)=0.606+(temp(num)-293)/80*(0.68-.606);%liquid conductivity
      area(num)=geo(22,num);%flow area
```

```
    Resub(num)=mdot*Dh(num)/area(num)/(279*10^-6);%Reynolds number
    h(num)=k(num)/Dh(num)*0.023*(Resub(num))^0.8*(Pr(num))^0.4;%heat transfer coefficient,
Dittus-Boelter
    walltemp(num)=qdot(num)*10^6/h(num)+temp(num);
    flow(1,num)=enthalpy(num);
    flow(2,num)=0;%quality
    flow(3,num)=0;%void fraction
    flow(4,num)=rhol(num);
    flow(6,num)=Resub(num);%Reynolds Number

flow(7,num)=0.184/(flow(6,num))^0.2*geo(23,num)/geo(21,num)*mdot^2/(2*flow(4,num)*(geo(22,
num))^2);%pressure loss
    accout(num)=0;
    accin(num)=0;
    flow(9,num)=accout(num)-accin(num);%acceleration term
    flow(20,num)=xe(num);
    flow(21,num)=temp(num);%bulk temperature
    flow(22,num)=qdot(num)*10^6*geo(13,num)*2*3.14159*geo(17,num);%power
    if theta(num)>=(3.14159/2)
      theta(num)=(3.14159/2);
      phi(num)=(3.14159/2);
    end
    SA0=(0.65444)+(-1.2018)*0.076*log(mdot/geo(22,num))+(-
0.008388)/(0.1)^2+(0.000179)*(mdot/geo(22,num))+(1.36899)*0.076/0.1+(-
0.077415)*0.076/(0.1)^2+(0.024967)*0.1*(log(mdot/geo(22,num)))^2;
    SA1=(-0.086511)*(log(mdot/geo(22,num)))^2+(-4.49425)*0.076*log(mdot/geo(22,num));
    SA2=(9.28489)*0.076;
    SA3=(-
0.0066169)*(log(mdot/geo(22,num)))^2+(11.62546)*0.076*0.1+(0.855759)*xe(num)*log(mdot/geo
(22,num));
    SA4=(-1.74177)*0.1+(0.182895)*log(mdot/geo(22,num))+(-
1.8898)*xe(num)+(2.2636)*0.076;

flow(23,num)=(SA0+SA1*xe(num)+SA2*(xe(num))^2+SA3*theta(num)+SA4*(theta(num))^2)*10^
6;%critical heat flux
    if phi(num)>=150/180*(3.14159)
        flow(25,num)=(4.8*flow(23,num))*multiplier;%nanofluid critical heat flux (multiplier% of
graph)
    elseif phi(num)>135/180*(3.14159)
        flow(25,num)=((3+(phi(num)-135/180*(3.14159))/(15/180*(3.14159))*(4.8-
3))*flow(23,num))*multiplier;
    elseif phi(num)>120/180*(3.14159)
        flow(25,num)=((2.5+(phi(num)-120/180*(3.14159))/(15/180*(3.14159))*(3-
2.5))*flow(23,num))*multiplier;
    elseif phi(num)>90/180*(3.14159)
        flow(25,num)=((2.1+(phi(num)-90/180*(3.14159))/(30/180*(3.14159))*(2.5-
2.1))*flow(23,num))*multiplier;
    else
    end
    flow(24,num)=flow(23,num)/(qdot(num)*10^6);%dnbr
    flow(26,num)=flow(25,num)/(qdot(num)*10^6);%nanofluid dnbr
    num=num+1;
  else
    enthalpy(num)=flow(1,num-
1)+qdot(num)*10^6*geo(13,num)*2*3.14159*geo(17,num)/mdot;%enthalpy [J/kg]
```

```
    P(num)=P(num-1)-flow(7,num-1)-flow(9,num-1)-1/vf(temp(num-1)-273)*9.81*(geo(10,num)-
geo(10,num-1));
    Dh(num)=geo(21,num);%hydraulic diameter [m], Dh=Do-Di
    hf1=461300;%saturated liquid enthalpy at 1.4 atm [J/kg]
    hfg1=2230200;%heat of vaporization at 1.4 atm [J/kg]
    tf(num)=381.865+(P(num)-137169)/(152810-137169)*(385.086-381.865);%saturated liquid
temperature [K]
    xe(num)=(enthalpy(num)-(hf1))/(hfg1);%equilibrium quality
    temp(num)=xe(num)*(hfg1)/4183+385;%bulk temperature of subcooled liquid [K]
    rhol(num)=998-(temp(num)-293)/80*(998-958.313);%subcooled liquid density [kg/m3]
    rhog(num)=0.59773+(P(num)-101400)/(143300-101400)*(0.82645-0.59773);
    Pr(num)=6-(temp(num)-293)/80*(6-1.76);%Prandtl number
    k(num)=0.606+(temp(num)-293)/80*(0.68-.606);%liquid conductivity
    %k(num)=Kf(temp(num)-273);%liquid conductivity
    area(num)=geo(22,num);%flow area
    Resub(num)=mdot*Dh(num)/area(num)/(279*10^-6);%Reynolds number
    h(num)=k(num)/Dh(num)*0.023*(Resub(num))^0.8*(Pr(num))^0.4;%heat transfer coefficient,
Dittus-Boelter
    walltemp(num)=qdot(num)*10^6/h(num)+temp(num);
    flow(1,num)=enthalpy(num);
    flow(2,num)=0;%quality
    flow(3,num)=0;%void fraction
    flow(4,num)=rhol(num);
    flow(6,num)=Resub(num);%Reynolds Number

flow(7,num)=0.184/(flow(6,num))^0.2*geo(23,num)/geo(21,num)*mdot^2/(2*flow(4,num)*(geo(22,
num))^2);%pressure loss
    if flow(3,num)==0
        accout(num)=2*mdot^2/(geo(22,num)+geo(22,num-
1))*(1/(rhol(num)*geo(22,num)));%acceleration out term
        accin(num)=accout(num-1);%acceleration in term
        flow(19,num)=rhol(num);
    else
        accout(num)=2*mdot^2/(geo(22,num)+geo(22,num-
1))*((flow(2,num))^2/(flow(3,num)*0.88)+(1-flow(2,num))^2/((1-
flow(3,num))*950))/geo(22,num);%acceleration out term
        accin(num)=accout(num-1);%acceleration in term
        rhop(num)=((flow(2,num))^2/(flow(3,num)*0.88)+(1-flow(2,num))^2/((1-
flow(3,num))*950))^-1;
        flow(19,num)=rhop(num);
    end
    flow(9,num)=accout(num)-accin(num);%acceleration term
    flow(20,num)=xe(num);
    flow(21,num)=temp(num);%bulk temperature
    flow(22,num)=qdot(num)*10^6*geo(13,num)*2*3.14159*geo(17,num);%power
    if theta(num)>=(3.14159/2)
      theta(num)=(3.14159/2);
      phi(num)=(3.14159/2);
    end
    SA0=(0.65444)+(-1.2018)*0.076*log(mdot/geo(22,num))+(-
0.008388)/(0.1)^2+(0.000179)*(mdot/geo(22,num))+(1.36899)*0.076/0.1+(-
0.077415)*0.076/(0.1)^2+(0.024967)*0.1*(log(mdot/geo(22,num)))^2;
    SA1=(-0.086511)*(log(mdot/geo(22,num)))^2+(-4.49425)*0.076*log(mdot/geo(22,num));
    SA2=(9.28489)*0.076;
```

```
    SA3=(-
0.0066169)*(log(mdot/geo(22,num)))^2+(11.62546)*0.076*0.1+(0.855759)*xe(num)*log(mdot/geo
(22,num));
    SA4=(-1.74177)*0.1+(0.182895)*log(mdot/geo(22,num))+(-
1.8898)*xe(num)+(2.2636)*0.076;

flow(23,num)=(SA0+SA1*xe(num)+SA2*(xe(num))^2+SA3*theta(num)+SA4*(theta(num))^2)*10^
6;%critical heat flux
    if phi(num)>=150/180*(3.14159)
        flow(25,num)=(4.8*flow(23,num))*multiplier;%nanofluid critical heat flux
    elseif phi(num)>135/180*(3.14159)
        flow(25,num)=((3+(phi(num)-135/180*(3.14159))/(15/180*(3.14159))*(4.8-
3))*flow(23,num))*multiplier;
    elseif phi(num)>120/180*(3.14159)
        flow(25,num)=((2.5+(phi(num)-120/180*(3.14159))/(15/180*(3.14159))*(3-
2.5))*flow(23,num))*multiplier;
    elseif phi(num)>90/180*(3.14159)
        flow(25,num)=((2.1+(phi(num)-90/180*(3.14159))/(30/180*(3.14159))*(2.5-
2.1))*flow(23,num))*multiplier;
    else
    end
    flow(24,num)=flow(23,num)/(qdot(num)*10^6);%dnbr
    flow(26,num)=flow(25,num)/(qdot(num)*10^6);%nanofluid dnbr
    if walltemp(num)>=tf%saturated liquid temperature at 1.5 atm [385 K]
      phase=1;
      xc=geo(9,num);
      yc=geo(10,num);
      hlonb=enthalpy(num);
      xeonb=xe(num);
    else
    end
    num=num+1;
  end
end
  for i=[num:n]
      if flow(1,i-1)<=2676100%below bulk boiling
        flow(1,i)=flow(1,i-1)+qdot(i)*10^6*geo(13,i)*2*3.14159*geo(17,i)/mdot;%enthalpy [J/kg]
        xe(i)=(flow(1,i)-hf1)/hfg1;
        Dh(i)=geo(21,i);%hydraulic diameter [m], Dh=Do-Di
        P(i)=P(i-1)-flow(7,i-1)-flow(9,i-1)-rhol(i-1)*9.81*(geo(10,i)-geo(10,i-1));
        tsat(i)=373.15+(P(i)-101400)/(152330-101400)*(385-373.15);
        tsat(num-1)=373.15+(P(num-1)-101400)/(152330-101400)*(385-373.15);
        temp(i)=xe(i)*hfg1/4183+385;%bulk temperature of subcooled liquid [K]
        if temp(i)>=tsat(i)
          temp(i)=tsat(i);
        else
        end
        rhol(i)=998-(temp(i)-293)/80*(998-958.313);%subcooled liquid density [kg/m3]
        Pr(i)=6-(temp(i)-293)/80*(6-1.76);%Prandtl number
        k(i)=0.606+(temp(i)-293)/80*(0.68-.606);%liquid conductivity
        %k(i)=Kf(temp(i)-273);
        area(i)=geo(22,i);%flow area
        Re(i)=mdot*Dh(i)/area(i)/(279*10^-6);% Reynolds number
        h(i)=k(i)/Dh(i)*0.023*(Re(i))^0.8*(Pr(i))^0.4;%heat transfer coefficient, Dittus-Boelter
        walltemp(i)=qdot(i)*10^6/h(i)+temp(i);
        flow(3,num-1)=0;
```

```
            alphabub(num-1)=flow(3,num-2);
            alphabub(i)=flow(3,i-1);
            tlc(num-1)=tsat(num-1)-(4183*(tsat(num-1)-temp(num-1))+hfg1*flow(2,num-
1))/(4183*(1-flow(2,num-1)));
            tl(num-1)=tlc(num-1);
            dz(num-1)=geo(23,num-1);
            dz(i)=geo(23,i);
            if alphabub(num-1)<10^-5
               F4(num-1)=flow(3,num-2)*10^5;
               alphabub(num-1)=10^-5;
            else
               F4(num-1)=1;
            end
            F3(num-1)=F4(num-1);
            if alphabub(i)<10^-5
               F4(i)=flow(3,i-1)*10^5;
               alphabub(i)=10^-5;
            else
               F4(i)=1;
            end
            F3(i)=F4(i);
            rhof=955;%saturated liquid density
            rhog(i)=0.59773+(P(i)-101400)/(143300-101400)*(0.82645-0.59773);
            if alphabub(num-1)<0.25
               vflux(num-1)=mdot/rhol(num-1)/area(num-1)/(1-flow(2,num-2));
               if abs(vflux(num-1))>0.61
                  phihif(num-1)=(1.639344*abs(vflux(num-1)))^0.47;
               else
                  phihif(num-1)=1;
               end
               C(num-1)=65-(5.69*10^-5)*(P(num-1)-10^5);
               F5(num-1)=1.8*phihif(num-1)*C(num-1)*exp(-45*alphabub(num-1))+0.075;
            else
               F5(num-1)=0.075;
            end
            Hif(num-1)=(F3(num-1)*F5(num-1)*hfg1*rhog(num-1)*rhof*alphabub(num-1))/(rhof-
rhog(num-1));
            if alphabub(i)<0.25
               vflux(i)=mdot/rhol(i)/area(i)/(1-flow(2,i-1));
               if abs(vflux(i))>0.61
                  phihif(i)=(1.639344*abs(vflux(i)))^0.47;
               else
                  phihif(i)=1;
               end
               C(i)=65-(5.69*10^-5)*(P(i)-10^5);
               F5(i)=1.8*phihif(i)*C(i)*exp(-45*alphabub(i))+0.075;
            else
               F5(i)=0.075;
            end
            Hif(i)=(F3(i)*F5(i)*hfg1*rhog(i)*rhof*alphabub(i))/(rhof-rhog(i));
            if qdot(i)==0
               if tl(i-1)>=temp(i-1)
                  tl(i)=tl(i-1);
                  flow(2,i)=flow(2,i-1);
               else
                  tl(i)=tl(i-1)+(Hif(i-1)*(tsat(i-1)-tl(i-1))*area(i-1)*dz(i-1))/((1-flow(2,i-1))*mdot*4183);
```

```
            collapse=300;
            flow(2,i)=flow(2,i-1)-(Hif(i-1)*(tsat(i-1)-tl(i-1))*collapse*area(i-1)*dz(i-
1))/(mdot*hfg1);
            if flow(2,i)<=0
               flow(2,i)=0;
            else
            end
          end
        else
          tl(i)=tlc(i-1);
          flow(2,i)=xe(i)-xeonb*exp((xe(i)/xeonb)-1);%quality, Levy Model
        end
        hf2(i)=(419.04+(tsat(i)-373)/10*(461.30-419.04))*1000;
        hfg2(i)=(2257+(tsat(i)-373)/10*(2230.2-2257))*1000;
        if hf2(i)<=flow(1,i)
            flow(2,i)=(flow(1,i)-hf2(i))/(hfg2(i));
        else
        end
        onephvis=0.000281832;%one phase viscosity
        %onephvis=muf(temp(i)-273);
        onephden(i)=rhol(i);%one phase density
        onephre(i)=mdot*geo(21,i)/(geo(22,i)*onephvis);%one phase Re
        [flow(3,i),jg(i),jf(i),c0(i)]=epri(flow(2,i),mdot,geo(22,i),angle(i),geo(21,i));
        flow(4,i)=flow(3,i)*rhog(i)+(1-flow(3,i))*onephden(i);%density [kg/m^3]
        flow(5,i)=flow(3,i)*0.000012+(1-flow(3,i))*0.000281832;%viscosity [N*s/m^2]
        flow(6,i)=mdot*geo(21,i)/(geo(22,i)*flow(5,i));%Reynolds Number
        flow(8,i)=onephre(i);
        if flow(3,i)==0
          flow(10,i)=100000;
        else
          flow(10,i)=jg(i)/jf(i)*(1-flow(3,i))/flow(3,i);%slip ratio
        end
        flow(11,i)=jg(i);
        flow(12,i)=jf(i);
        flow(13,i)=jg(i)/jf(i);
        flow(16,i)=[1+flow(2,i)*(onephden(i)/.59773-1)];
        rhobar=(flow(2,i)/0.59773+(1-flow(2,i))/onephden(i))^-1;
        We=mdot^2*geo(21,i)/((geo(22,i))^2*rhobar*0.0589);
        Fr=mdot^2/(9.81*geo(21,i)*(rhobar)^2*(geo(22,i))^2);
        A1=(1-flow(2,i))^2+((flow(2,i))^2)*(onephden(i)/0.59773)*(0.0000012/0.000281832)^0.2;
        A2=(flow(2,i))^0.78*(1-flow(2,i))^0.224;
        A3=(onephden(i)/0.59773)^0.91*(0.0000012/0.000281832)^0.19*(1-
0.0000012/0.000281832)^0.7;
        flow(18,i)=A1+3.24*A2*A3/(Fr^0.045*We^0.035);%two phase flow friction factor Friedel
correlation

flow(7,i)=0.184/onephre(i)^0.2*geo(23,i)/geo(21,i)*mdot^2/(2*onephden(i)*(geo(22,i))^2)*flow(18,i)
;%pressure loss
        if flow(3,i)==0
          accout(i)=2*mdot^2/(geo(22,i)+geo(22,i-
1))*(1/(onephden(i)*geo(22,i)));%acceleration out term
          accin(i)=accout(i-1);%acceleration in term
          flow(19,i)=rhol(i);
        else
          accout(i)=2*mdot^2/(geo(22,i)+geo(22,i-1))*((flow(2,i))^2/(flow(3,i)*rhog(i))+(1-
flow(2,i))^2/((1-flow(3,i))*onephden(i)))/geo(22,i);%acceleration out term
```

```
            accin(i)=accout(i-1);%acceleration in term
            rhop(i)=((flow(2,i))^2/(flow(3,i)*rhog(i))+(1-flow(2,i))^2/((1-flow(3,i))*onephden(i)))^-1;
            flow(19,i)=rhop(i);
          end
          flow(9,i)=accout(i)-accin(i);%acceleration pressure loss
          flow(20,i)=xe(i);
          if flow(20,i)<=0
            flow(21,i)=temp(i);%bulk temperature
          else
            flow(21,i)=373;
          end
          flow(22,i)=qdot(i)*10^6*geo(13,i)*2*3.14159*geo(17,i);%power
          tlc(i)=tsat(i)-(4183*(tsat(i)-temp(i))+hfg1*flow(2,i))/(4183*(1-flow(2,i)));
          if theta(i)>=(3.14159/2)
            theta(i)=(3.14159/2);
            phi(i)=(3.14159/2);
          end
          SA0=(0.65444)+(-1.2018)*0.076*log(mdot/geo(22,i))+(-
0.008388)/(0.1)^2+(0.000179)*(mdot/geo(22,i))+(1.36899)*0.076/0.1+(-
0.077415)*0.076/(0.1)^2+(0.024967)*0.1*(log(mdot/geo(22,i)))^2;
          SA1=(-0.086511)*(log(mdot/geo(22,i)))^2+(-4.49425)*0.076*log(mdot/geo(22,i));
          SA2=(9.28489)*0.076;
          SA3=(-
0.0066169)*(log(mdot/geo(22,i)))^2+(11.62546)*0.076*0.1+(0.855759)*xe(i)*log(mdot/geo(22,i));
          SA4=(-1.74177)*0.1+(0.182895)*log(mdot/geo(22,i))+(-1.8898)*xe(i)+(2.2636)*0.076;
          flow(23,i)=(SA0+SA1*xe(i)+SA2*(xe(i))^2+SA3*theta(i)+SA4*(theta(i))^2)*10^6;%critical
heat flux
          if phi(i)>=150/180*(3.14159)
            flow(25,i)=(4.8*flow(23,i))*multiplier;%nanofluid critical heat flux
          elseif phi(i)>135/180*(3.14159)
            flow(25,i)=((3+(phi(i)-135/180*(3.14159))/(15/180*(3.14159))*(4.8-
3))*flow(23,i))*multiplier;
          elseif phi(i)>120/180*(3.14159)
            flow(25,i)=((2.5+(phi(i)-120/180*(3.14159))/(15/180*(3.14159))*(3-
2.5))*flow(23,i))*multiplier;
          elseif phi(i)>90/180*(3.14159)
            flow(25,i)=((2.1+(phi(i)-90/180*(3.14159))/(30/180*(3.14159))*(2.5-
2.1))*flow(23,i))*multiplier;
          else
          end
          if qdot(i)==0
            flow(24,i)=25;
            flow(26,i)=25;
          else
            flow(24,i)=flow(23,i)/(qdot(i)*10^6);%dnbr
            flow(26,i)=flow(25,i)/(qdot(i)*10^6);%nanofluid dnbr
          end
        else
          bulkboiling=1
        end
      end
flow(14,:)=geo(22,:);
flow(15,:)=c0;
flow(17,1)=cn;

%EPRI void fraction correlation
```

```
function [alpha,jg,jf,c0]=epri(x,mdot,area,angle,dh)
epsilon=0.00005;
for alpha1=[0:epsilon:1]
   ang=angle*180/3.14159;
   fr=(90-ang)/90;
   jg=x*mdot/area/0.59773;
   jf=(1-x)*mdot/area/958.313;
   c1=4*221.2^2/(220.2);
   L=(1-exp(-c1*alpha1))/(1-exp(-c1));
   liqRe=jf*958.313*dh/0.000281832;
   vapRe=jg*0.59773*dh/0.000012;
   if liqRe>vapRe
      Re=liqRe;
   else
      Re=vapRe;
   end
   a1=1/(1+exp(-Re/60000));
   b1=min(0.8,a1);
   k0=b1+(1-b1)*(0.59773/958.313)^0.25;
   r=(1.0+1.57*0.59773/958.313)/(1-b1);
   c0v=L/(k0+(1-k0)*alpha1^r);
   c0h=(1+alpha1^0.05*(1-alpha1)^2)*c0v;
   c0=fr*c0v+(1-fr)*c0h;
   c5=(150/958.313*0.59773)^0.5;
   c2=1/(1-exp(-c5/(1-c5)));
   c3=max(0.50,2*exp(-Re/60000));
   c7=(0.09144/dh)^0.6;
   c8=c7/(1-c7);
   if c7>=1
      c4=1;
   else
      c4=1/(1-exp(-c8));
   end
   c9=(1-alpha1)^b1;
   vgjv=c9*1.41*c2*c3*c4*(957.715*0.0589*9.81/958.313^2)^0.25;
   vgjh=vgjv;
   vgj=fr*vgjv+(1-fr)*vgjh;
   if (c0*(jg+jf)+vgj)==0
      alpha2=0;
   elseif jg==0
      alpha2=0;
   else
      alpha2=jg/(c0*(jg+jf)+vgj);
   end
   alpha2;
   error=abs(alpha2-alpha1);
   if error<0.00005
      break
   else
   end
end
alpha=0.5*(alpha1+alpha2);

%Evaluator for AP1000 for power uprate
function evaluator6(mdot,uprate)
[geo,dth,angle]=ap1000modinlet;
```

```
[flow]=flow6001(geo,mdot,dth,angle,uprate);
mdot=mdot;%mass flow used in energy
[rn,cn]=size(geo);
n=cn;
dsum=0;
hsum=0;
for i=[1:n-1]
   dsum=dsum+((geo(10,i+1)-geo(10,i))*0.5*(flow(4,i+1)+flow(4,i)))^2;
   hsum=hsum+(geo(10,i+1)-geo(10,i))^2;
end
aveden=(dsum/hsum)^.5;
gravity=(geo(10,n)-geo(10,1))*9.81*(952-aveden)
friction=sum(flow(7,:))
acceleration=sum(flow(9,:))
inletform=0.5*mdot^2*vf(373-273)/2/0.145209
form=gravity-friction-acceleration-inletform%[N/m^2]
tpff=flow(18,262)%Friedel friction factor at limiting area
dens=955;
koutlet=(form)*2*dens*1.0/mdot^2/tpff
power=sum(flow(22,:))
mdotcalc=(2*dens*form*(1.27*tpff)^-1)^0.5
error=mdotcalc-mdot

%Graph Generator
function graphgenerator
mdot=860;
[geo,dth,angle]=ap1000modinlet;
[flow]=flow6001(geo,mdot,dth,angle,2.1);
enthalpy=flow(1,:);
quality=flow(2,:);
voidf=flow(3,:);
density=flow(4,:);
Re=flow(6,:);
pressloss=flow(9,:)+flow(7,:);
onephre=flow(8,:);
slip=flow(10,:);
jg=flow(11,:);
jf=flow(12,:);
vfluxratio=flow(13,:);
area=flow(14,:);
c0=flow(15,:);
rhomplus=flow(19,:);
xe=flow(20,:);
temp=flow(21,:);
power=flow(22,:);
chf=flow(23,:);
dnbr=flow(24,:);
nanodnbr=flow(26,:);
qdot=flow(27,:);
tpff=flow(18,:);
[rn,cn]=size(geo);
n=cn;
cumploss(1)=0;%cumulative pressure loss
for i=[1:n]
   ycoord(i)=geo(10,i)+2.16;
   cumploss(i+1)=cumploss(i)+pressloss(i);
```

```
   G(i)=mdot/area(i);
   diff(i)=density(i)-rhomplus(i);
end
plot(flow(9,:),ycoord)
xlabel('CHF (W/m^2)')
ylabel('Height (m)')
```

NOMENCLATURE

A	area	[m^2]
C_0	distribution parameter in EPRI correlation	
D_H	hydraulic diameter	[m]
Fr	Froude number	
G	mass flux	[$kg/m^2 \cdot s$]
H	height	[m]
K	form loss coefficient	
L	length of channel	[m]
N_p	phase change (Zuber) number	
N_s	subcooling number	
P	decay power	[W]
P	pressure	[MPa]
P_0	reactor operating power	[W]
Pr	Prandtl number	
$\dot{Q}$	power	[MW]
Q_0	maximum power	[W]
Re	Reynolds number	
T	temperature	[K]
V_{gi}	drift flux parameter in EPRI correlation	
We	Weber number	
f	friction factor	
g	acceleration due to gravity	[m/s^2]
h	enthalpy	[J/kg]
h	height	[m]
j	superficial velocity	[m/s]
k	form loss coefficient	
k	thermal conductivity	[W/m·K]
l	average length of incremental volume	[m]

$\dot{m}$	mass flow rate	[kg/s]
q''	heat flux	[W/m^2]
q''_{CHF}	critical heat flux	[MW/m^2]
s	channel gap size	[m]
t	time after shutdown	[s]
t_1	time to core relocation	[s]
t_2	time in which water can remove the same amount of decay power as a nanofluid	[s]
x	flow quality	
x_e	equilibrium quality	

Subscript

acceleration	due to acceleration
bulk	of the bulk fluid
cavity	inside the cavity but outside the channel
channel	inside the channel
crit	at the critical point
exit	at the channel exit
f	of the liquid
fg	difference between the vapor and liquid values
form	due to form
friction	due to friction
g	of the vapor
gravity	due to gravity
i	at the inlet
inlet	at the inlet
l	of the liquid
m	of the mixture

o	at the outlet
onb	at the outset of nucleate boiling
tp	two-phase
sat	at saturation
surface	of the surface
wall	of the wall

Greek

Δh	subcooled enthalpy	[J/kg]
ΔP	pressure loss	[Pa]
Θ	angle from horizontal	[rad]
Φ^2	two-phase friction multiplier	
α	void fraction	
η	non-dimensional power	
θ	angle from vertical	[deg]
μ	dynamic viscosity	[Pa·s]
ξ	non-dimensional mass flow rate	
ρ	density	[kg/m^3]
ρ^+	two-phase momentum density	[kg/m^3]
σ	surface tension	[N/m]

REFERENCES

1. T-N. Dinh, J.P. Tu, T. Salmassi, T.G. Theofanous, "Limits of Coolability in the AP1000-Related ULPU-2400 Configuration V Facility," CRSS-03/06 (2003).

2. S. J. Kim, I. C. Bang, J. Buongiorno, L. W. Hu, "Surface Wettability Change during Pool Boiling of Nanofluids and its effect on Critical Heat Flux", *International Journal of Heat and Mass Transfer,* (in press), (2007).

3. N. Todreas, M. Kazimi, *Nuclear Systems I: Thermal Hydraulic Fundamentals*, Hemisphere Publishing Corporation, New York (1990).

4. B. Chexal, G. Lellouche, J. Horowitz, J. Healzer "A Void Fraction Correlation for Generalized Applications," *Progress in Nuclear Energy*, **Vol. 27**, *No. 4*, pp. 255-295 (1992).

5. S. Rouge, *SULTAN Test Facility Large Scale Vessel Coolability in Natural Convection at Low Pressure, NURETH-7 Conference Proceedings*, Saratoga Springs, NY USA (September 1995).

6. S. M. You, J. Kim, K. H. Kim, "Effect of nanoparticles on critical heat flux of water in pool boiling heat transfer", *Applied Physics Letters*, **Vol. 83**, *No. 16*, pp. 3374-3376 (2003).

7. U.S. Rohatgi, R.B. Duffey, "Stability, DNB, and CHF in Natural Circulation Two-Phase Flow," *Int. Comm. Heat Mass Transfer*, Vol. 25, No. 2, pp. 161-174 (1998).

8. P. Saha, M. Ishii, N. Zuber, "An Experimental Investigation of the Thermally Induced Flow Oscillations in Two-Phase Systems", *J. Heat Transfer*, Vol. 98, pp. 616-622 (1976).

9. Y.-Y. Hsu, R. W. Graham, *Transport Processes in Boiling and Two-Phase Systems*, American Nuclear Society (1987).

10. D. L. Knudson, J. L. Rempe, *In-Vessel Retention Modeling Capabilities of SCDAP/RELAP5-3D©, ICONE-10 Conference Proceedings*, Arlington, VA USA (April 2002).

11. Gianfranco Saiu, Monica Linda Frogheri, "AP1000 Nuclear Power Plant Overview," ANSALDO Energia S.p.A, Genoa, Italy, <http://www.ansaldonucleare.it/TPap0305/NNPP/NPP_37.pdf> (April 30, 2007).

12. Westinghouse AP1000 Design Control Document, Rev. 3, APP-GW-GL-700 (2003).

13. Westinghouse AP1000 Probabilistic Risk Assessment Report, Rev. 0, APP-GW-GL-022 (2003).

14. J.P. Tu, T.N. Dinh, T.G. Theofanous, *Enhancing Resistance to Burnout via Coolant Chemistry, NURETH-10 Conference Proceedings*, Seoul, Korea (October 2003).

15. Nyacol AL20, AL20DW Material Safety Data Sheet, Nyacol Nano Technologies, Inc. (June 8, 2000).

16. T. Lucas, L.W. Hu, J. Buongiorno, *Investigation of Gamma Radiation Effect on Nanofluids for Nuclear Applications, ANS Summer Meeting Proceedings,* Boston, MA USA (June 2007).

17. Personal communication with Richard Wright, Westinghouse Electric Company (February 2006).

18. International Occupational Safety and Health Information Centre (CIS) Material Data Card, < http://www.ilo.org/public/english/protection/safework/cis/products/icsc/dtasht/_icsc03/icsc0351.htm> (April 27, 2007).

19. Personal communication with Professor Ronald G. Ballinger, Massachusetts Institute of Technology (March 2006).

20. *ASM Handbook, Vol. 13: Corrosion*, pp. 547-565, 669-706 (1990).

21. Personal communication with Robert Moscardini and Bob Taylor, AT&F Advanced Metals, LLC (October 2006).

22. W.E. Cummins, M.M. Corletti, T.L. Schulz, *Westinghouse AP1000 Advanced Passive Plant, ICAPP '03 Conference Proceedings*, Cordoba, Spain (May 2003).

23. Personal communication with Carolyn Shull, Customer Service, Nano Technologies Inc. (March 2007).

24. Personal communication with Al Gunnarson, Warren Controls (April 2007).

25. Personal communication with Lisa Jones, Tioga Pipe (March 2007).

26. Personal communication with Jay Cheema, Senior Project Engineer, Fluid Energy Controls (March 2007).

27. Westinghouse AP1000 Final Safety Evaluation Report (2004).

28. Title 10, Part 52 of the United States Code of Federal Regulations.

29. NRC Policy Statement, "The Use of Probabilistic Risk Assessment Methods in Nuclear Regulatory Activities," (60 FR 42622 dated August 16, 1995).

30. NRC Policy Statement, "Safety Goals for the Operations of Nuclear Power Plants," 51 FR 28044 (August 4, 1986).

31. Nuclear Regulatory Commission Generic Letter 95-02, "Use of NUMARC/EPRI Report TR-102348, 'Guideline on Licensing Digital Upgrades,' in Determining the Acceptability of Performing Analog-to-Digital Replacements under 10 CFR 50.59," Washington, D.C. (April 26, 1995).

32. J. Palomar, R. Wyman, "The Programmable Logic Controller and Its Application in Nuclear Reactor Systems," NUREG/CR-6090, UCRL-ID-112900 (September 1993).

33. United States Federal Register, 57FR36680 (August 14, 1992).

34. T. Aldemir, D.W. Miller, M.P. Stovsky, J. Kirschenbaum, P. Bucci, A.W. Fentiman, L.T. Mangan, "Current State of Reliability Modeling Methodologies for Digital Systems and Their Acceptance Criteria for Nuclear Power Plant Assessments," NUREG/CR-6901 (February 2006).

35. "Guideline on Licensing Digital Upgrades," Nuclear Management and Resources Council/Electrical Power Research Institute Report, TR-102348 (December 1993).

36. International Atomic Energy Agency, "Safety-related Terms for Advanced Nuclear Power Plants," IAEA–TECDOC-626, Vienna (September 1991).

37. Nuclear Energy Agency, "Passive System Reliability - A Challenge to Reliability Engineering and Licensing of Advanced Nuclear Power Plants," NEA/CSNI/R(2002)10 (March 2002).

38. R. Eul, K. Ahn, S-P. Kao, P. Hejzlar, and M.S. Kazimi, "Comparison of Active and Passive Safety Systems in Advanced Light Water Reactors," MIT-ANP-TR-111 (September 2006).

39. Annabelle Hett, *Nanotechnology – Small matter, many unknowns*, Swiss Reinsurance Company (2004).

40. Toxic Substances Control Act, 15 U.S.C. §2601 *et seq.*

41. Peter Tomasco, "Note: Manufactured Nanomaterials: Avoiding TSCA and OSHA Violations for Potentially Hazardous Substances," Boston College Environmental Affairs Law Review, 33 B.C. Envtl. Aff. L. Rev. (2006).

42. The Occupational Safety and Health Act of 1970, 29 U.S.C. §651 *et seq.*

43. NIOSH official website, <http://www.cdc.gov/niosh/topics/nanotech/ohrisks.html> (April 27, 2007).

44. MIT Environment, Health, and Safety Office website, "Potential Risks of Nanomaterials and How to Safely Handle Materials of Uncertain Toxicity," <http://web.mit.edu/environment/ehs/topic/nanomaterial.html> (April 27, 2007).

45. *Risk Assessment in the Federal Government: Managing the Process*, National Academy Press, Washington, D.C. (1983).

46. G. M. Masters, Introduction to Environmental Engineering and Science, 2nd Edition, Englewood Cliffs: Prentice Hall (1998).

47. Health and Safety Executive (UK), "Nanoparticles: an occupational hygiene review," Research Report 274 (2004).

48. David Rejeski, "The Next Small Thing," *The Environmental Forum*, March/April 2004, pp. 42-49.

49. G. Oberdörster, Z. Sharp, V. Atudorei, A. Elder, R. Gelein, W. Kreyling, C. Cox, "Translocation of Inhaled Ultrafine Particles to the Brain," *Inhalation Toxicology*, Volume 16, Issue 6 & 7 June 2004 , pp. 437-445.

50. K. Peters, R. E. Unger, C. J. Kirkpatrick, A. M. Gatti, E. Monari, "Effects of nano-scaled particles on endothelial cell function in vitro: Studies on viability, proliferation and inflammation," *J. Mater. Sci.: Mater. Med.* **2004**, 15, 321-325.

51. M. D. Cheng, "Effects of nanophase materials (<) 20 nm) on biological responses," *J. Environ. Sci. Health, Part A: Toxic/Hazard. Subst. Environ. Eng.* **2004**, *39*, 2691-2705.

52. Q. Rahman, M. Lohani, E. Dopp, H. Pemsel, L. Jonas, D. G. Weiss, D. Schiffmann, "Evidence that ultrafine titanium dioxide induces micronuclei and apoptosis in Syrian hamster embryofibroblasts," *Environ. Health Perspect.* **2002**, *110*, 797-800.

53. Katherine A. Dunphy, Guzman, Margaret R. Taylor, Jillian F. Banfield, "Environmental Risks of Nanotechnology: National Nanotechnology Initiative Funding, 2000-2004," *Environmental Science & Technology*, Vol. 40, No. 5, **2006**, p. 1405.

54. G. Oberdörster, J.N. Finkelstein, C. Johnson, R. Gelein, C. Cox, R. Baggs, A.C. Elder, "Acute pulmonary effects of ultrafine particles in rats and mice," *Research Report, Health Effects Institute*, **2000** Aug;(96):5-74; disc. 75-86.

55. "DOE Handbook: Primer on Tritium Safe Handling Practices," DOE-HDBK-1079-94, U.S. Department of Energy, Washington, D.C. (December 1994).

56. Veerle Heyvaert, "Reconceptualizing Risk Assessment," *Reciel* 8(2): 135-143 (1999).

57. "U.S. Environmental Protection Agency White Paper on Nanotechnology," U.S. Environmental Protection Agency, Washington D.C., EPA 100/B-07/001 (February 2007).

58. Sonia Miller, "A Matter of Torts: Why Nanotechnology Must Develop Processes of Risk Analysis," *New York Law Journal*, Vol. 232, No. 67 (October 5, 2004).

59. Henry G. Grabowski, John M. Vernon, "The Regulation of Pharmaceuticals: Balancing the Benefits and the Risks," American Enterprise Institute, Washington D.C. (1983).

60. Nicholas A. Ashford, Claudia S. Miller, "Low-Level Chemical Exposures: A Challenge for Science and Policy," Environmental Science and Technology, November 1, 1998 / Volume 32, Issue 21 / pp. 508 A-509 A.

61. Harvey M. Sapolsky, "The Politics of Risk," *Daedalus*; Fall 1990; 119,4.

62. M. Granger Morgan, "Risk Analysis and Management," *Scientific American*, July 1993, pp. 24-30.